FIELAX Gesellschaft für wissenschaftliche Datenverarbeitung mbH
Schleusenstr. 14, D-27568 Bremerhaven, GERMANY
Fon: +49 (0)471 30015-0, Fax: +49 (0)471 30015-22, Mail: info@fielax.de

Heat Flow Measurements

Great Australian Bight

Deepwater Marine Program

Client: CSIRO

Contractor: FIELAX GmbH

Contact:

FIELAX Gesellschaft für wissenschaftliche Datenverarbeitung mbH
Schleusenstraße 14, D-27568 Bremerhaven, GERMANY
Fon: +49 (0)471 30015-0, Fax: +49 (0)471 30015-22
Mail: info@fielax.de

Ref.: HF_report_IN2015_C01_v1.4.pdf	Vers.: 1.4	Date: 27.11.2015	Status: preliminary

Report history

Rev.	Author	Company	Date	Comments / Changes
1.0	C. Müller	FIELAX	14.11.2015	First draft
1.1	C. Müller	FIELAX	16.11.2015	Preliminary
1.4	C. Müller	FIELAX	27.11.2015	Preliminary

Content

1 Introduction

In October/November 2015, heat flow measurements were performed as part of the CSIRO Great Australian Bight Deepwater Marine Program on board the vessel “R.V. Investigator”. For the determination of heat flow values from marine sediments, the measurement of the temperature gradient and thermal conductivity is required to calculate the heat flow value according to Fourier’s law:

$$q = -\lambda(z) \cdot \frac{d}{dz} T(z)$$

where q is heat flow in mW/m^2, $\lambda(z)$ the depth dependent thermal conductivity in W/(m K) and dT/dz the temperature gradient. Heat flow measurements were performed at 10 locations using the FIELAX HeatFlowProbe (**Figure 1**). This report presents the method description, the measured data and its quality assessment, and processing results with respect to steady-state heat flow values.

Figure 1: The FIELAX HeatFlowProbe during its deployment on board the vessel “R.V. Investigator”.

2 Heat flow survey overview

- 21-Oct-2015, 13:00 (local time) arrival of the FIELAX operator in Hobart, boarding “R.V. Investigator”, arrival of freight

- 22-Oct-15, mobilization, setup/check/test of HF equipment (HF-electronics serial# CTM1000, NTC sensor-string serial# T113SD). 20:00 (local) leaving harbor for trial/test journey

- 24-Oct-15, toolbox meeting HF: discussion of deployment/recovery procedure using the starboard side crane

- 24-Oct-15, 18:15 (24-Oct-15, 05:15 UTC), HF-Test (TPRBE_006), calibration at 2413 m depth, two penetrations, Pen 1: failed; Pen 2: not stable, temperature gradient determined, thermal conductivity assumed for HF determination

- 24-Oct-15, 06:00 (local) arrival Hobart, 20:00 (local) leaving Hobart

- 04-Nov-15, 16:39 (04-Nov-15 05:39 UTC), HF08 (TPRBE_030), two penetrations, both ca. 2.5 m but sufficient for HF processing

- 07-Nov-15, due to hard sediments and thus, poor penetration, additional weights of 280 kg mounted to the head of the heat flow probe, Toolbox meeting HF,

- 07-Nov-15, 19:58 (07-Nov-15, 08:58 UTC), HF07 (TPRBE_046), two penetrations, both sufficient

- 08-Nov-15, 21:00 (07-Nov-15, 08:00 UTC), HF04 (TPRBE_047), two penetrations, both sufficient

- 08-Nov-15, 18:01 (08-Nov-15, 07:01), HF03 (TPRBE_048), two penetrations, due to strong currents probe moved (steady tilt) during both penetrations, temperature gradients determined, thermal conductivities assumed for HF determination, measurement repeated:

- 08-Nov-15, 21:00 (08-Nov-15, 08:00 UTC), HF03 (TPRBE_049), one penetration, again due to strong currents probe moved (steady tilt) during penetration, temperature gradient determined, thermal conductivity assumed for HF determination

- 10-Nov-15, 12:04 (10-Nov-15, 01:04 UTC), HF06 (TPRBE_056), two penetrations, Pen 1: poor, unstable in the ground, Pen 2: failed

- 13-Nov-15, toolbox meeting HF: discussion to overcome poor stable penetration problems due to lightweight Dynema-deep sea cable: Using standard deep sea cable from A-frame

- 19-Nov-15, toolbox meeting HF: discussion to overcome poor stable penetration problems due to lightweight Dyneema-deep sea cable: Using standard deep sea cable from A-frame

- 19-Nov-15, 12:35 (19-Nov-15, 01:35 UTC), HF05 (TPRBE_088) using standard deep sea cable from A-frame, no stability problems, two penetrations, Pen 1: ok, Pen 2: failed, deep sea cable entangled head of probe: 2nd penetration started with 15° tilt.

- 21-Nov-15, toolbox meeting HF for improving deployment

- 22-Nov-15, 8:18 (22-Nov-15, 19:18 UTC), HF02 (TPRBE_109) using standard deep sea cable from A-frame, no stability problems. Nevertheless, cable strongly damaged. Both penetrations were successful with 4.5 m for the first and 5.5 m full penetration for the second.

- 25-Nov-15, VSM03 and HF01 delayed because of too much wind/swell

-

3 Measuring procedure and data

3.1 The FIELAX HeatFlowProbe

The FIELAX HeatFlowProbe is a scientific device for measurement of temperature gradients and in-situ thermal conductivities. With these two parameters, the heat flux density can be determined. The standard design of a heat flow probe follows the violin bow concept of Lister (Hyndman et al., 1979; Lister 1979) where a sensor string equipped with thermistors and heating wires mounted parallel to a strength member penetrates by its own weight into soft deep sea sediments. The probe is designed to measure in-situ thermal parameter values in the sediments of the seafloor down to a penetration depth of 6 m.

Thermal measurements with the heat flow probe have been conducted in a wide range of deep-sea environments, with the device using its own weight and gravity to penetrate the seafloor. The probe can be operated in water depths up to 6000 m.

The thermal measurement equipment consists of the following components:

- Sensor string, with 22 temperature sensors (FIELAX Serial#: T113SD)
- Data acquisition unit (FIELAX Serial#: CTM1000)
- Power supply unit for heat pulse generation

Here, the temperatures are recorded with 22 thermistors that are placed within a sensor string at a spacing of 250 mm, resulting in an active length of 5.5 m. The sensors are temperature sensitive resistors (NTC, Negative Temperature Coefficient) designed for temperature ranges of -2°C to 60°C with a resolution better than 1 mK and accuracy within 2 mK after deep sea calibration. The sensor string also contains a heating wire which allows the release of a distinct amount of thermal energy into the sediments. The amount of energy dissipates from the heating wire is determined by high precision voltage and current measurements. The data acquisition and the power supply units are built in Grade-5 titanium pressure housings.

3.2 Measuring principle

A full measuring cycle (**Figure 2**) starts with the penetration process. The system is lowered to the seabed and penetrates the sediment during which the temperature usually rises due to frictional heating followed by convergence towards undisturbed sediment temperatures. From the frictional heat and subsequent decay relative sediment temperatures as a function of depth are derived and the temperature gradient can be determined. After a certain period of stability time (12 min) to allow dissipation of the frictional heat, a heat pulse with duration of 20 seconds is released and heats up the sensor tube and the surrounding sediment resulting in a sharp temperature peak. The probe remains in the sediment for another 20 minutes to record the decay of this artificial thermal energy. The decay of the heat allows the depth-dependent determination of the thermal parameters as conductivity, diffusivity and capacity of the sediment.

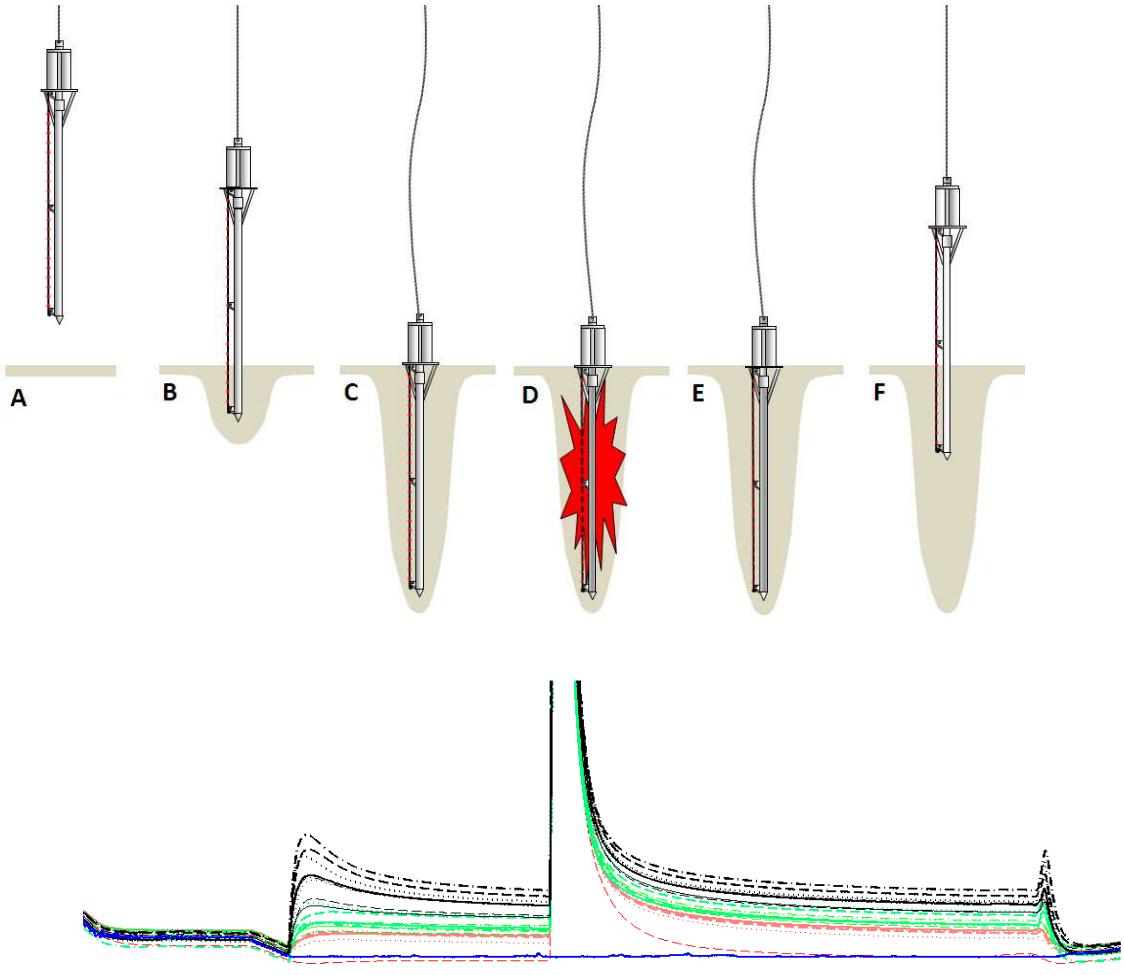

Figure 2: Principle of a heat flow measurement. A: HeatFlowProbe lowering to the seabed. B: Penetrating into seabed. C: Recording temperatures of thermal decay of frictional heat (12 minutes). D: Artificial heat pulse. E: Recording temperatures of thermal decay of heat pulse (approximately 20 minutes). F: Retrieval to surface.

3.3 Operation mode

The probe was operated in autonomous mode, i.e. no direct, online control by a direct cable connection was possible. The control of time of the heat pulse release was configured as being enabled if tilt during penetration was less than 30° and the probe was stable in the sediment for 12 min. This stability time was controlled from acceleration stability being less than 0.03 g. After heat pulse release a further heat pulse was blocked until the next relative change of pressure by 50 dbar. Thus, for enabling a second penetration was moved for 100 m above the seabed before lowered and penetrated again.

3.4 Data Processing

The processing of temperature data includes calibration of sensors, inversion of in-situ sediment temperatures and temperature gradients, correction for probe tilt during penetration, calculation of thermal conductivities and thermal diffusivities. The depth dependent in-situ temperatures, thermal conductivities and thermal diffusivities are determined by an iterative inversion procedure based on the method developed by Hartmann & Villinger (2002). Both, thermal conductivity and also thermal diffusivity are derived independently from the temperature data, which also allows determining the volumetric heat capacity. Thus, true undisturbed in-situ temperatures and in-situ thermal conductivities can be determined. It should be taken into account, that due to the geometry of the measuring system, thermal conductivities λ are determined in horizontal direction. Due to anisotropy of thermal conductivities in layered sediments, for an evaluation of conductivities in vertical direction this should be accounted for. Following Pribnow et al. (2000), the anisotropy in layered sediments is in the range of $\lambda_{horizontal}/\lambda_{vertical} \sim 1.2$.

3.5 Sensor string calibration and water temperature

For determination of the temperature gradients, the temperatures must be measured within a relative accuracy of up to 1 mK. To guarantee this, the sensor strings NTCs values are compared to the laboratory calibrated high precision PT100 water sensor. The measuring range of the NTCs (here: -2°C -30°C) is calibrated in the laboratory for linearization in this range using the Steinhart & Hart (1968) method. The deep sea is a perfect homogeneous temperature environment suitable for determining temperature sensor offsets with respect to the PT100 sensor. Thus, for final evaluation of the temperature data for heat flow, the temperature offsets data from the deep sea HF site HF08 (TPTBE_56) were used. These

offsets were determined in a water depth of 5385 m. Temperature-depth data from the ODV database (**Zitat???**) and measured temperatures show, that the temperature depth distribution ibn this region and depth is sufficient homogenous (**Figure 3**).

In addition, the use of this calibrated, high precision PT100 enables to conduct complete temperature-depth profiles from the sea surface completely down towards the sea floor. A compilation of all temperature-depth profiles measured during this project is provided in the **Appendix 9**.

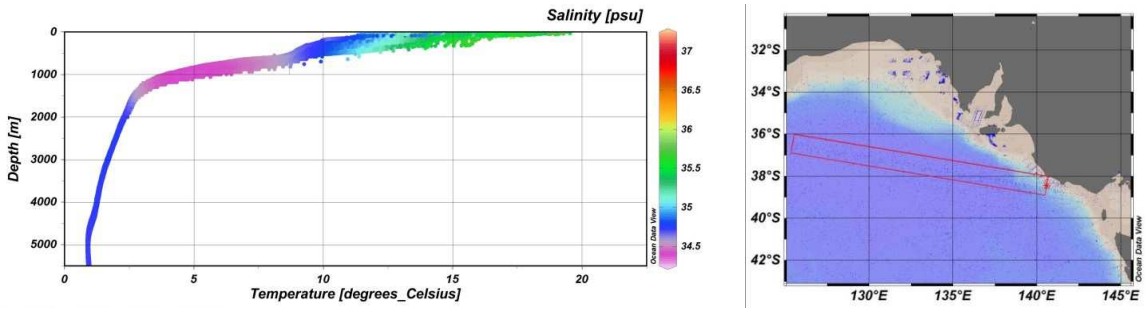

(**a**)

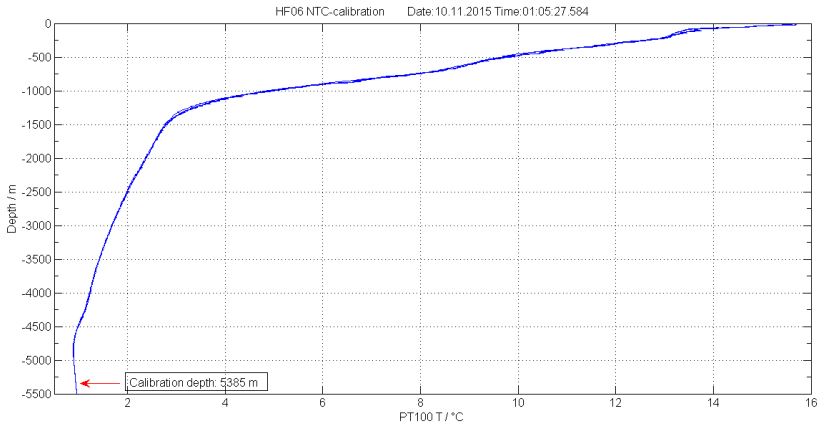

(**b**)

Figure 3: Water temperatures in the Great Australian Bight and sensor string calibration: (**a**) Temperature and salinities from the ODV database (**Zitat?**) and (**b**) temperature-depth distribution from the PT100 sensor of HF site HF08 (TPRBE_056), were NTC sensor string T113SD was calibrated in the depth of 5385 m).

3.6 Data quality control

After each heat flow deployment, a quick evaluation of the measured data was performed using FIELAX standard quality control plots. As an example, **Figure 4** shows these quality control plots for site HF07 (TPRBE_046). This station was performed as a pogo measurement, i.e. two penetrations/measurements were carried out during one deployment. The temperature data are not yet offset compensated in this stage.

Quality control plots for all measurements performed in this project are provided in the **Appendix 7**.

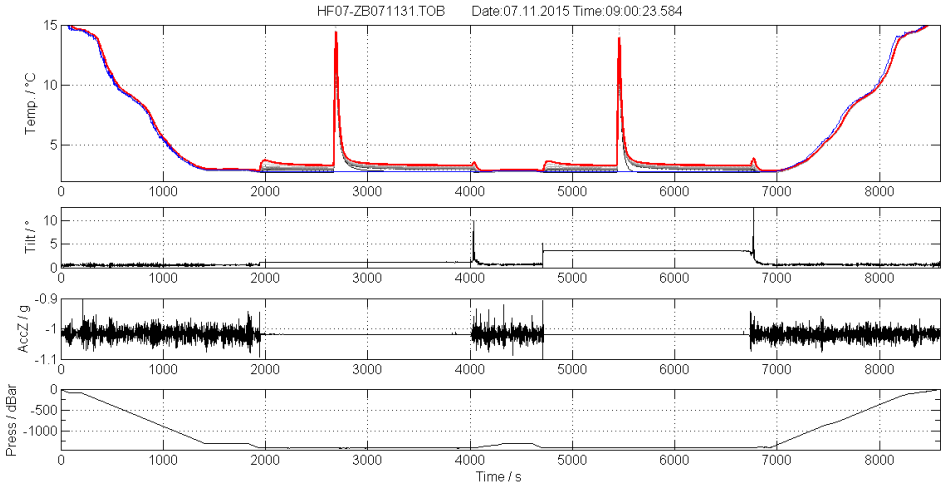

(**a**)

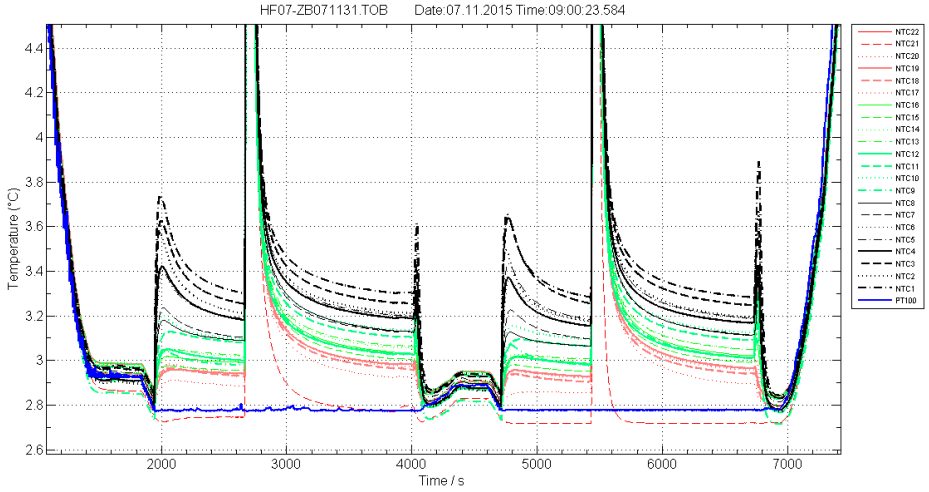

(**b**)

Figure 4: Typical quality control plots (HF07) enabling a very first view on measured data (**a**) time dependent properties as temperatures, horizontal tilt, acceleration, and pressure, corresponding to depths in meters and (**b**) a closer view to the temperature evolution of all 22 NTC thermistors.

4 Heat flow stations

The map **Figure 5** shows the sites of heat flow measurements performed. A summarize of heat flow stations is provided in **Table 1**. All stations were planned to be measured in double penetration mode, i.e. for redundancy and repeatability of measured values. Two penetrations at the same site were performed during each deployment.

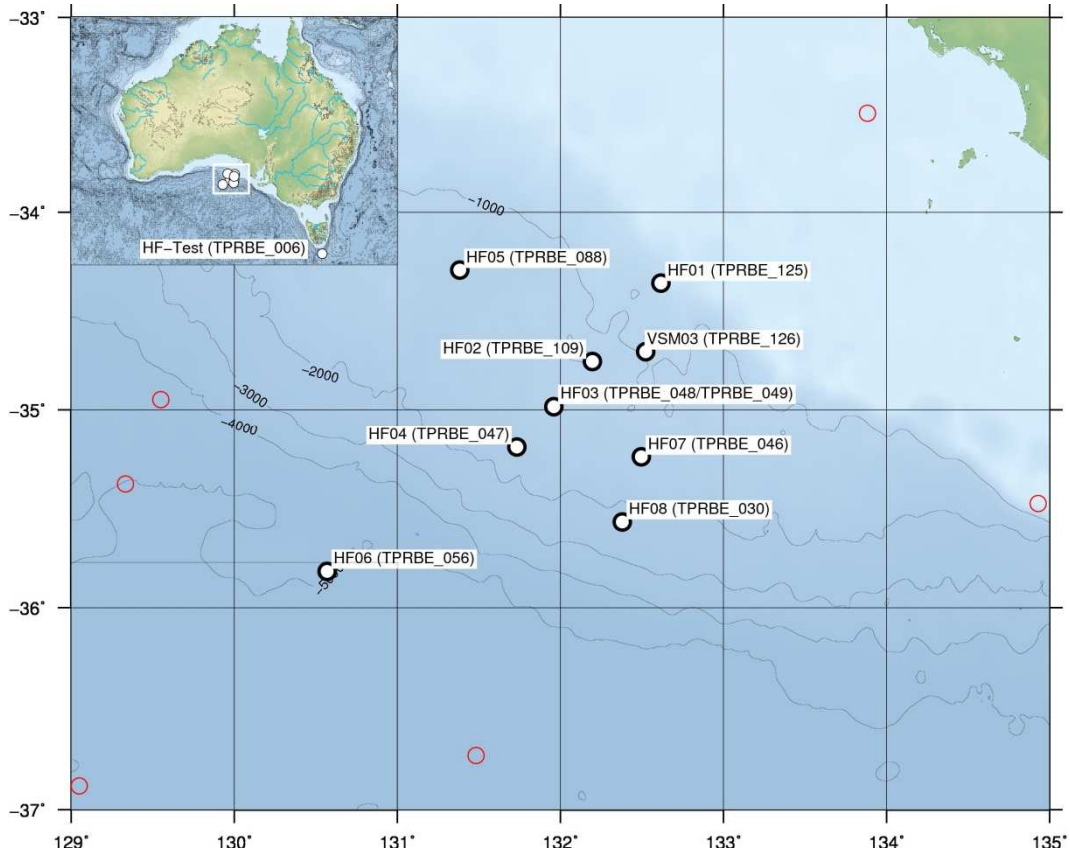

Figure 5: Map showing the location and station identification of the heat flow measurements performed. Red circles are heat flow sites as retrieved from the Global Heat Flow Database (2011). The bathymetry used is from the GEBCO data set (2014).

4.1 HF-Test (TPRBE_006):

On the short mobilization test voyage south of Tasmania, also a test deployment of the heat flow probe was performed (HF-Test, TPRBE_006, 24-Oct-15, 03:11 UTC). This deployment was used for NTC-calibration in a depth of 2413 m. Two penetrations were attempted. The first failed with no penetration. The second penetrated with the lowermost four sensors (~ 1 m) and after that starting a strong motion with further penetration but strong tilt and being unstable for the rest of penetration time (**Figure 6**). Nevertheless, the initial, stable phase of little penetration could be used for a temperature gradient determination.

4.2 HF08 (TPRBE_030):

The first HF deployment in the survey area, HF08 (TPRBE_030) was performed on 4-Nov-15 06:26 (UTC, first penetration) with two penetrations within one deployment. Again, these both penetrations were only partly: 1.7 m and 2.2 m. Nevertheless, data and processing results of both measurements are of very good quality.

The penetration depths at these first sites were very low due to extremely stiff sediments. Thus, due to these little penetrations, it was decided to mount additional weights (ca. 280 kg) to the head of the heat flow probe. This turned out to yield better penetration depths at following HF sites (**Table 1**).

Table 1: Overview of heat flow sites performed and equipment used; sorted by date of deployment.

Station name	Cast_ID HF	Pen. #	Date yyyy-mm-dd	Pen time hh:mm:ss	Lat dd.dddd	Lon dd.dddd	Depth m	Sens. pen.	Comments deployment
HF-Test	TPRBE_006	1	2015-10-24	04:09:00	-44.3802	147.5483	2562 (pressure)	-	No penetration
HF-Test	TPRBE_006	2	2015-10-24	05:03:00	-44.3812	147.5483	2562 (pressure)	1-4	Partial penetration, not stable
HF08	TPRBE_030	1	2015-11-04	06:26:20	-35.568197	132.380953	2120	1-7	Partial penetration
HF08	TPRBE_030	2	2015-11-04	07:15:20	-35.568197	132.380953	2120	1-9	Partial penetration
HF07	TPRBE_046	1	2015-11-07	09:32:40	-35.243246	132.494955	1418	1-21	
HF07	TPRBE_046	2	2015-11-07	10:18:50	-35.243246	132.494955	1418	1-20	
HF04	TPRBE_047	1	2015-11-07	21:43:00	-35.191869	131.733369	1686	1-13	
HF04	TPRBE_047	2	2015-11-07	22:30:00	-35.191869	131.733369	1686	1-21	Partial penetration
HF03	TPRBE_048	1	2015-11-08	07:30:50	-34.983634	131.958528	1263	1-14	Strong current, Not stable
HF03	TPRBE_048	2	2015-11-08	08:11:00	-34.983634	131.958528	1263	1-15	Strong current, not stable
HF03	TPRBE_049	3	2015-11-08	10:32:50	-34.983729	131.958444	1263	1-13	Strong current, not stable
HF06	TPRBE_056	1	2015-11-10	02:43:10	-35.820164	130.563621	5432	1-5	Calibration
HF06	TPRBE_056	2	2015-11-10	03:36:30	-35.820164	130.563621	5432	-	No penetration
HF05	TPRBE_088	1	2015-11-19	02:08:30	-34.294436	131.3843443	1314	1-15	
HF05	TPRBE_088	2	2015-11-19	02:46:00	-34.294436	-34.294436	1314	-	Np penetration
HF02	TPRBE_109	1	2015-11-22	19:46:10	-34.757075	132.197948	1137	1-21	
HF02	TPRBE_109	2	2015-11-22	20:26:10	-34.757075	132.197948	1137	1-21	
HF01	TPRBE_125	1	2015-11-26	04:51:00	-34.359189	132.615812	701	1-22	
HF01	TPRBE_125	2	2015-11-26	05:29:00	-34.359189	132.615812	701	1-22	
VSM03	TPRBE_126	1	2015-11-26						
VSM03	TPRBE_126	2	2015-11-26						

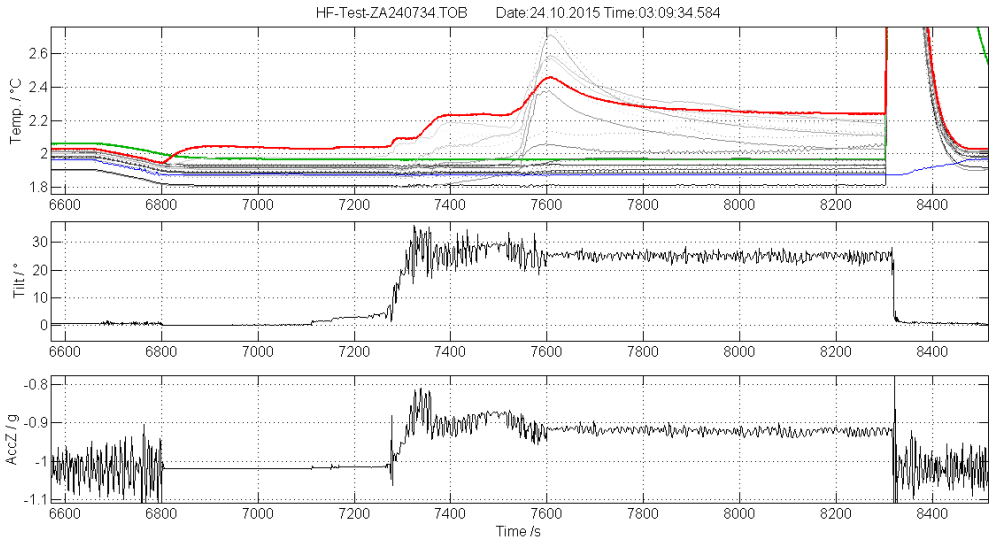

Figure 6: Second penetration of HF-Test (TPRBE_006) showing stable (~0° tilt) penetration of lowermost 4 sensors (~1 m) for a duration of 5 minutes after second 6800 followed by strong movement, further penetration down to sensor 14 and strong tilt of the probe after second 7300. Due to this movement the heat pulse was delayed and temperatures strongly disturbed and thus, not usable for processing. Nevertheless, the initial 5 min of stable penetration could be used for a temperature gradient determination.

4.3 HF07 (TPRBE_046):

The penetration depths of site HF07 (TPRBE_046, 07-Nov-15, 08:58 UTC) were quite sufficient with 5.3 m and 5.0 m. The temperature data could be processed without any restrictions.

4.4 HF04 (TPRBE_047):

The penetration depths of site HF04 (TPRBE_047, 07-Nov-15, 08:00 UTC) differed by 3.2 m and 5.2 m. Nevertheless, temperature data of both penetrations could be processed without any restrictions.

4.5 HF03 (TPRBE_048, TPRBE_049):

The HF deployment HF03 (TPRBE_048) was performed on 8-Nov-15 07:30 (UTC, first penetration) with two penetrations within one deployment. Due to extremely strong bottom water currents, the probe was not stable in the ground and suffered from steady tilt of the probe resulting in thermal disturbances of the temperature sensors from steady frictional heating (**Figure 7**). A second deployment at the same site (HF03 (TPRBE_049, Pen 3, 08-Nov-15 10:32 (UTC)) was performed with the lower end of the deep sea cable fixed to the

ground by additional weights but leading to no reasonable better results. Penetrations were sufficient with 4.5 m (HF03 Pen 1), 5.2 m (HF03 Pen2), and 4.5 m (HF03 Pen 3).

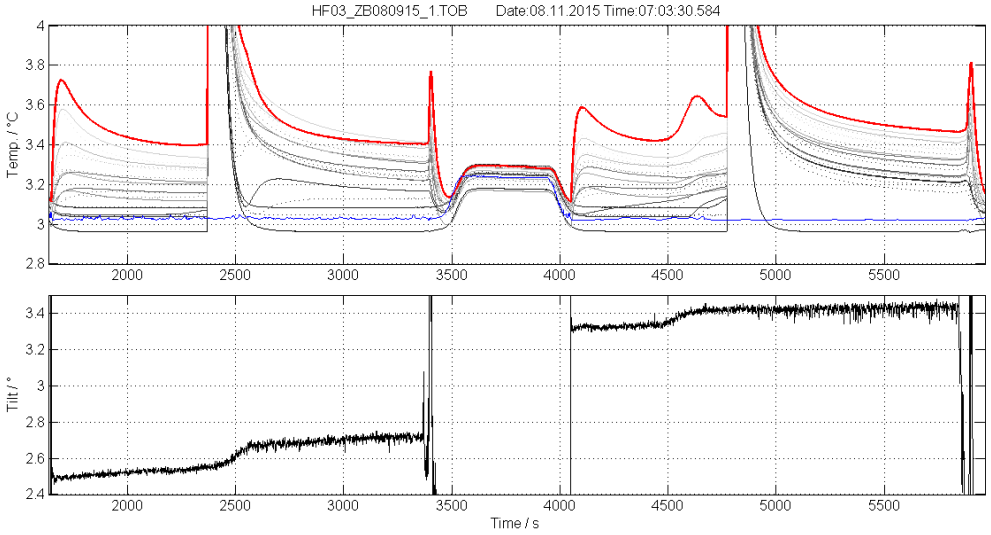

Figure 7: Both penetrations of HF03 showing NTC temperatures and tilts during penetrations. Note steady tilt change and temperature rise from frictional heating during phases of tilt acceleration.

4.6 HF06 (TPRBE_056):

The deep (5432 m) HF deployment HF06 (TPRBE_056) was performed on 10-Nov-15 02:43 (UTC) with two penetrations within one deployment. The first penetration was 1.3 m in the sediment and the second did not penetrate at all. Due to extremely strong bottom water currents, the probe was not stable in the ground and suffered from steady tilt of the probe resulting in thermal disturbances of the temperature sensors from steady frictional heat. A sudden, string movement of the probe ca. 10 min following the heat pulse made the temperature data unusable from this point on. Nevertheless, a reliable temperature gradient could be retrieved from HF06 Pen 1 and thermal conductivities could be inverted.

As the reason for these stability problems during penetration (HF-Test, HF03, HF06), the use of the lightweight Dyneema deep sea cables were identified. Due to being nearly buoyant in the water, it has no resistance against friction forces from water currents and the penetrated probe is continuously forced to horizontal tilt movement. These tilt movements produce frictional heat to the sensor string so that temperature measurements are disturbed and thermal conductivity determination not possible. **Figure 8** gives an impression of these frictional forces on the cable for various probe depths in the water column.

To overcome this problem, for the following HF sites a standard deep sea cable deployed from the A-frame was used.

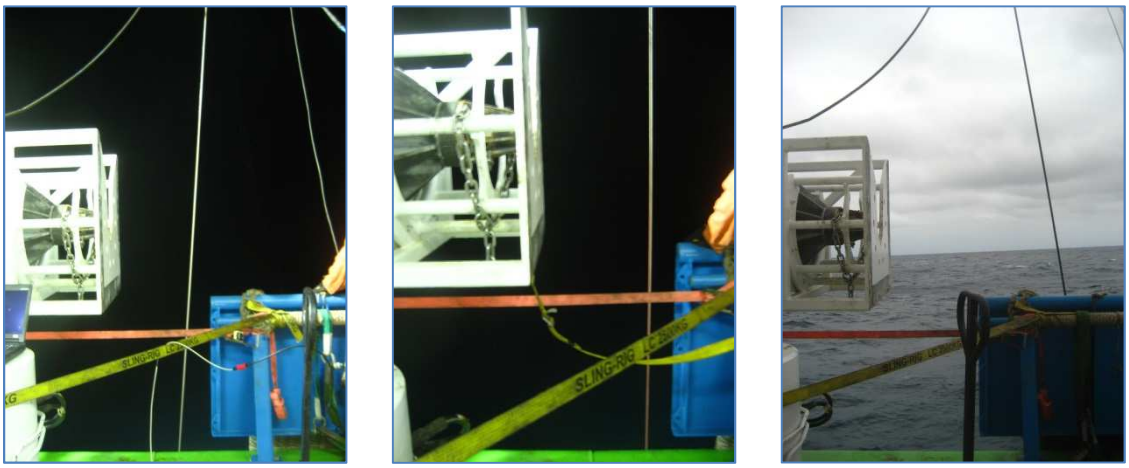

Figure 8: Deflection of the deep sea cable just after recovery from the penetration of HF03 (TPRBE_049) in ca. 1000 m depth (left) indicating extreme strong bottom water current, near the sea surface (middle), and for HF06 (TPRBE_030) just after recovery from the sea bed in ca. 5000 m depth.

4.7 HF05 (TPRBE_088):

Using the standard deep sea cable, HF05 (TPRBE_088, 19-Nov-15, 02:08 UTC) was not disturbed by movement of the probe during penetration. Pen 1 had a depth of nearly 4 m and Pen2 did not penetrate. From analysis of the tilts it is obvious that the cable was tangled around the head of the probe and penetration started with a tilt angle of 15° leading to failure (**Figure 9**). Nevertheless, temperature data of Pen 1 could be processed without any restrictions.

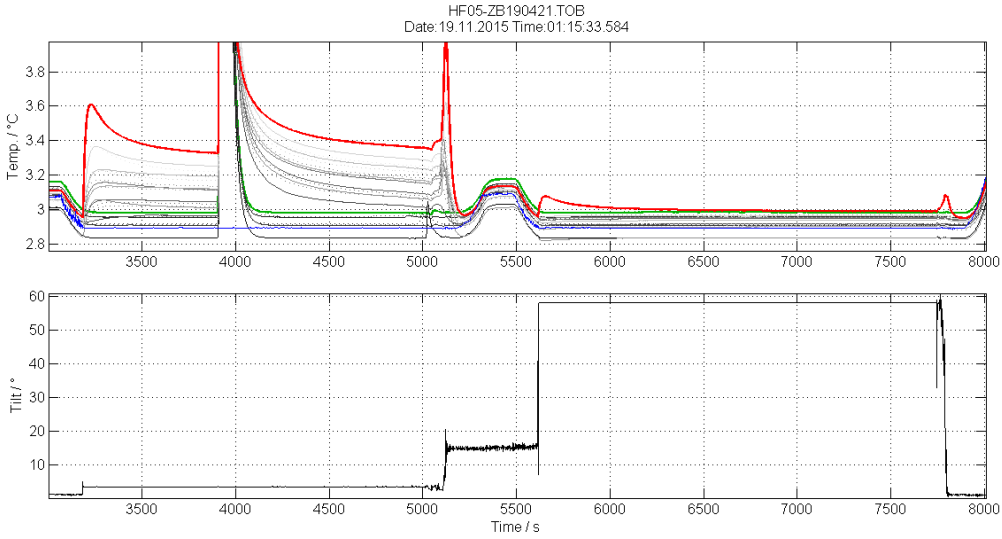

Figure 9: Pen1 HF05 using standard deep sea cable showing no tilt disturbances anymore. Nevertheless, entangled cable around the probes head lead to tilt of 15° during pullout and second penetration. Thus, Pen 2 fall to the side and did not penetrate.

4.8 HF02 (TPRBE_109):

The HF deployment HF02 (TPRBE_109) was performed 22-Nov-2015 20:46 (UTC, first penetration) with two penetrations within one deployment. Both penetrations were successful with 4.5 m for the first and 5.5 m full penetration for the second. Data and processing results of both measurements were of excellent quality.

4.9 HF01 (TPRBE_125):

The HF deployment HF01

4.10 VSM03 (TPRBE_126):

The HF deployment VSM03

5 Heat flow determination and results

The aim of this project was to measure the steady-state heat flow. In order to decide if steady-state heat flow is prevailing, the so-called Bullard method is applied. Steady-state heat flow means that the sediment is in the state of thermal equilibrium and no transient processes are active. This means that the heat transfer equation is independent of time, no material transport (advection).takes place and no heat sinks or sources are present:

$$\partial_z(\lambda \partial_z T) = 0.$$

This in turn means that heat flow q_0 is independent of time and the Fourier law

$$q_0 = \lambda(z)\frac{dT}{dz}$$

(here, $\lambda(z)$ is the depth (z) dependent thermal conductivity and dT/dz the temperature gradient) can be integrated according to depth. This yields

$$T(z) = T(z_0) + q_0 \int_{z_0}^{z} \frac{dz'}{\lambda(z')} = T(z_0) + q_0\, R(z)$$

or

$$T(R) = T_0 + q_0 R$$

with

$$R(z) = \int_{z_0}^{z} \frac{dz'}{\lambda(z')},$$

the “integrated thermal resistance”. Plotting T versus R yields the so-called Bullard plot (Bullard, 1939). In case of conductive steady-state processes, $T(R)$ shall be linear with the slope q_0 yielding a constant heat flow value. Nonlinear deviations may be caused by transient processes such as high sedimentation rates, seasonal temperature fluctuations, advection processes, or heat generation.

The sites, which were measured in pogo style i.e. at the same position, reveal nearly identical results (see **Table 2** and the **Appendix 8**). **Figure 10** as an example shows the Bullard plots for stations HF04 (TPRBE_047) for both Pen 1 and Pen 2.

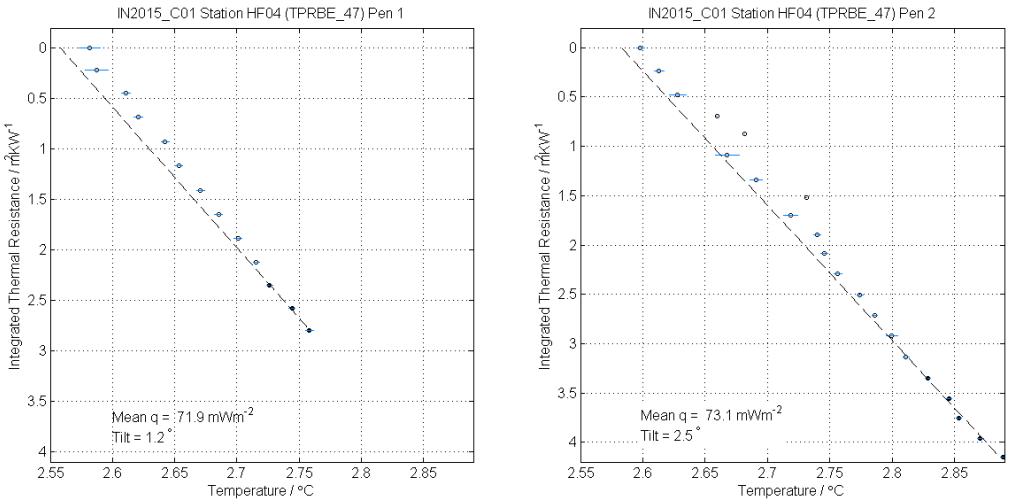

Figure 10: Example for Bullard plots from heat flow sites HF04 (TPRBE_047) Pen 1 and Pen 2. In general, temperatures are quite linear but with slight deviations in the upper part. Thus, for heat flow determination, only the lowermost five sensors were used. Deviations in the upper layers might originate from advective processes like fluid flow and/or degassing, change of sedimentation rates with time, or transient processes like bottom water temperature variations. In addition, this figure nicely shows nearly identical temperature distribution for two pogo measurements at the same position but different penetration depths.

Table 2: Heat flow results showing temperature gradients, mean thermal conductivity λ, diffusivity κ, capacity ρc and heat flow q. For details and depth dependent parameters see **Appendix 8**.

Station	Cast_ID	Pen.	Mean conductivity λ	Mean diffusivity κ	Mean capacity ρc	Temp-gradient	Heat flow q	Comments / quality
name	HF	#	W/(m K)	1e-7 m^2/s	MJ/(m^3 K)	K/m	mW/m^2	
HF-Test	TPRBE_006	1	-	-	-	-	-	No penetration
HF-Test	TPRBE_006	2	1.0 (assumed)	-	-	0.0737	73.7	fairly good
HF08	TPRBE_030	1	0.995	3.167	3.145	0.0723	71.3	very good
HF08	TPRBE_030	2	1.021	3.294	3.105	0.0716	73.2	very good
HF07	TPRBE_046	1	1.214	4.054	2.994	0.0680	77.1	excellent
HF07	TPRBE_046	2	1.102	3.698	3.009	0.0671	75.5	excellent
HF04	TPRBE_047	1	1.080	3.578	3.022	0.0640	71.9	very good
HF04	TPRBE_047	2	1.228	4.340	2.868	0.0584	73.1	excellent
HF03	TPRBE_048	1	1.1 (assumed)	-	-	0.0627	68.9	fairly good
HF03	TPRBE_048	2	1.1 (assumed)	-	-	0.0691	76.0	fairly good
HF03A	TPRBE_049	3	1.1 (assumed)	-	-	0.0672	73.9	fairly good
HF06	TPRBE_056	1	1.162	4.003	3.025	0.0646	65.0	good
HF06	TPRBE_056	2	-	-	-	-	-	No penetration
HF05	TPRBE_088	1	1.007	3.236	3.133	0.0718	70.73	excellent
HF05	TPRBE_088	2	-	-	-	-	-	No penetration
HF02	TPRBE_109	1	1.101	3.694	2.993	0.0663	72.25	excellent
HF02	TPRBE_109	2	1.131	3.833	2.958	0.696	80.64	excellent
HF01	TPRBE_	1	0.931	2.871	3.249	0.0844	79.87	excellent
HF01	TPRBE_	2	0.938	2.905	3.233	0.0794	75.54	excellent
VSM03	TPRBE_126	1						
VSM03	TPRBE_126	2						

All heat flow stations reveal non-linear variations of the temperatures in the upper ~4 m in the sediment, which might originate from advective processes like fluid flow and/or degassing, change of sedimentation rates with time, or transient processes like bottom water temperature variations. Thus, only lowermost sensors which show linear characteristics in the Bullard plots (**Figure 10**, **Appendix 8**) were used for heat flow evaluation. **Table 2** provides an overview of the heat flow measurements performed. All data and heat flow inversion results are provided in the **Appendix 8**.

The results of heat flow processing are shown in maps for mean thermal conductivities (**Figure 11**), temperature gradients (**Figure 12**), and the geothermal heat flow (**Figure 13**), each in small and large scale maps. Included are the values from the Global Heat Flow Database (2011).

5.1 HF-Test (TPRBE_006):

From the stable first five minutes of Pen 2, a temperature gradient of 0.0737 K/m was determined. Inversion for thermal conductivities was not possible due to following instability of the probe and thus failure of the heat pulse. With an assumed homogeneous thermal conductivity value of 1.0 W/(m K) a heat flow value of 73.7 mW/m^2 was determined.

5.2 HF08 (TPRBE_030):

The small penetration depths here were sufficient to determine the undisturbed, steady state geothermal heat flow with good reproducible values of 7.31 mW/m^2 (temperature gradient: 0.0723 K/m) and 73.2 mW/m^2 (0.0716 K/m) for both penetrations, respectively. Thermal conductivities were very homogeneous with depth representing values around 1.0 W/(m K), which are quite normal for deep sea sediments. The relationship between temperatures and integrated thermal resistivity (Bullard plots) are linear with minor deviations in the upper 0.7 m indicating very weak disturbance from transient sources (bottom water temperature variations) and/or advective processes.

5.3 HF07 (TPRBE_046):

From both (nearly full) penetrations the undisturbed, steady state geothermal heat flow with good reproducible values of 77.1 mW/m^2 (temperature gradient: 0.0680 K/m) and

75.5 mW/m^2 (0.0671 K/m) were determined. The thermal conductivities are not homogeneous with respect to depth (Pen 1) and also vary between both penetrations, thus laterally. Mean values (1.2 W/(m K) for Pen 1 and 1.1 W/(m K) for Pen 2 are slightly larger than normal for deep sea sediments. The relationship between temperatures and integrated thermal resistivity (Bullard plots) are linear with minor deviations in the upper first meter indicating very weak disturbance from transient sources (bottom water temperature variations) and/or advective processes.

5.4 HF04 (TPRBE_047):

From both penetrations the undisturbed, steady state geothermal heat flow with good reproducible values of 71.9 mW/m^2 (temperature gradient: 0.0640 K/m) and 73.1 mW/m^2 (0.0584 K/m) were determined. These values are slightly above the global mean of marine, tectonically passive regions. Thermal conductivities are not homogeneous with respect to depth (Pen 1) and also vary between both penetrations, thus laterally. Mean values (1.08 W/(m K) for Pen 1 and 1.23 W/(m K) for Pen 2 are slightly larger than normal for deep sea sediments. The relationship between temperatures and integrated thermal resistivity (Bullard plots) are linear with minor deviations in the upper 2 m indicating very weak disturbance from transient sources (bottom water temperature variations) and/or advective processes.

5.5 HF03 (TPRBE_048, TPRBE_049):

The HF deployment HF03 was severely disturbed from extremely strong bottom water currents; the probe was not stable in the ground and suffered from steady tilt of the probe resulting in thermal disturbances of the temperature sensors from steady frictional heat. It was not possible to determine reliable thermal conductivity values. Nevertheless, temperature gradients could be determined with some scattering but sufficiently stable, reproducible results from all three penetrations: Pen 1: 0.0627 K/m; Pen 2: 0.0691 K/m and Pen 3: 0.0672 K/m). Thermal conductivities could not be inverted from none of these three penetrations. With an assumed thermal conductivity of 1.1 W/(m K) based on previous conductivity determinations in the region, heat flow values of 68.9 mW/m^2 , 76.0 mW/m^2, and 73.9 mW/m^2 were determined.

5.6 HF06 (TPRBE_056):

Again, due to extremely strong bottom water currents, the probe was not stable in the ground and suffered from steady tilt of the probe resulting in thermal disturbances of the temperature sensors from steady frictional heat. Nevertheless, a temperature gradient 0.0665 K/m, mean thermal conductivity of 1.16 W/(K m) and heat flow 66.2 mW/m^2 could be determined with sufficient reliability.

5.7 HF05 (TPRBE_088):

From the successful Pen 1, a steady state geothermal heat flow value of 70.7 mW/m^2 temperature gradient 0.0718 K/m) was determined. This value is slightly above the global mean of marine, tectonically passive regions. The mean value of thermal conductivity of 1.0 W/(m K) for Pen 1 is slightly larger than normal for deep sea sediments The relationship between temperatures and integrated thermal resistivity (Bullard plots) are linear with minor deviations in the upper 2 m indicating very weak disturbance from transient sources (bottom water temperature variations) and/or advective processes.

5.8 HF02 (TPRBE_109):

The penetration depth was sufficient to determine the undisturbed, steady state geothermal heat flow of 72.3 mW/m^2 (geothermal gradient 0.066 K/m) for the first and 80.6 mW/m^2 (geothermal gradient 0.070 K/m) for the second penetration. These heat flow values are slightly above the global mean of marine, tectonically passive regions. Thermal conductivities are nearly homogeneous with respect to depth with a mean value at 1.10 W/(m K) for the first penetration and 1.13 W/(m K) for the second. These values are slightly larger than normal for deep sea sediments. The relationship between temperatures and integrated thermal resistivity (Bullard plots) are linear with minor deviations in the upper 2 m indicating very weak disturbance from transient sources (bottom water temperature variations) and/or advective processes. Noticeable is the relatively large deviation between both measured heat flow (geothermal gradient) values. This might be a consequence of minor advective processes active all over the penetration depth.

5.9 HF01 (TPRBE_125):

5.10 VSM03 (TPRBE_126):

5.11 Sediment thermal properties

The observed mean thermal conductivities are quite homogeneous in depth and also little variations laterally. The mean values vary between 1.0 W/(m K) and 1.23 W/(m K). These values are upper range as typical for normal deep sea sediments. Thermal conductivities of marine sediments are in the range 0.6 - 1.2 W/(m K) (e.g. Stein, 1995). Since being near the shelf of the south Australian continental margin they may be influenced by high conductivity terrigenous sediments. As can be seen from **Figure 11**, thermal conductivities on and in the vicinity of the continental margin are in general smaller than deep sea values.

A valuable control of measured thermal parameters is the volumetric thermal capacity ρc (density ρ), which can be derived from inverted thermal conductivity λ and thermal diffusivity κ simply by $\rho c = \lambda / \kappa$. For all heat flow measurements, ρc values are nearly constant between 2.87 MJ/(m^3 K) and 3.15 MJ/(m^3 K), which is quite normal for deep sea sediments.

5.12 Heat flow results

At each station the Bullard method could be applied successfully i.e. all measurements provided steady-state crustal heat flow values. The accuracy and thus, comparability of the results strongly depends on the depth of penetration and stability in the ground during penetration. This mainly affects station HF03 with less accurate gradient estimation and as a consequence assumed thermal conductivity used.

The temperature gradients are shown in **Figure12**. The values represent the geothermal gradient since they are determined according to the Bullard method representing the thermal steady state. Temperature gradient values are in the range 0.058 K/m- 0.072 K/m. Also displayed are thermal gradient values as reported from the Global Heat Flow Database (2011). In general, in marine sediment the temperature gradients are larger than those in continental and shelf areas.

The determined heat flow values are in the range of 65 mW/m^2 (HF06) and 81 mW/m^2 (HF02). Heat flow values from the Global Heat Flow Database (2011) in this area show a large variety of values with lower values (~50 mW/m^2) to the north on the continental shelf (**Figure 13**, top) and very high values along the southern Australian continental margin (**Figure 13**, bottom). These include two sites with extremely high values of 341 mW/m^2 and 566 mW/m^2 just in the vicinity to the west of the investigation area.

We tried to get more information about these sites. The database includes as the source of these data a cruise of the Lamont Doherty Earth Observatory (LDEO, cruise V33 in 2004). Geli et al. (2008) used other data from that cruise and published quite reasonable temperature-depth and heat flow values. Nevertheless, no more additional information for those two, extremely high heat flow sites could be found. Goutorbe et al. (2008) discuss and re-evaluates heat flow data in and around Australia but did not take into account the mentioned LDEO data.

The global average oceanic heat flow is 100 mW/m^2 (e.g. Stein, 1995), depending of the age of the oceanic plate and tectonic processes active. It also might be affected by hydrothermal circulation processes, sedimentation rates and changes of sedimentation rates and by transient processes like bottom water temperature variations. In addition, strong topographic features lead to apparent heat flow values which could be accounted for by a topographic correction of the heat flow values. Some of these issues will be discussed in the following subsections in as more or less speculative investigations and suggestions.

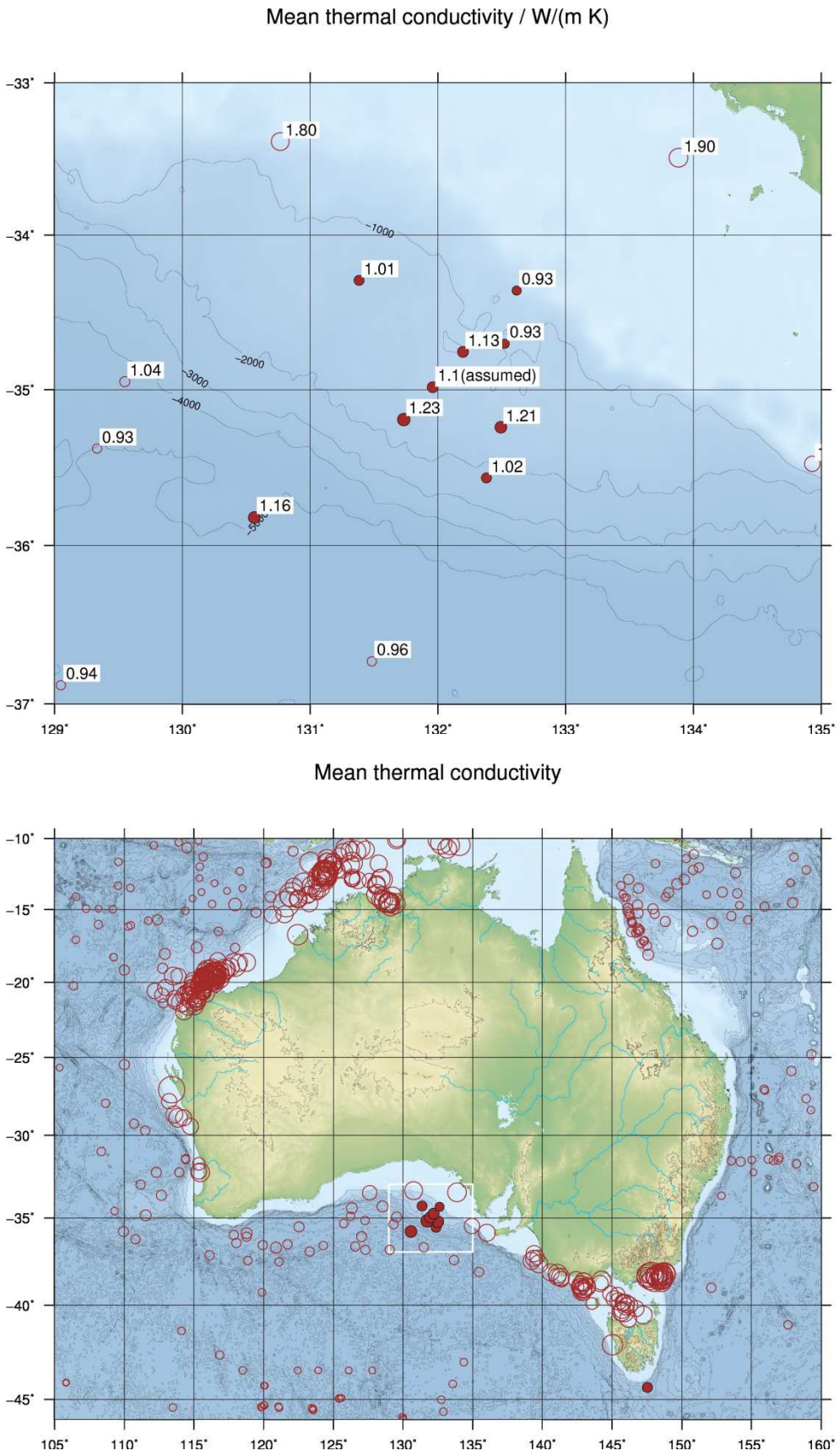

Figure 11: Mean thermal conductivity values λ (solid symbols) along with heat flow values of the Global Heat Flow Database (2011, open symbols). The sizes of the symbols scale with thermal conductivity values. The bathymetry used is from the GEBCO data set (2014). In general, thermal conductivities in marine sediment reveal conductivities < 1 W/(m K) and higher values for the continent and regions with sedimentation of continental material as in the shelf areas.

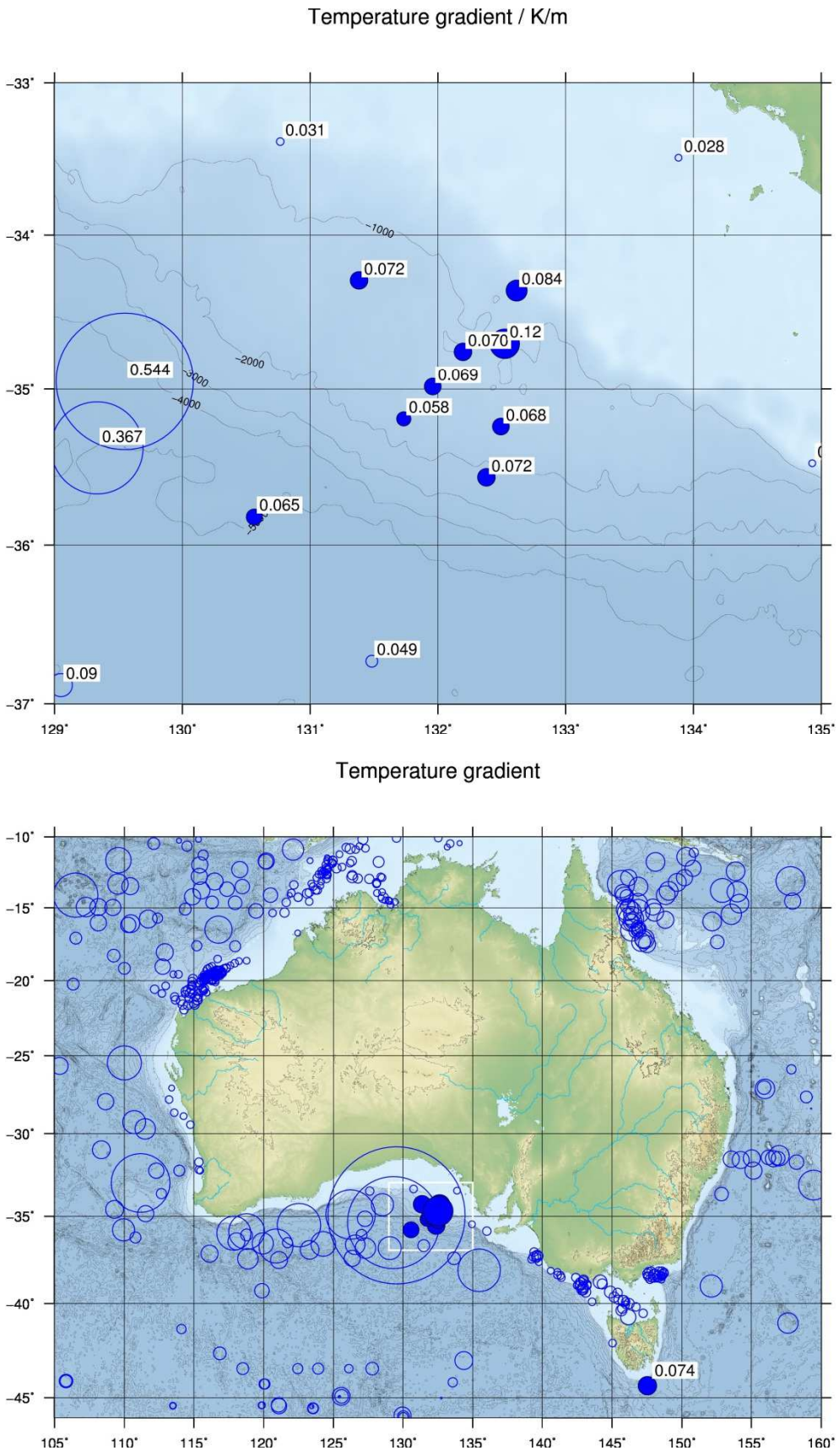

Figure 12: Temperature gradients dT/dz (solid symbols) along with values of the Global Heat Flow Database (2011, open symbols). The sizes of the symbols scale with values for temperature gradients. The bathymetry used is from the GEBCO data set (2014). In general, in marine sediment the temperature gradients are larger than those in continent and shelf areas.

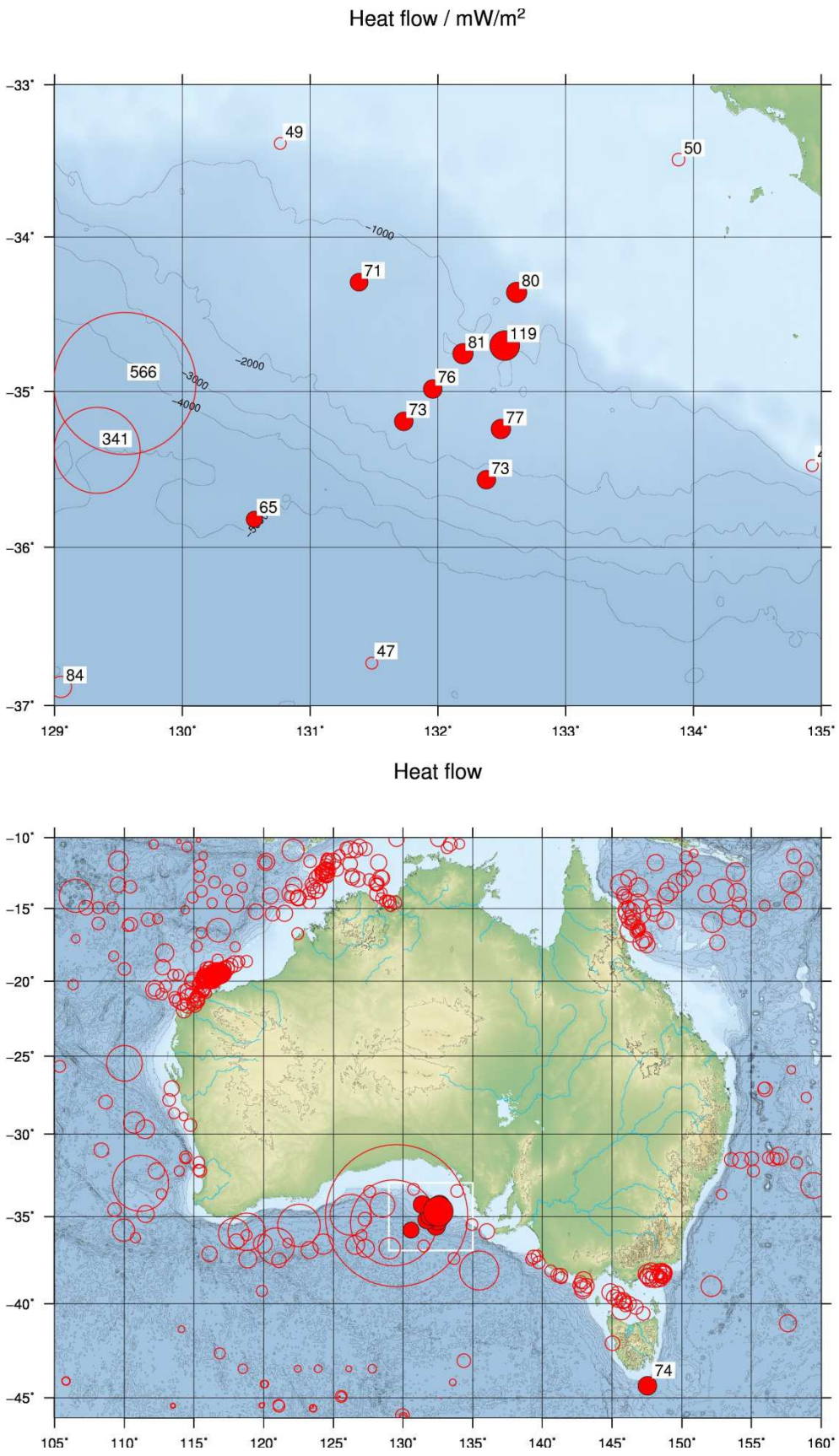

Figure 13: Measured heat flow values q (solid symbols) along with heat flow values of the Global Heat Flow Database (2011, open symbols). The sizes of the symbols scale with heat flow values. The bathymetry used is from the GEBCO data set (2014).

5.12.1 Lithospheric age

Sea floor heat flow is highest at mid ocean ridges, and decreases with the age of the lithosphere. This variation is one of the key features in the models of plate tectonics, where the oceanic lithosphere cools as it spreads away from mid ocean ridges and reheats upon returning to the mantle at subduction zones. Stein & Stein (1992) set up a model describing this relation of heat flow and crustal thickness depending on lithospheric age.

According to Müller et al. (1997), lithospheric ages of the Great Australian Bight area (GAB, including the area of investigation, **Figure 14**) are of greater age than 90 Ma and originated after disintegration of Australia and Antarctica during Gondwana break-up ~160 Ma ago. Initial rifting was slow after disintegration but accelerated 50 Ma ago.

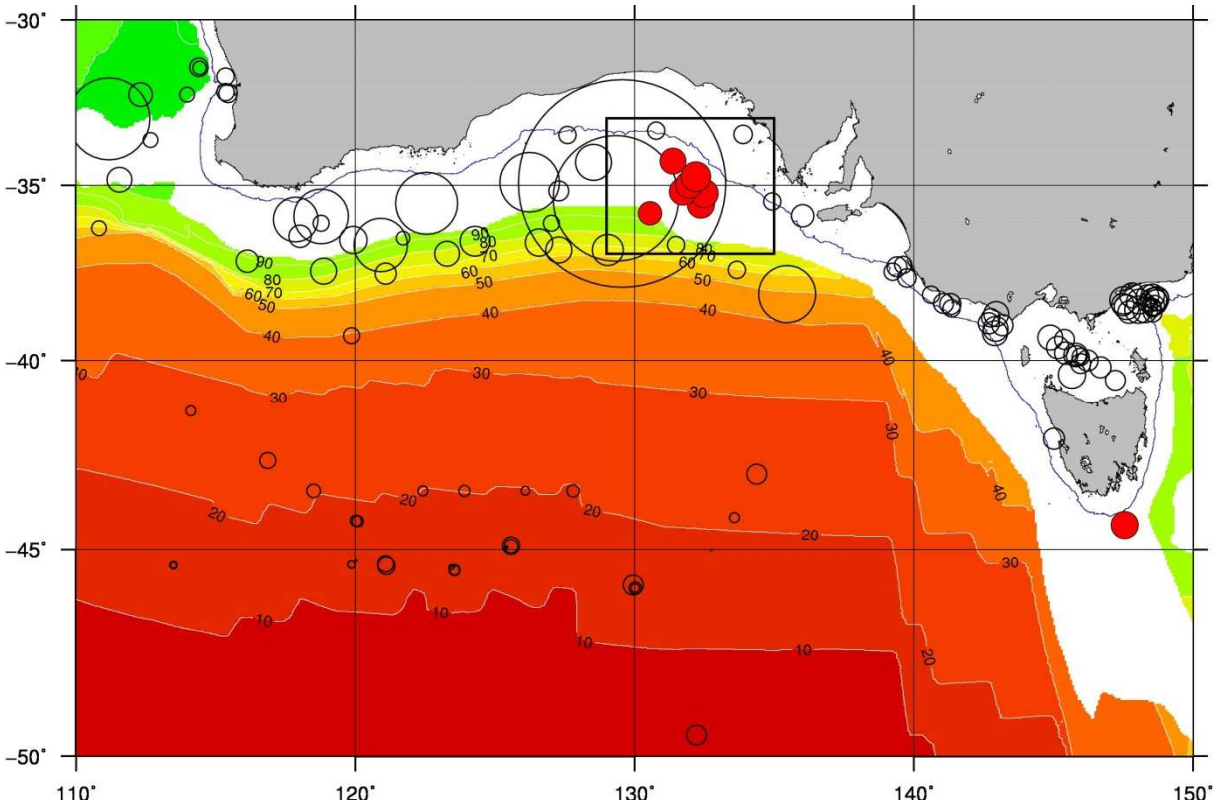

Figure 14: Heat flow and lithospheric age. Map showing lithospheric age after Müller et al. (1997) including heat flow values in the area of investigation and from the Global Heat Flow Database (2011). Heat flow values are high in coastal regions and compared to these, low in regions of smaller age.

Comparison of heat flow values and lithospheric age in **Figure 14** show no obvious simple relation of low heat flow at high ages and vice versa. In general, heat flow values along the continental margin measured in this project and those from the Heat Flow Database show significant higher values than those of younger crust. **Figure 15** displays the relationship

between heat flow and lithospheric age from the global model of variation in oceanic depth and heat flow with lithospheric age (GDH1) of Stein & Stein (1992). The recent measured heat flow values from the GAB would suggest lithospheric ages 40-53 Ma, far too young, values of the Global Heat Flow Database even significant younger. A heat flow prediction from this model with crustal ages of more than 90 Ma would suggest heat flow values of ca. 50 mW/m^2.

As a conclusion, a standard, simple relationship between heat flow and crustal age cannot explain the observed high heat flow values in the GAB and southwestern Australian continental margin at all.

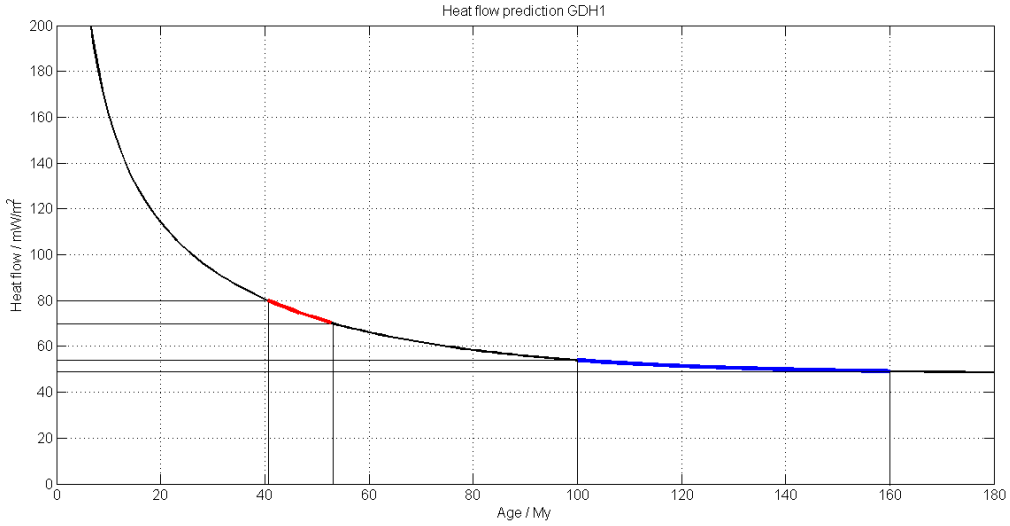

Figure 15: Heat flow prediction as a function of lithospheric age according to the model GDH1 of Stein & Stein (1992). The heat flow q (mW/m^2) is related to the age t (Ma) by $q(t) = 510\ t^{-1/2}$, $t \leq 55$ Ma and $q(t) = 48 + 96 \exp(-0.0278\ t)$, $t > 55$ Ma. According to this model, measured heat flow values in the range of 70 – 80 mw/m^2 represent ages of 40 - 53 Ma. The crustal age model of Müller et al. (1997, t > 90 Ma) would predict heat flow values of ~50 mW/m^2.

5.12.2 Topographic disturbance and correction

Since the region of interest is at the continentals' margin, a large step of 4000 m covers the water depths between the southwestern-most (HF06) and the northeastern-most (HF01) heat flow sites. The presence of a step in topographic relief leads to deflections of isothermal curves near the surface. Thus, a topographic correction to the measured heat flow values was calculated using the simple model of Lachenbruch (1968). This simple model describes heat flow modified by a topographic relief change from two levels of ocean depth with a certain slope of sea floor in between (**Figure 16**, bottom). The crust is assumed to be homogeneous and isotropic, and the surface is represented by a plane segment inclined at an angle to horizontal surfaces beyond the toe and behind the brink which are at an elevation difference. In this case, horizontal distance of the slope from toe to brink is about 250 km and the corresponding vertical distance of 4 km represent a shallow slope angle of 0.05°.

This topographic effect would mainly influence heat flow values measured near the toe (HF06, measured heat flow > 5% to large) and the brink (HF01, measured heat flow value > 5% to low) of the slope (**Figure 16**, top). These effects are small and thus, deviations from topographic relief most likely may be discarded.

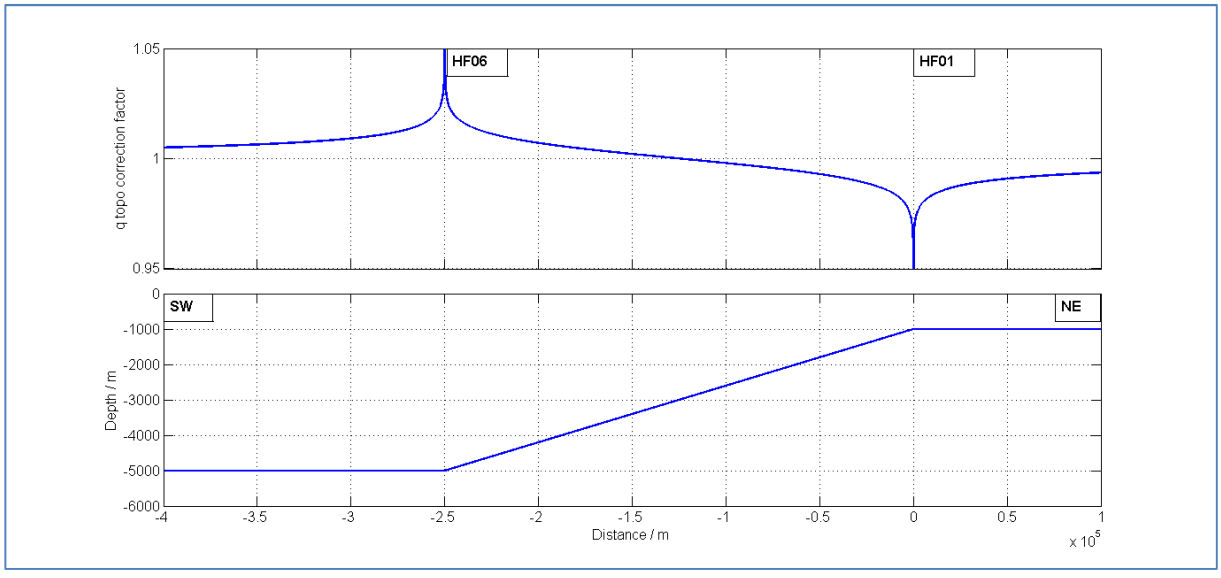

Figure 16: Simple topographic profile between deep sea in the southwest and continental shelf at the northeast and simple terrain correction estimates according to Lachenbruch (1968). At the toe of the slope station HF06 might be affected with an apparent heat flow value with a maximum of 5% higher and station HF01 at the brink with apparent values 5% lower than expected.

5.12.3 Sedimentation/erosion

Higher heat flow values as expected from crustal age may be explained by sediment erosion processes, thus removing parts of the sediment cover. A simple model according Von Herzen & Uyeda (1963) describing thermal gradient changes due to surface elevation changes by sedimentation/erosion will give clues on heat flow alterations.

There is evidence of erosional removal of 200 m during last glacial ice ages. Here, we consider the influence of 200 m sediment removal in the last 200000 years and its influence on basal heat flow. Sedimentation has a blanketing effect and decreases surface heat flow values with respect to the basal heat flow. On the other hand, removal or erosion of sediments has an increasing effect for heat flow values. From a theoretical view, removal or addition of sediment, can mathematically described by movement with respect to the medium (Carslaw & Jaeger, 1959), thus adding an apparent advective term to the heat transfer equation. The corresponding solution of the heat transfer is

$$q/q_0 = 1 - \mathrm{erf}(X) - \frac{2X}{\sqrt{\pi}}\exp(-X^2) + 2Xerfc(X), \qquad \text{with} \quad X = \frac{1}{2}U\sqrt{\frac{t}{\kappa}} \ ,$$

given the relation q/q0 between measured surface and basal heat flow. Here, erf() and erfc() denote the error function and its complement, U = -0.0001 m/y = -3.2 10^{-11} m/s is the erosion rate, κ = 4.0 10^{-7} m^2/s the thermal diffusivity as a mean value determined from the measurements and t = 200000 y = 6.3 10^{12} s the time since start of erosion. A solution with these values is q/q_0 = 1.15. Thus, measured values are 15% larger than basal heat flow values. For a measured q = 70 mW/m^2 follows a basal heat flow of q_0 = 60.8 mW/m^2. Thus, this erosion effect might be an explanation for too high heat flow according to crustal age.

5.12.4 Advection (vertical fluid/gas movements)

As seen from the temperature-depth distributions, advection effects at the measurement sites play a minor role. At some stations little temperature perturbations from the geothermal gradient exist which might be explained by fluid/gas movements but they cannot explain the overall high heat flow values in the region of investigation.

5.12.5 Transient disturbances (bottom water temperature variations)

As seen from the temperature-depth distributions, transient effects at the measurement sites play a minor role. At some stations little temperature perturbations from the geothermal gradient exist in the upper meter of penetration which might be explained by bottom water temperature variations but do not disturb temperature evaluation in terms of steady state heat flow. Seasonal bottom temperature in these water depths are of minor importance to be regarded.

5.12.6 Radiogenic heat generation

In basaltic oceanic crust, radiogenic minerals are mainly depleted and thus, have a minor contribution to crustal heat flow. In continental crust and continental shelves, radiogenic heat production may have a substantial but strongly variable contribution to crustal heat flow. Moreover, the heat flow depends critically on radioactive heat production in the crust. This holds for shelf regions and offshore sediments including a sedimentation fraction of radiogenic continental material.

Thus, the simple assumption of the oceanic heat flow is essentially a simple function of age described by the cooling plate model may be violated by the presents of radioactive elements abandoned in the crust or transported by sediment transfer from the continent. A detailed discussion of heat flow in Australian continental margins and the influence of radiogenic heat production can be found in Goutorbe et al. (2008).

A continental material influence on sediments in the GAB is supported by the high values of thermal conductivities being in the transition between oceanic deep sea and continental values.

5.12.7 Post-rifting geothermal activity

A further possible source of overall heated lithosphere in the WAB and thus enhanced heat flow are post-rift geothermal active processes like volcanic intrusions which happened during mid-Eocene volcanic activity.

6 Literature

Bullard EC, 1939. Heat Flow in Africa, *Proc. R. Soc. Lond.*, **173**, 474-502.

Carslaw HS & Jaeger, JC, 1959. Conduction of heat in solids. Oxford University Press, pp. 510.

Global Heat Flow Database, 2011. The International Heat Flow Commission, hosted by the University of North Dakota, http://www.heatflow.und.edu/

GEBCO bathymetric data set, 2014. General Bathymetric Chart of the Oceans, hosted by the British Oceanographic Data Centre (BODC), http://www.gebco.net/.

Geli L, Lee TC, Cochran JR, Francheteau J, Abbott D, Labails C & Appriou D, 2008. Heat flow from the Southeast Indian Ridge flanks between 80°E and 140°E: Data review and analysis, *J. Geophys. Res.*, **113**(B01101), doi:10.1029/2007JB005001.

Goutorbe B, Lucazeau F & Bonneville A, 2008. Surface heat flow and the mantle contribution on the margins of Australia, *Geochem, Geophys. Geosyst*., **9**(Q05011), doi:10.1029/2007GC001924.

Hartmann A & Villinger H, 2002. Inversion of marine heat flow measurements by expansion of the temperature decay function, *Geophys. J. Int.,* **148**(3), 628-636.

Hyndman R, Davis E & Wright J, 1979. The measurement of marine geothermal heat flow by a multi penetration probe with digital acoustic telemetry and in situ thermal conductivity, *Mar. Geophys. Res.*, **4**, 181-205.

Lachenbruch AH, 1968. Rapid estimation of the topographic disturbance to superficial thermal gradients. *Rev Geophys*., **6**(3), 365-400.

Müller RD, Roest WR, Royer J-Y, Gahagan, LM & Sclater JG, 1997. Digital isochrones of the world's ocean floor. *J. Geophys. Res.*, **102**(B2), 3211-3214.

Lister CRB, 1979. The pulse-probe method of conductivity measurement, *Geophys. J. R. astr. Soc.,* **57**, 451-461.

Pribnow DFC, Davis EE & Fisher AT, 2000. Borehole heat flow along the eastern flank of the Juan de Fuca Ridge, including effects of anisotropy and temperature dependence of thermal conductivity, *J. Geophys. Res.*, **105**(B6): 13449-13456.

Stein CA, 1995. Heat flow of the Earth*, Global Earth Physics, A Handbook of Physical Constants, AGU reference Shelf* 1: 144-158.

Stein CA & Stein S, 1992. A model for the global variation in oceanic depth and heat flow with lithospheric age. *Nature*, **359**, 123-129.

Steinhart JS & Hart SR, 1968. Calibration curves for thermistors, *Deep Sea Res. Ocean. Abstr.*, **15**(4), 497-503.

Von Herzen RP & Uyeda S, 1963. Heat flow through the Eastern Pacific Ocean floor. *J. Geophys. Res.*, **68**(14), 4219-4250.

7 Appendix 1: Quality control plots

This is a compilation of all quality control plots:

7.1 Cruise IN2015_C01 Station HFTest (TPRBE_006)

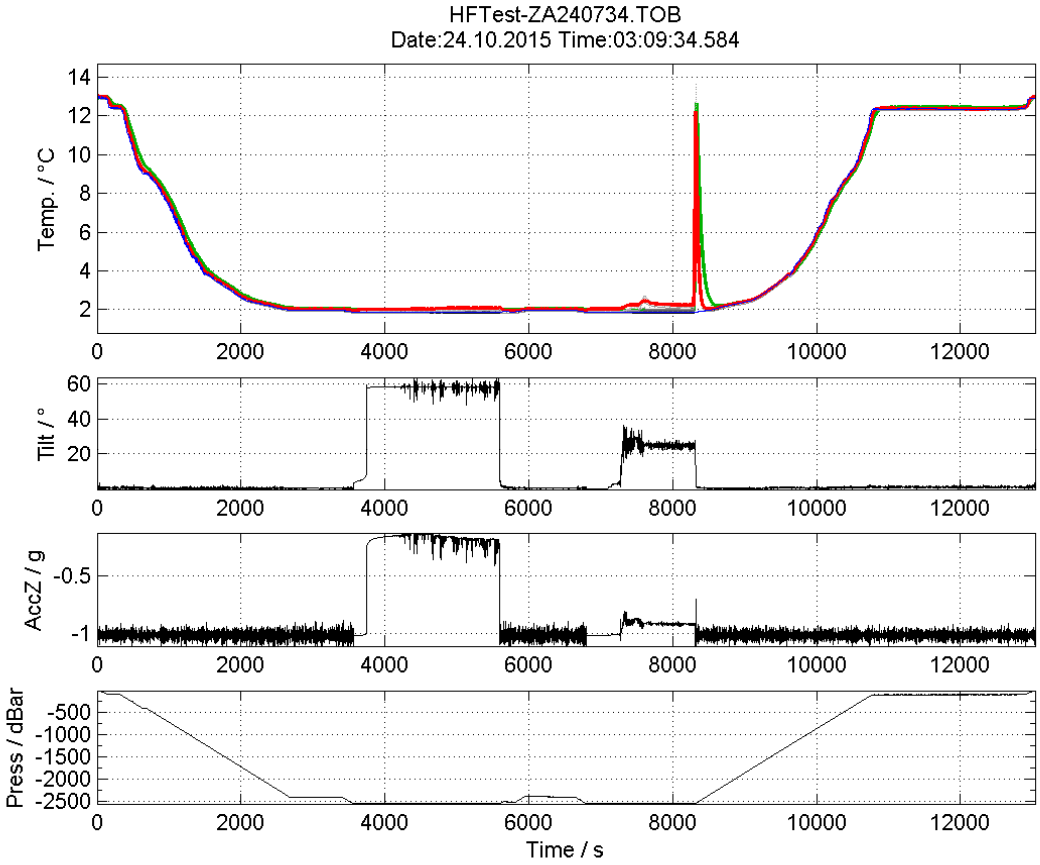

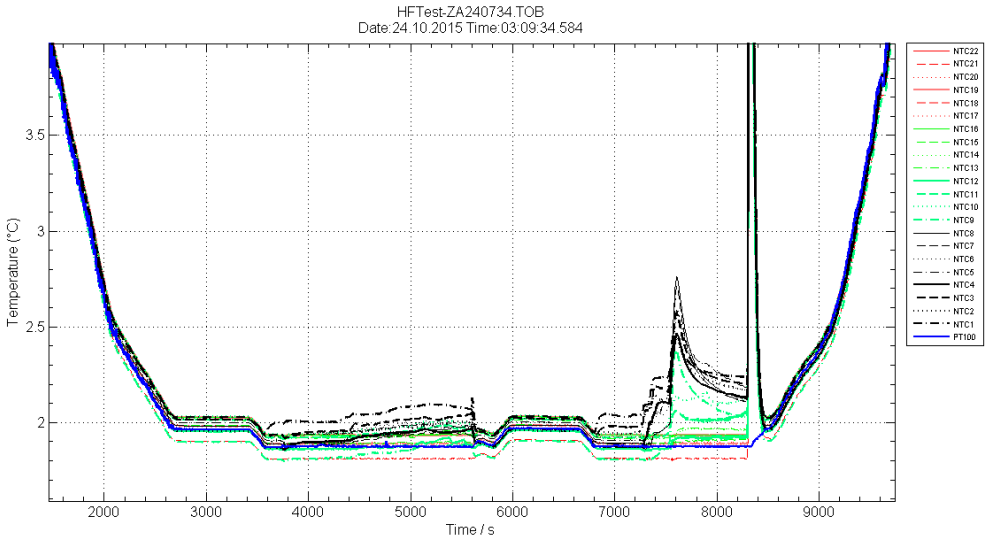

7.2 Cruise IN2015_C01 Station HF08 (TPRBE_030)

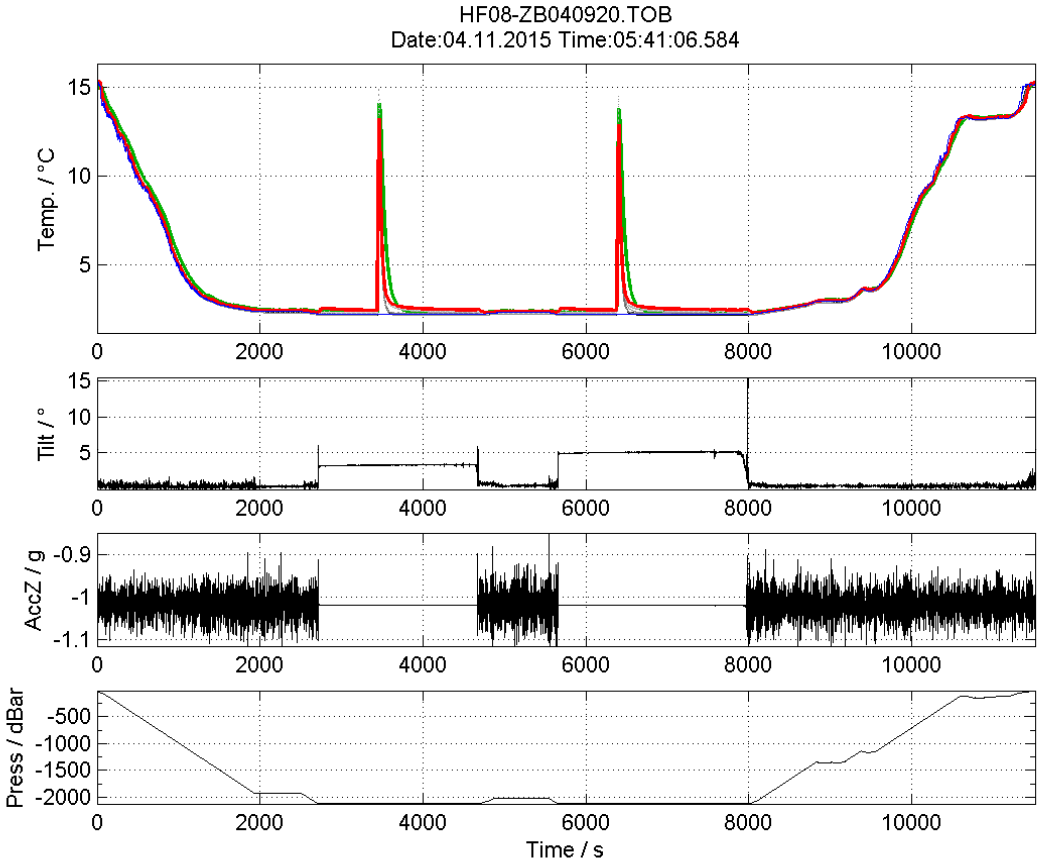

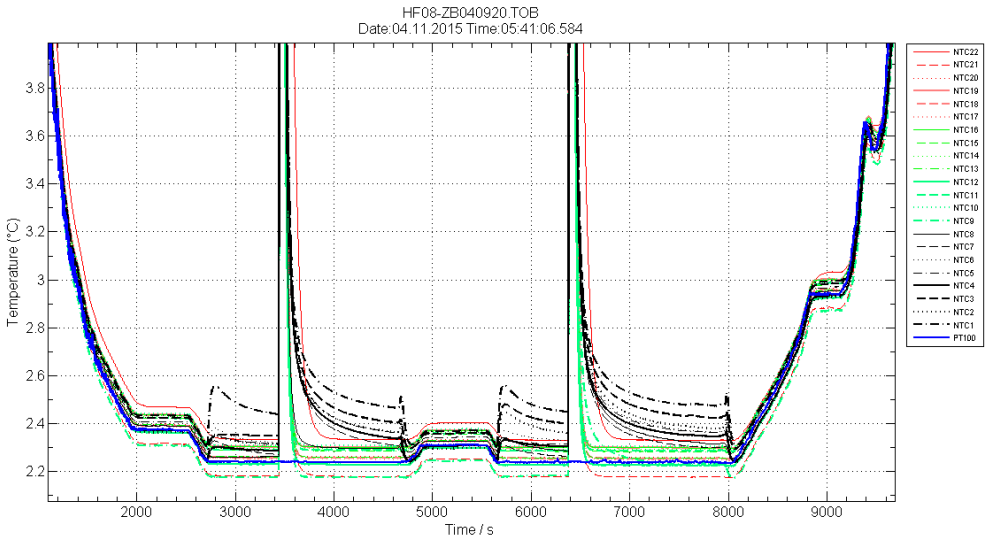

7.3 Cruise IN2015_C01 Station HF07 (TPRBE_046)

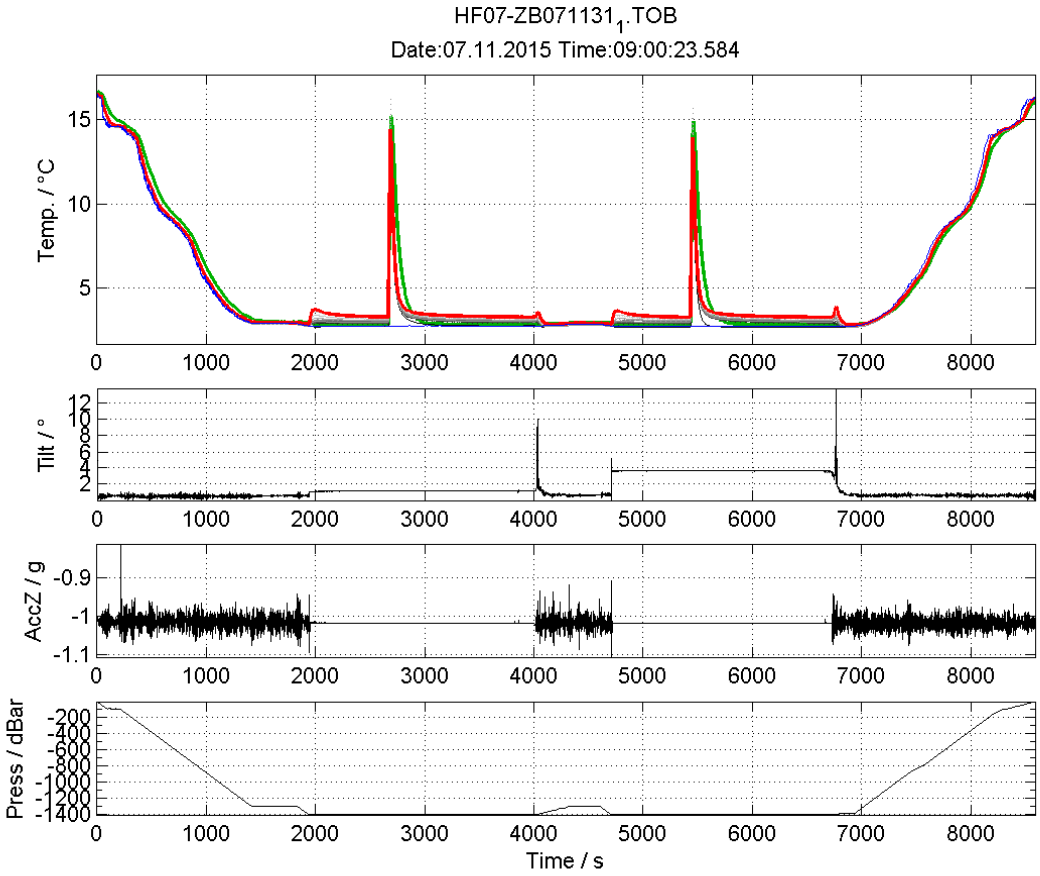

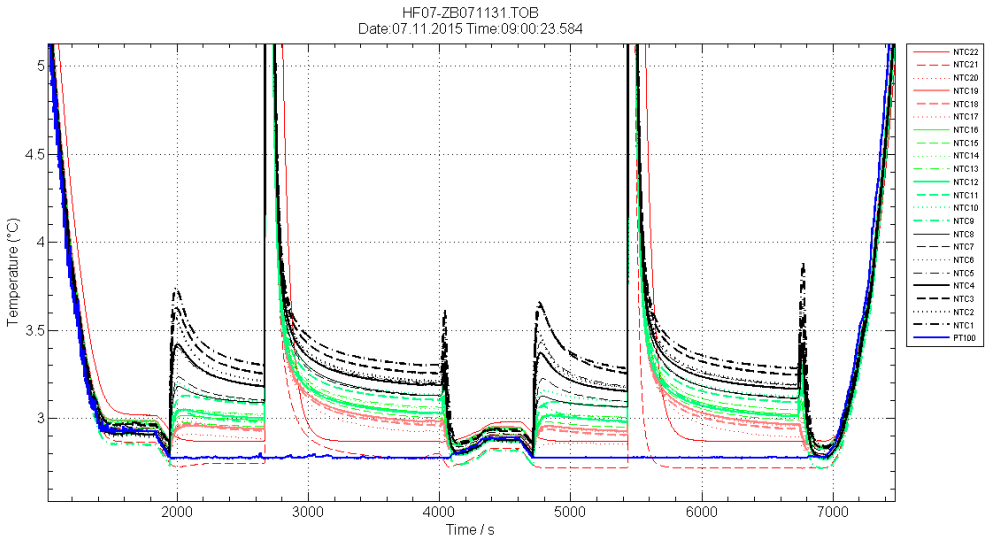

7.4 Cruise IN2015_C01 Station HF04 (TPRBE_047)

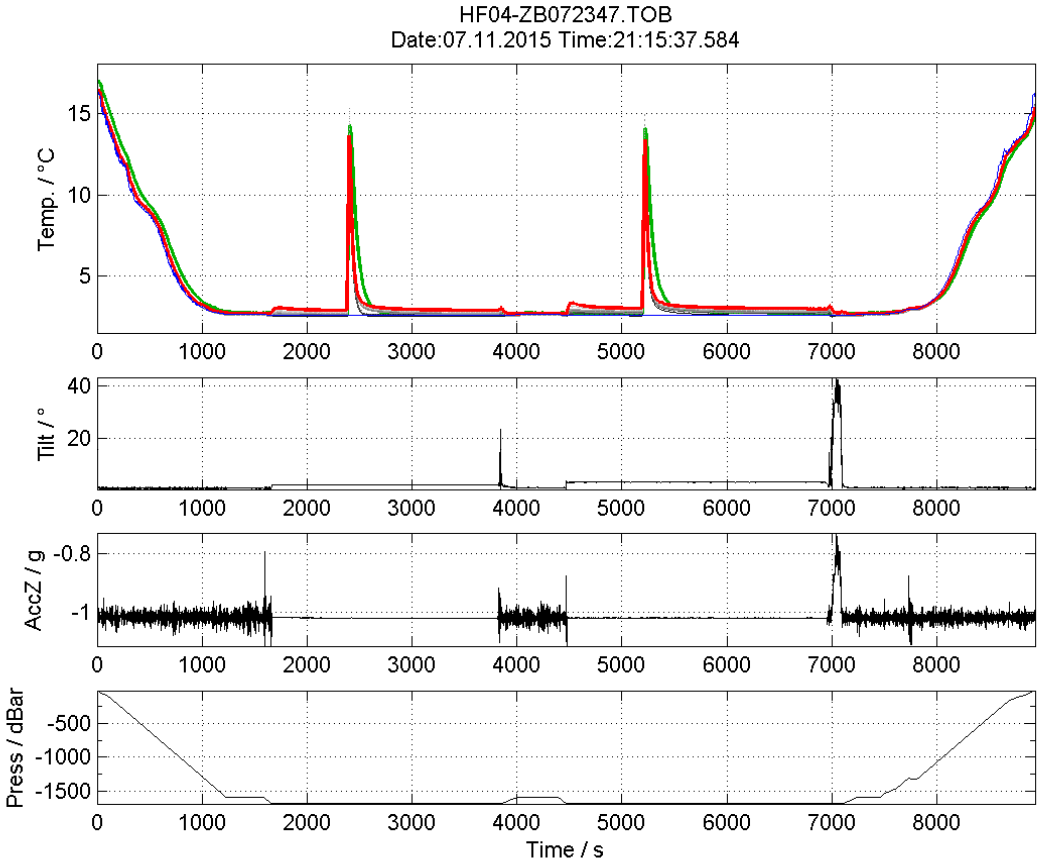

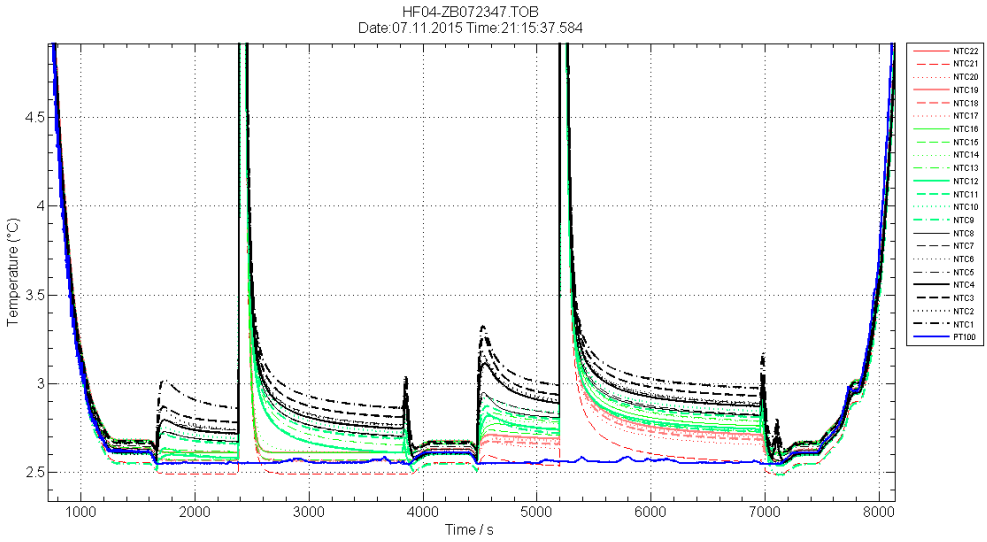

7.5 Cruise IN2015_C01 Station HF03 (TPRBE_048)

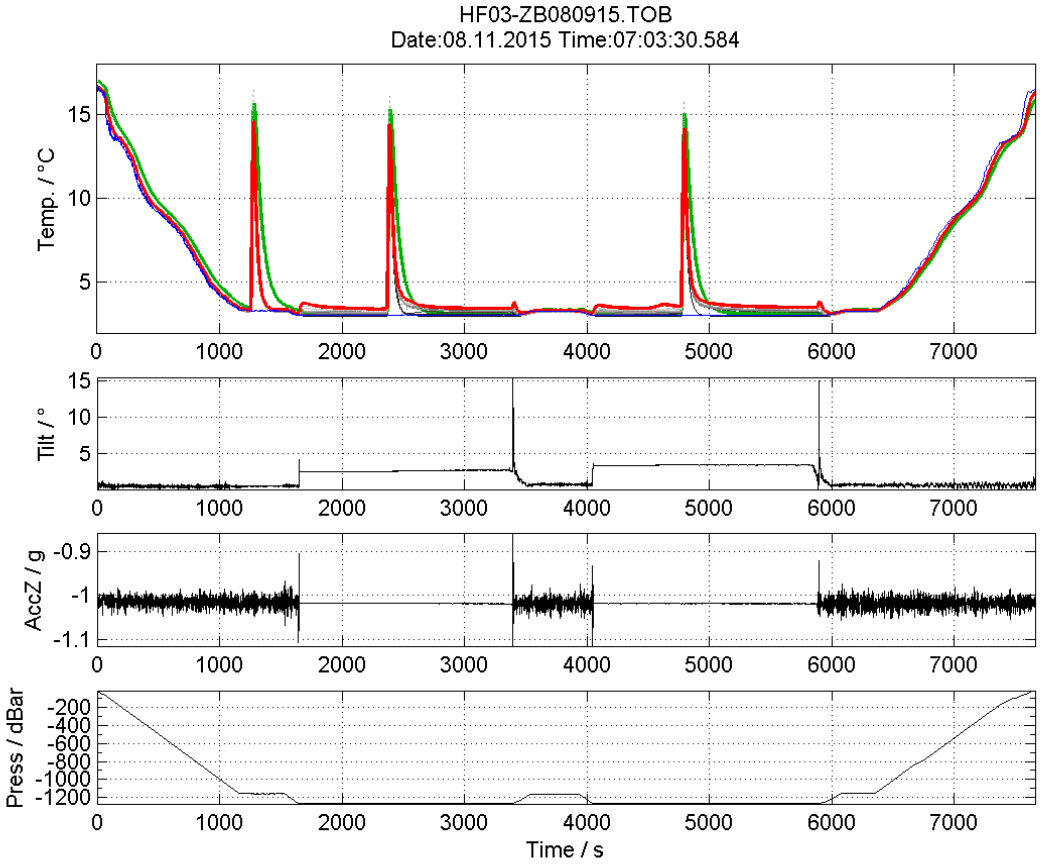

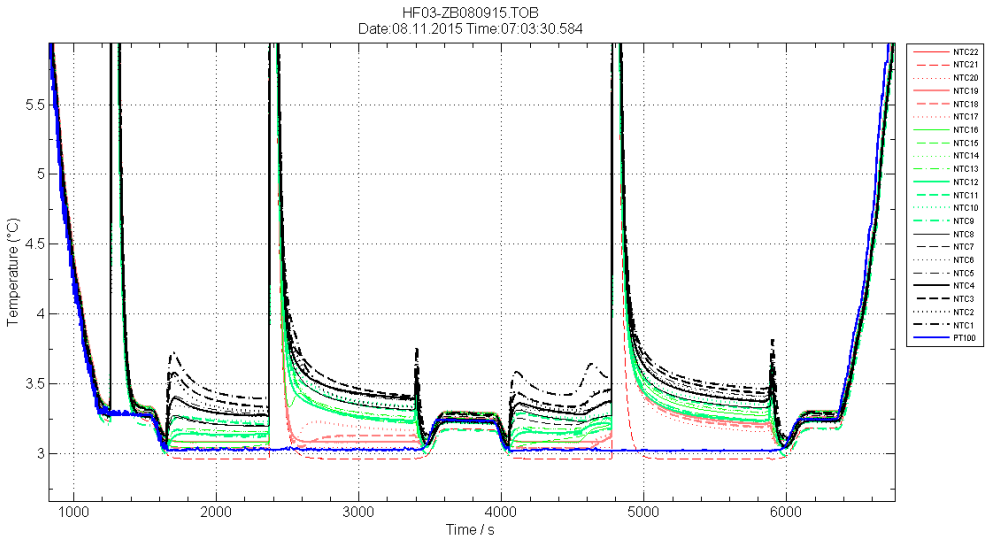

7.6 Cruise IN2015_C01 Station HF03 (TPRBE_049)

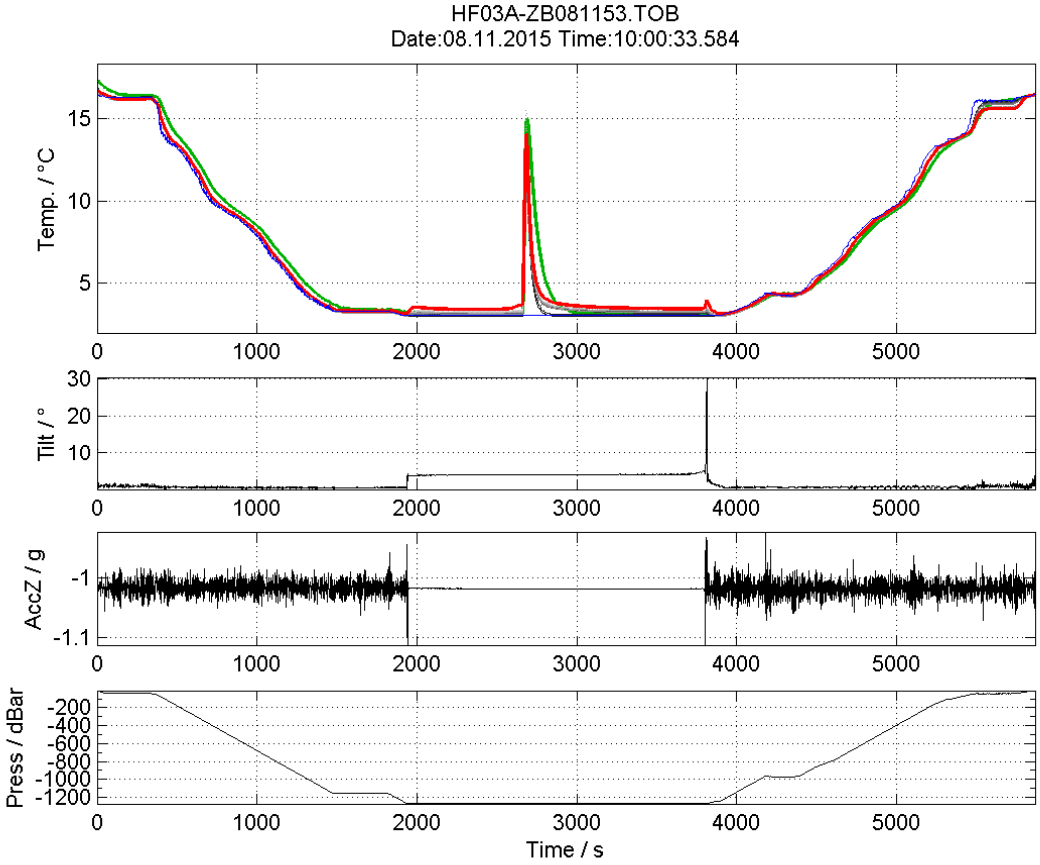

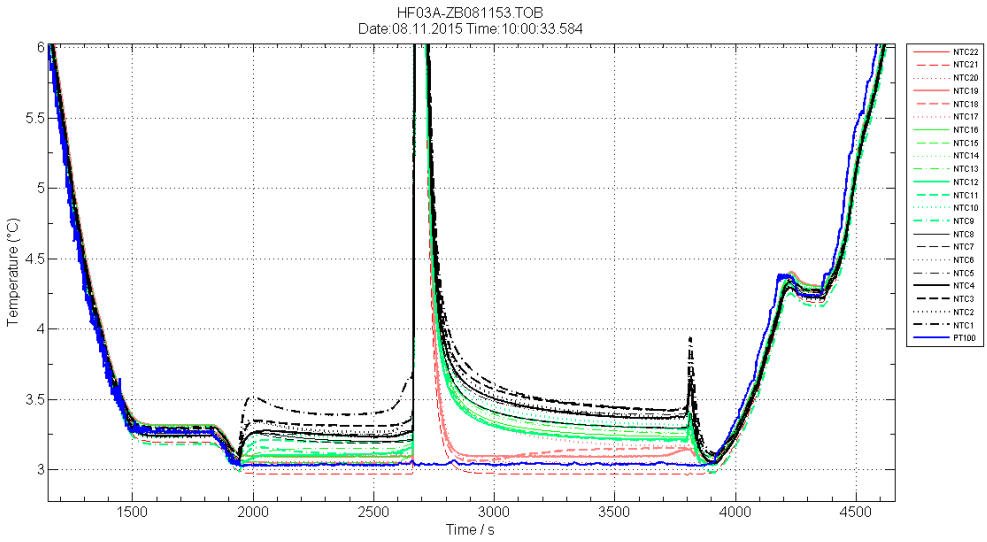

7.7 Cruise IN2015_C01 Station HF06 (TPRBE_056)

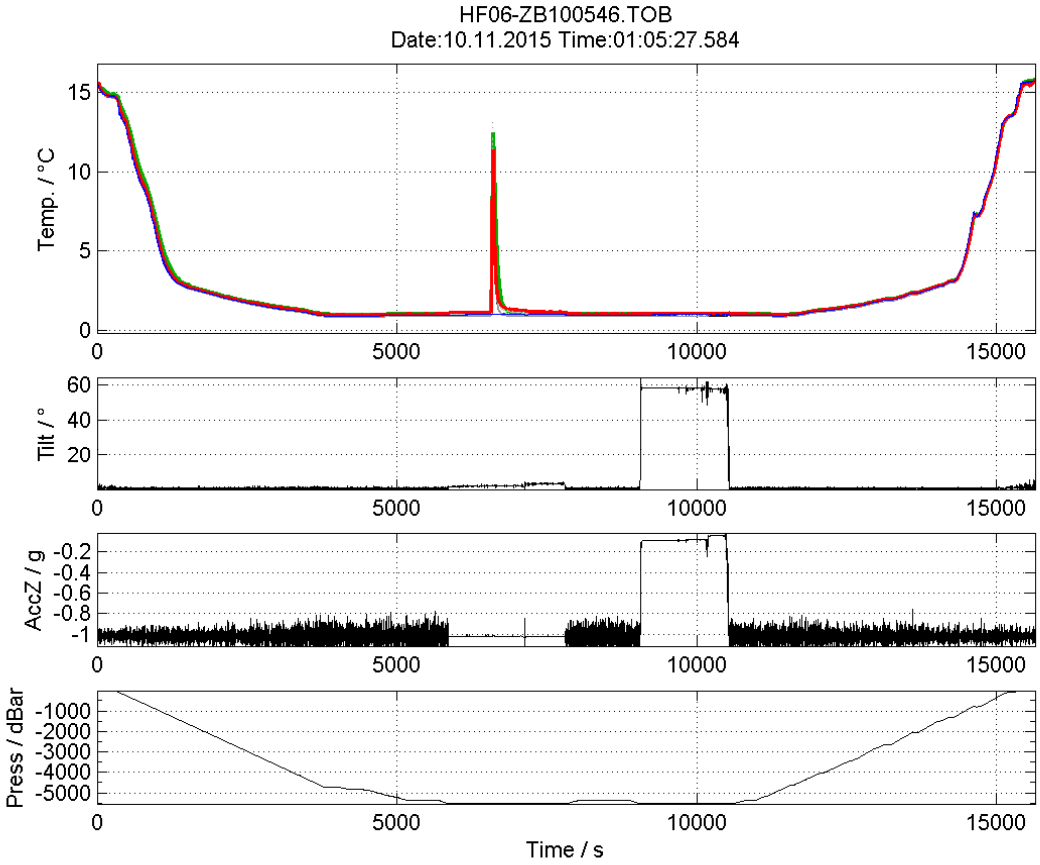

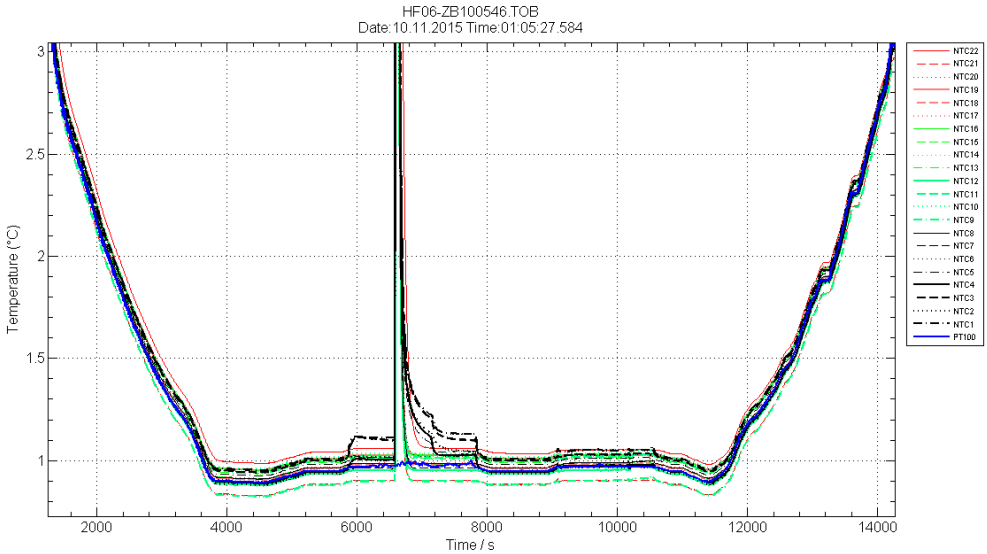

7.8 Cruise IN2015_C01 Station HF05 (TPRBE_088)

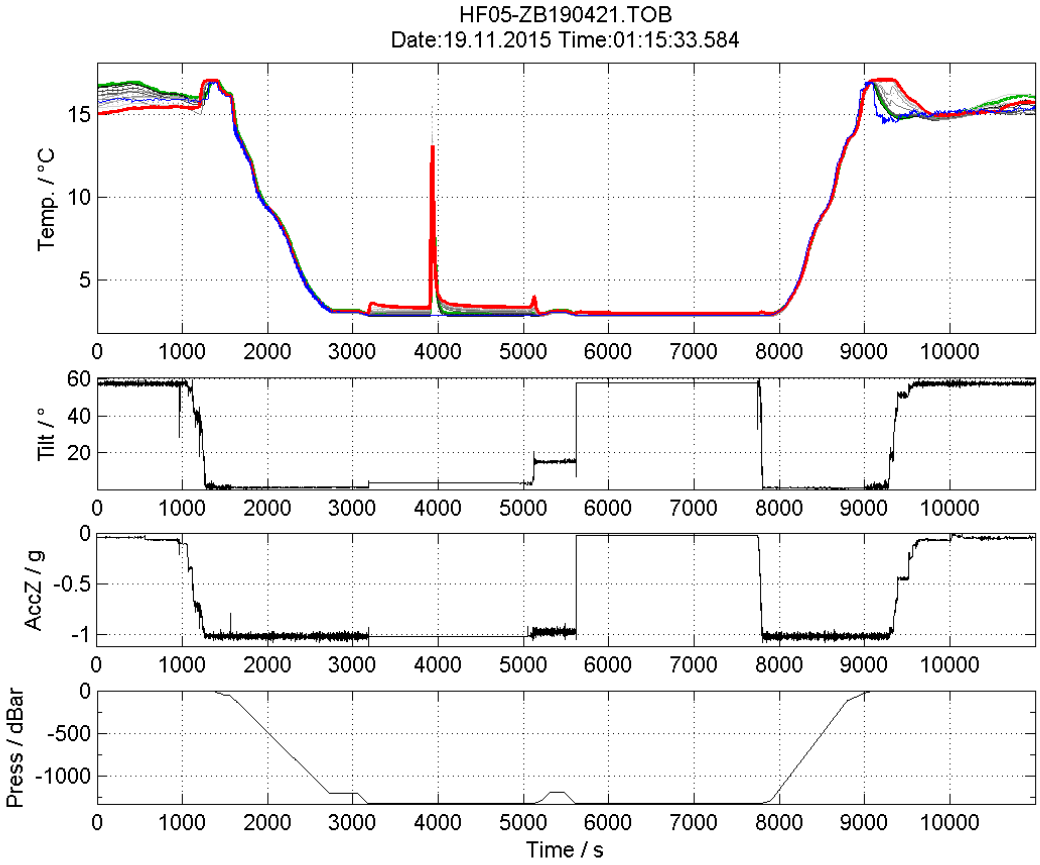

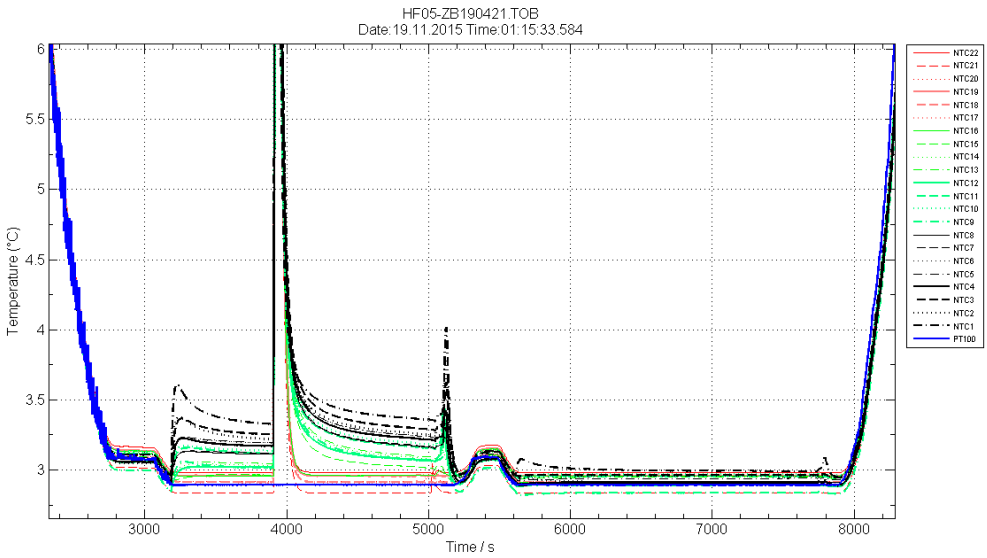

7.9 Cruise IN2015_C01 Station HF02 (TPRBE_109)

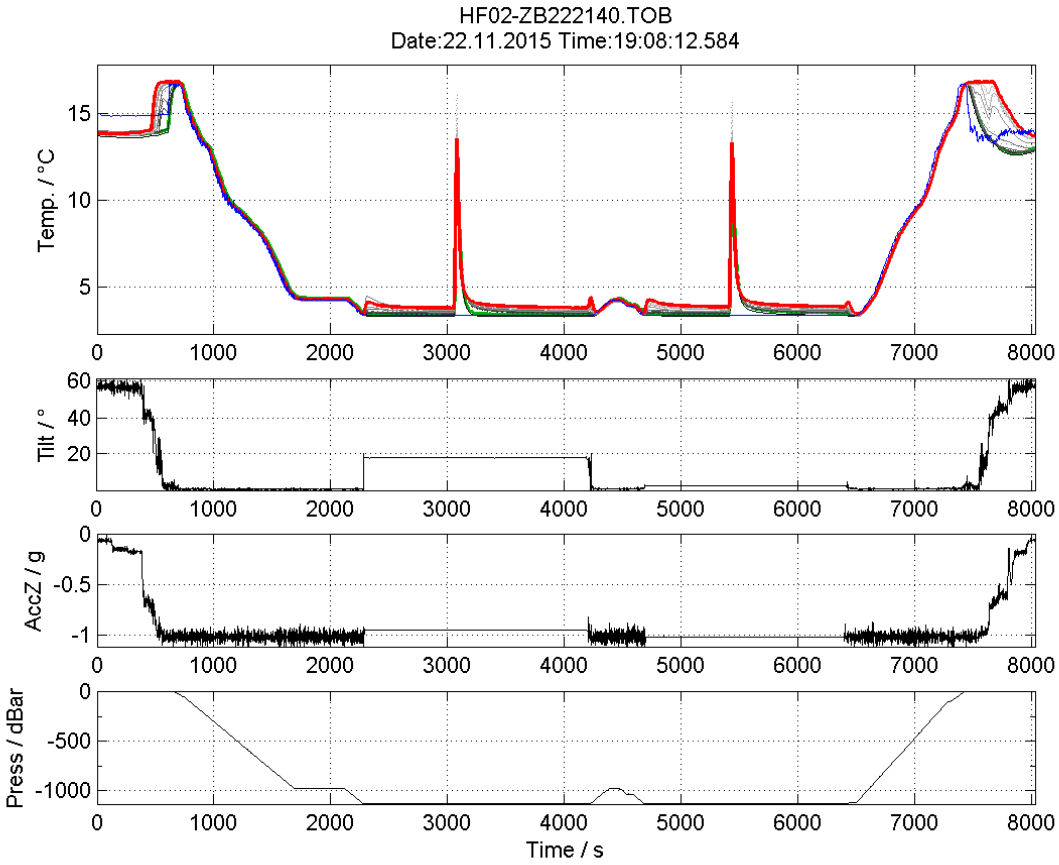

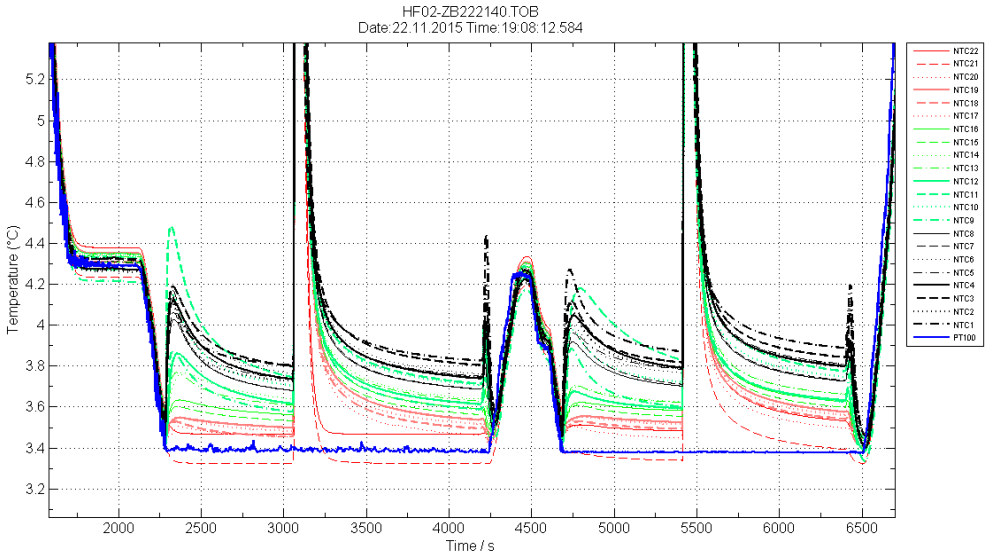

7.10 Cruise IN2015_C01 Station HF01 (TPRBE_125)

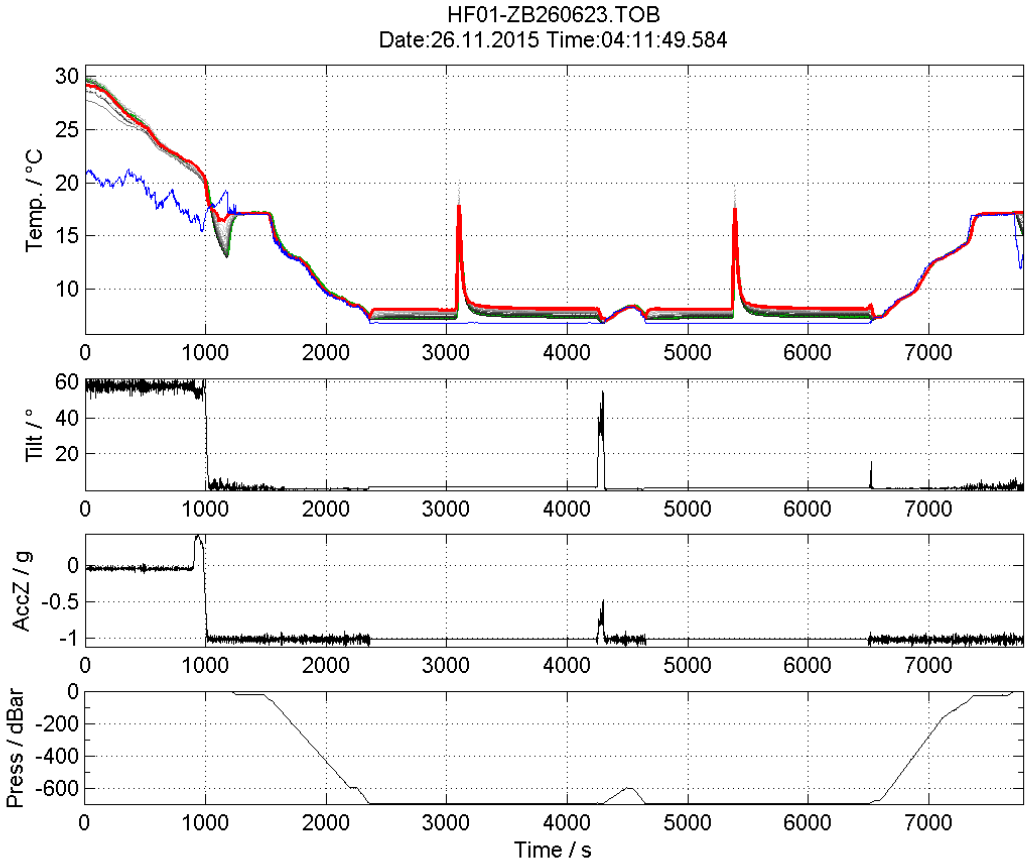

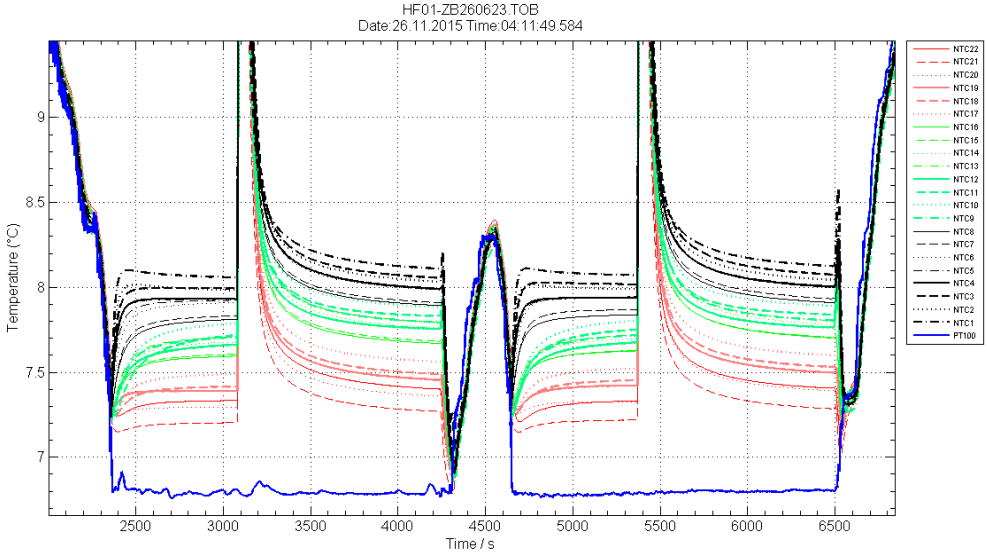

7.11 Cruise IN2015_C01 Station VMS03 (TPRBE_126)

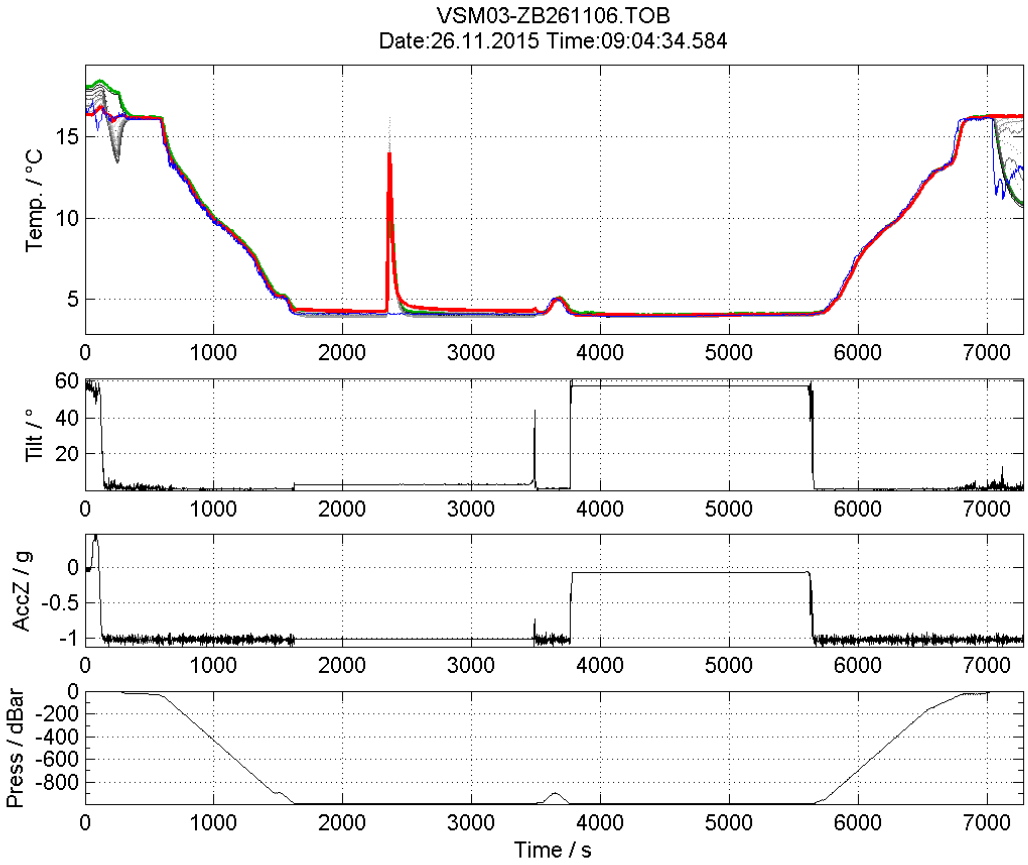

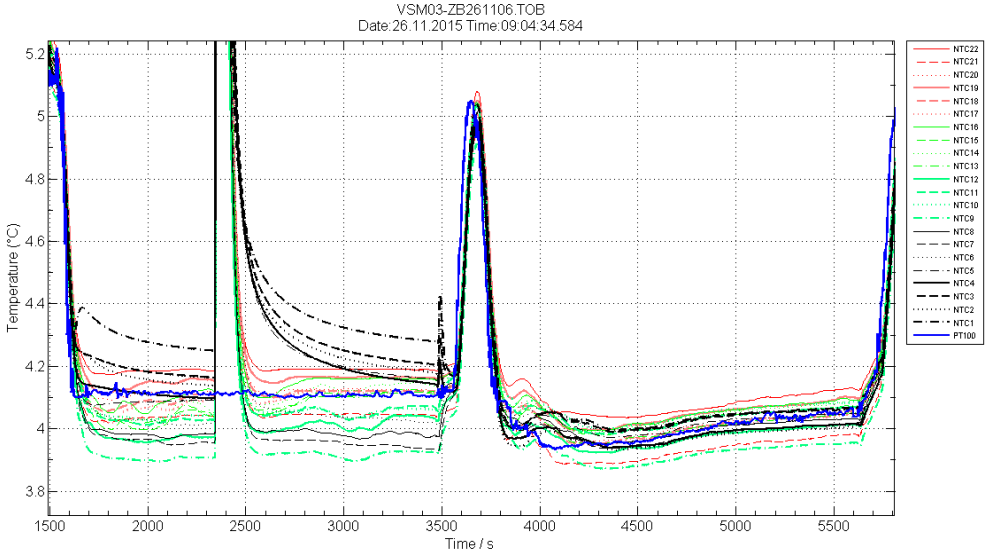

7.12 Cruise IN2015_C01 Station VMS03 (TPRBE_127)

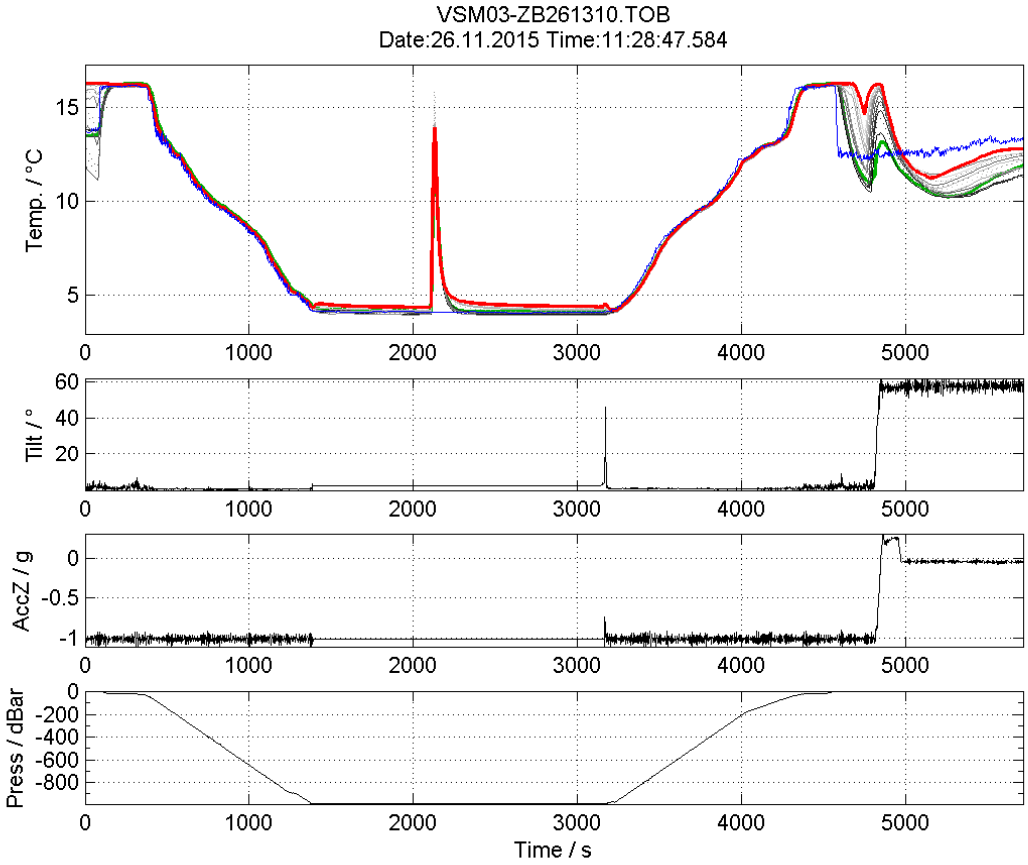

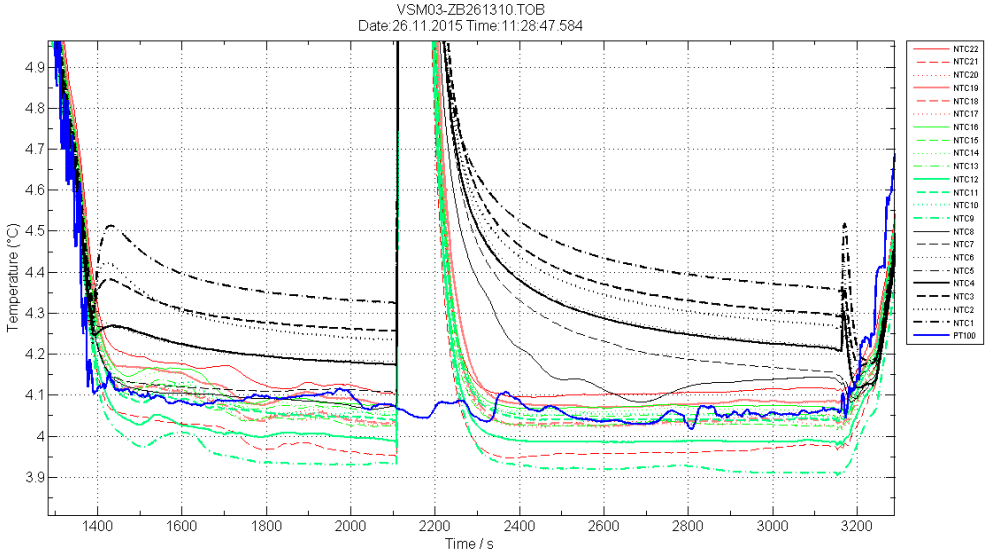

8 Appendix 2 Heat flow inversion results

All penetration sites are presented in appending figures and data:

- For each station, the figure to the left page on top shows temperature evolution of the sensors used for inversion.

- The plot on the left page at the bottom represents the relative in-situ temperatures (after calibration), the thermal conductivities, thermal diffusivities, and heat capacities, all plotted vs. depth. The horizontal error bars show the uncertainties of the inverted temperatures. The dashed lines resemble the respective mean values and mean gradient for the temperatures (here, only the solid symbols have been used).

- The plot on the right page on top shows the so-called Bullard plot in which temperatures are shown vs. integrated thermal resistivity and which is the basis of the heat flow calculations. Only the sensors showing a stationary gradient (solid symbols) have been included in the heat flow calculations. The calculated heat flow values for each station are summarized in **Table 2**. On right panel, three plots represent the errors of in-situ temperature, in-situ thermal conductivity, and residual temperatures from the linear fit of thermal resistances vs. temperature in the Bullard plot.

- Below, right page, the summary shows all meta data and inversion results in mean and depth (sensor) dependent values.

8.1 Cruise IN2015_C01 Station HF-Test (TPRBE_006)

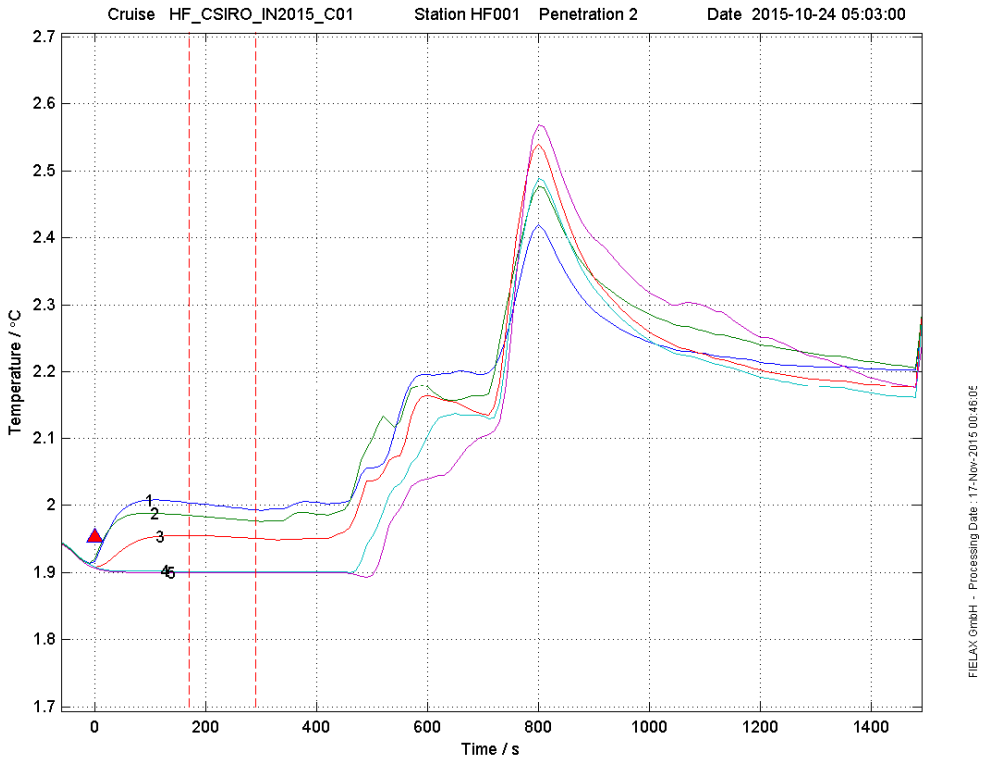

Sediment temperatures

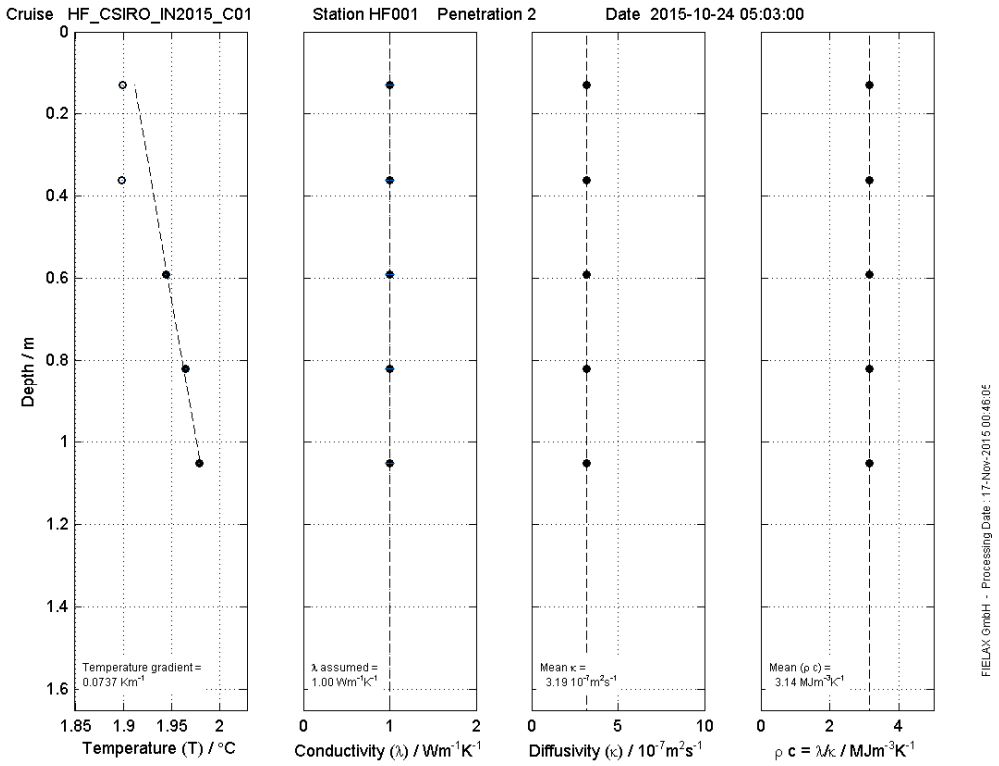

Sediment thermal properties

IN2015_C01 Station HF-Test (TPRBE_006)

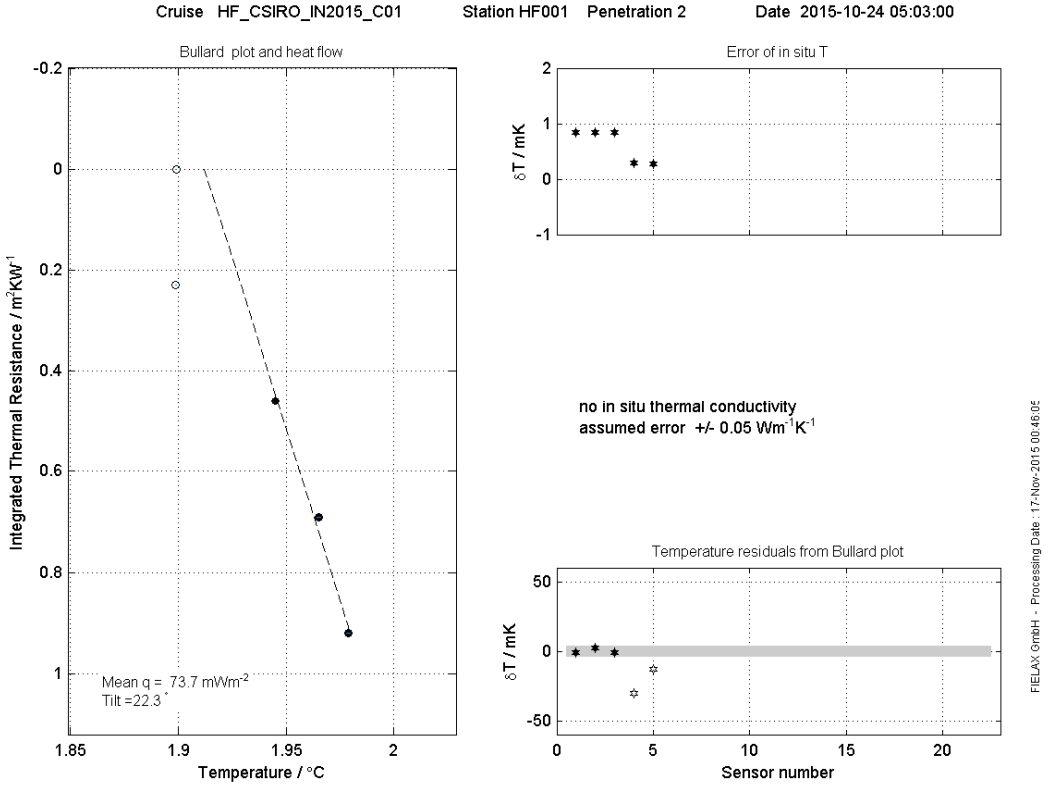

Bullard plot and error estimates

```
Cruise-Transect                          HF_CSIRO_IN2015_C01
Station                                  HF-Test (TPRBE_006)
Penetration No.                          2

Date/Time of Penetration                 2015-10-24 05:03:00
Latitude [°]                             44.3812 S
Longitude [°]                            147.5483 E
Depth [m]                                  0.00

Device ID                                CTM1000
String ID                                T113SD
Heating wire length [m]                  6.05

Pressure [dbar]                          2561.8
Tilt [°]                                 22.3
Bottom water temperature [°C]            1.874
Heating power [J/m]                      0.00

Mean th. conductivity (assumed) [W/(m K)] 1.000
Temperature gradient dT/dz [K/m]         0.0737
Heat flow Q [mW/m^2]                     73.72
```

Sens_used #	Sens_depth [m]	T_insitu [K]	Bull_depth [m^2 K/W]	lambda_assumed [W/m K]
5	0.130	1.899	0.000	1.000
4	0.360	1.899	0.230	1.000
3	0.590	1.945	0.460	1.000
2	0.820	1.965	0.690	1.000
1	1.050	1.979	0.920	1.000

8.2 Cruise IN2015_C01 Station HF08 (TPRBE_030)

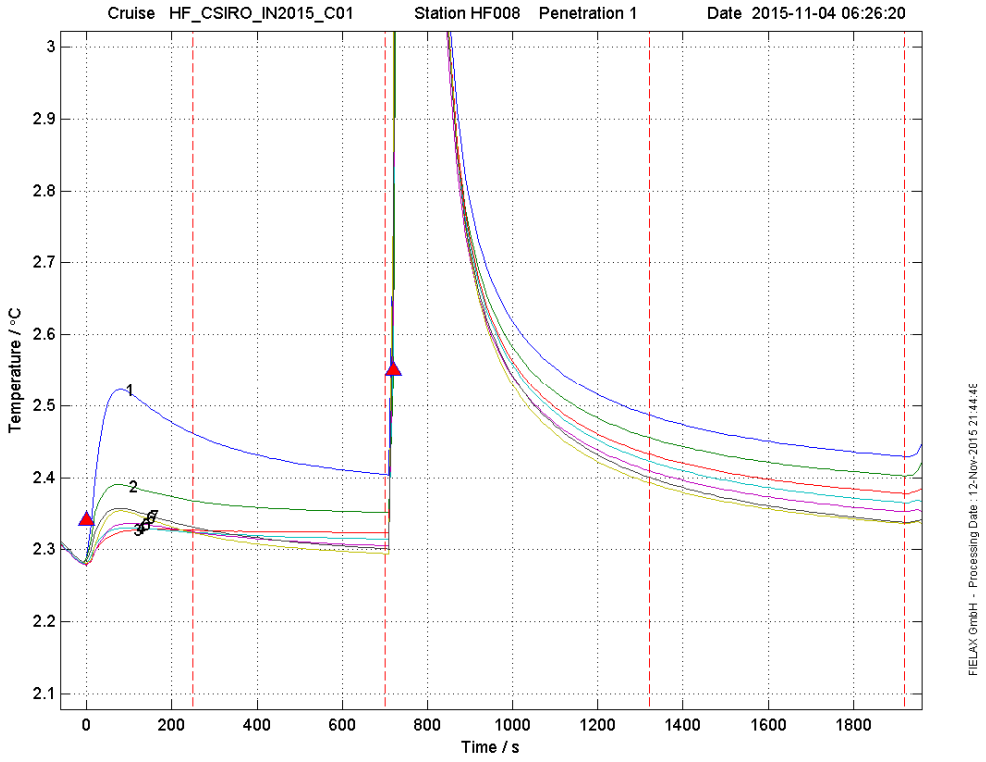

Sediment temperatures

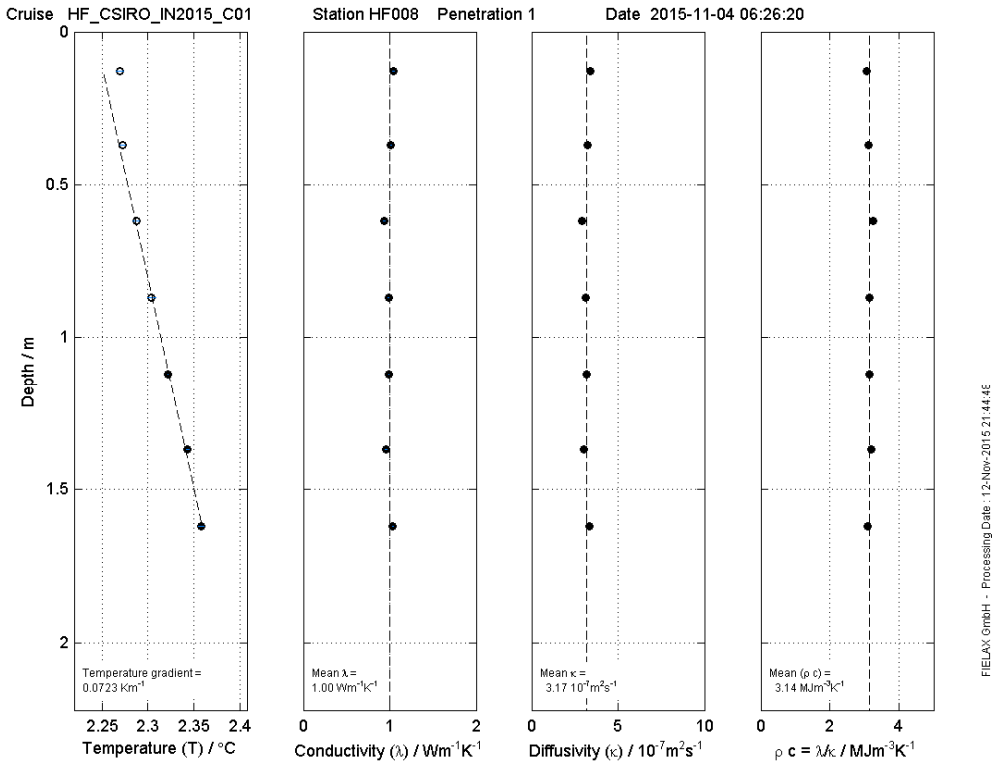

Sediment thermal properties

IN2015_C01 Station HF08 (TPRBE_030) Pen 1

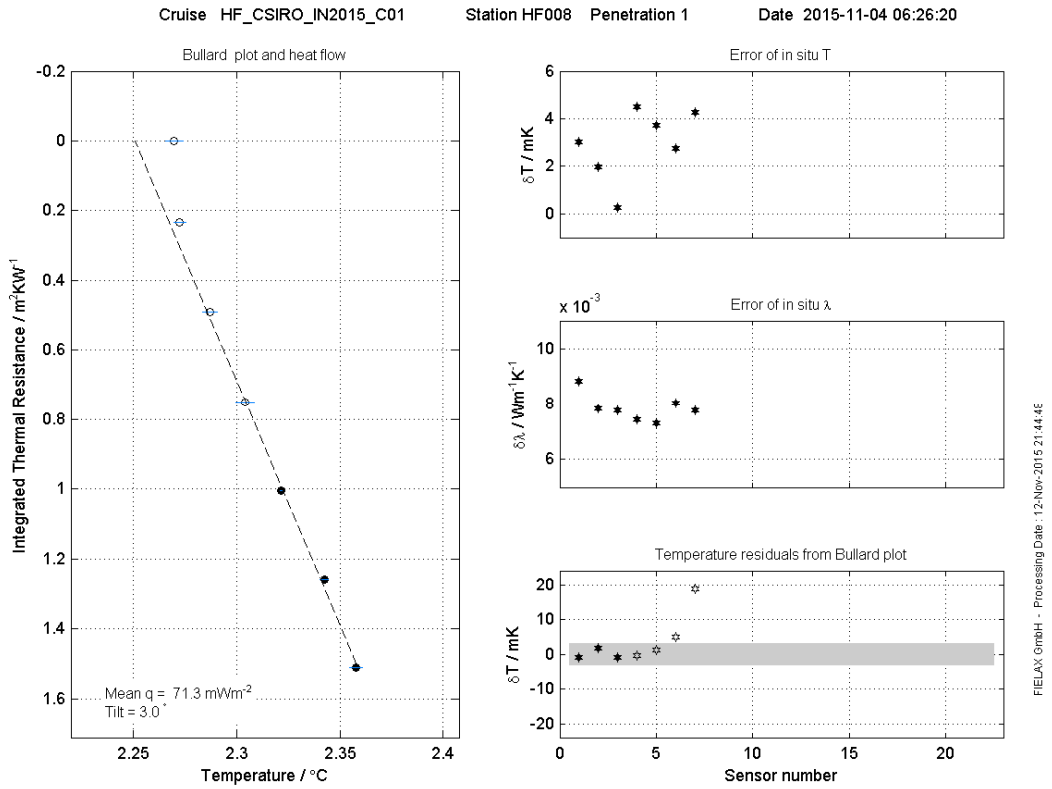

Bullard plot and error estimates

Cruise-Transect	HF_CSIRO_IN2015_C01
Station	HF008 (TPBRE_30)
Penetration No.	1
Date/Time of Penetration	2015-11-04 06:26:20
Latitude [°]	35.568197 S
Longitude [°]	132.380953 E
Depth [m]	2120.00
Device ID	CTM1000
String ID	T113SD
Heating wire length [m]	6.05
Pressure [dbar]	2126.5
Tilt [°]	3.0
Bottom water temperature [°C]	2.240
Heating power [J/m]	824.39
Mean thermal conductivity [W/(m K)]	0.995
Mean thermal resistivity [m K/W]	1.005
Mean thermal diffusivity [1e-07 m^2/s]	3.167
Mean volumetric capacity [MJ/m^3 K]	3.145
Temperature gradient dT/dz [K/m]	0.0723
Heat flow Q [mW/m^2]	71.33

Sens_used #	Sens_depth m	Temp. °C	Bullard depth m^2 K/W	Th. conduct. W/(m K)	Th. res. m K/W	Th. diffus. 1e-07 m^2/s	Vol. capac. MJ/(m^3 K)
7	0.130	2.270	0.000	1.043	0.959	3.395	3.072
6	0.370	2.272	0.234	1.009	0.991	3.232	3.122
5	0.620	2.287	0.491	0.937	1.068	2.894	3.237
4	0.870	2.304	0.751	0.988	1.012	3.132	3.155
3	1.120	2.322	1.004	0.993	1.007	3.156	3.147
2	1.370	2.342	1.260	0.959	1.043	2.995	3.201
1	1.620	2.358	1.511	1.037	0.964	3.367	3.081

IN2015_C01 Station HF08 (TPRBE_030) Pen 2

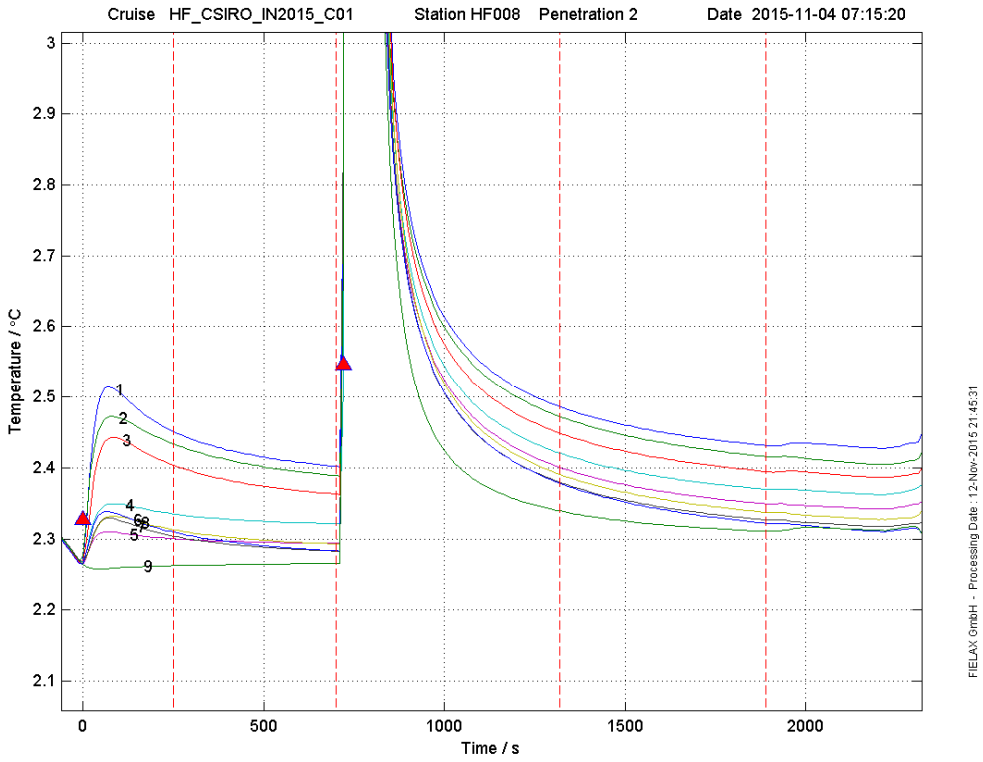

Sediment temperatures

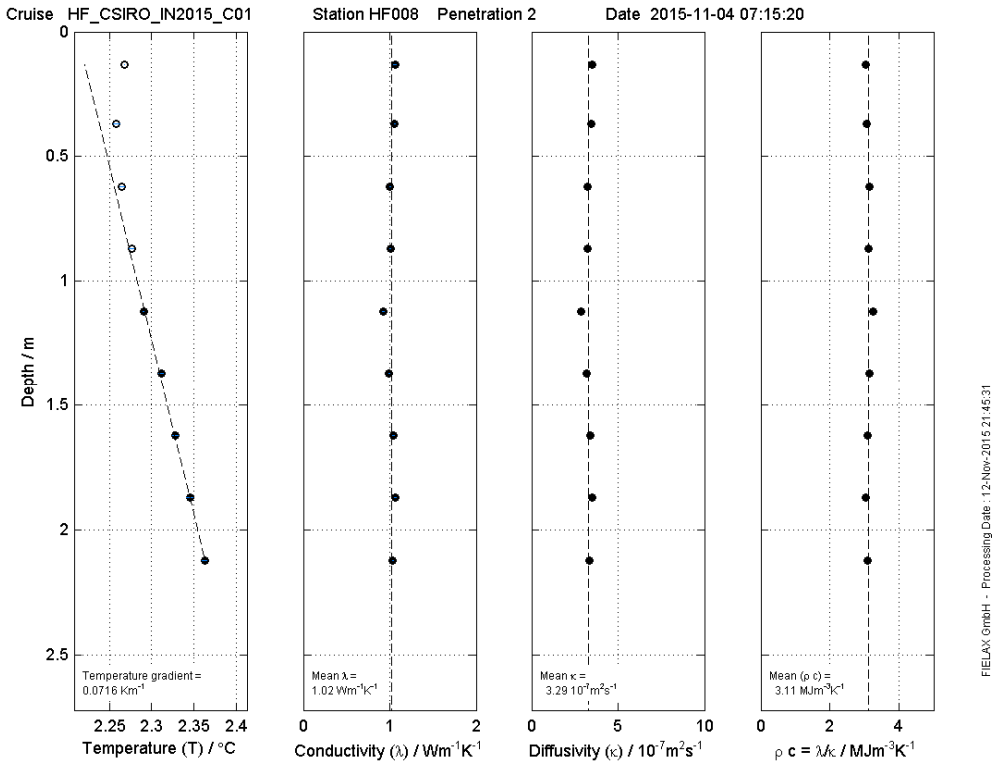

Sediment thermal properties

IN2015_C01 Station HF08 (TPRBE_030) Pen 2

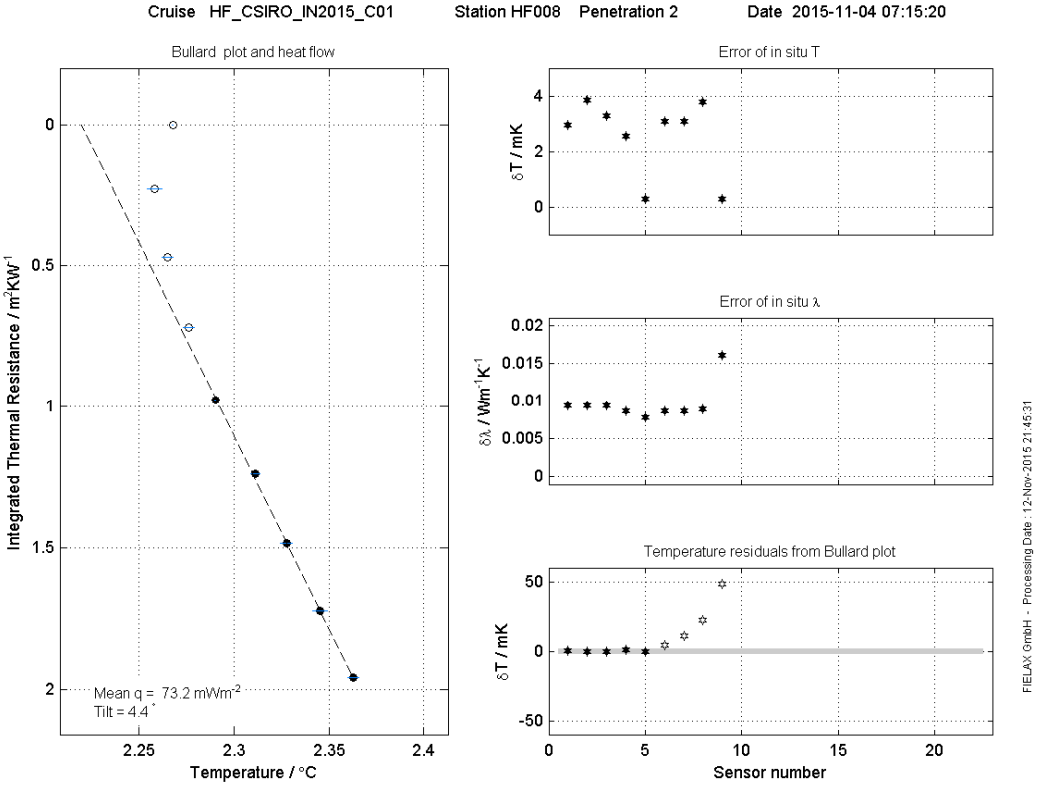

Bullard plot and error estimates

Cruise-Transect	HF_CSIRO_IN2015_C01
Station	HF08 (TPRBE_030)
Penetration No.	2
Date/Time of Penetration	2015-11-04 07:15:20
Latitude [°]	35.568197 S
Longitude [°]	132.380953 E
Depth [m]	2120.00
Device ID	CTM1000
String ID	T113SD
Heating wire length [m]	6.05
Pressure [dbar]	2126.5
Tilt [°]	4.4
Bottom water temperature [°C]	2.239
Heating power [J/m]	794.34
Mean thermal conductivity [W/(m K)]	1.021
Mean thermal resistivity [m K/W]	0.979
Mean thermal diffusivity [1e-07 m^2/s]	3.294
Mean volumetric capacity [MJ/m^3 K]	3.105
Temperature gradient dT/dz [K/m]	0.0716
Heat flow Q [mW/m^2]	73.21

Sens_used #	Sens_depth m	Temp. °C	Bullard depth m^2 K/W	Th. conduct. W/(m K)	Th. res. m K/W	Th. diffus. 1e-07 m^2/s	Vol. capac. MJ/(m^3 K)
9	0.130	2.268	0.000	1.059	0.944	3.477	3.046
8	0.370	2.258	0.227	1.059	0.945	3.471	3.049
7	0.620	2.265	0.469	1.004	0.996	3.209	3.130
6	0.870	2.276	0.718	1.007	0.993	3.222	3.125
5	1.120	2.290	0.977	0.927	1.078	2.851	3.253
4	1.370	2.311	1.237	0.993	1.007	3.156	3.147
3	1.620	2.328	1.483	1.040	0.961	3.381	3.076
2	1.870	2.345	1.721	1.067	0.938	3.510	3.039
1	2.120	2.363	1.959	1.037	0.964	3.365	3.081

8.3 Cruise IN2015_C01 Station HF07 (TPRBE_046)

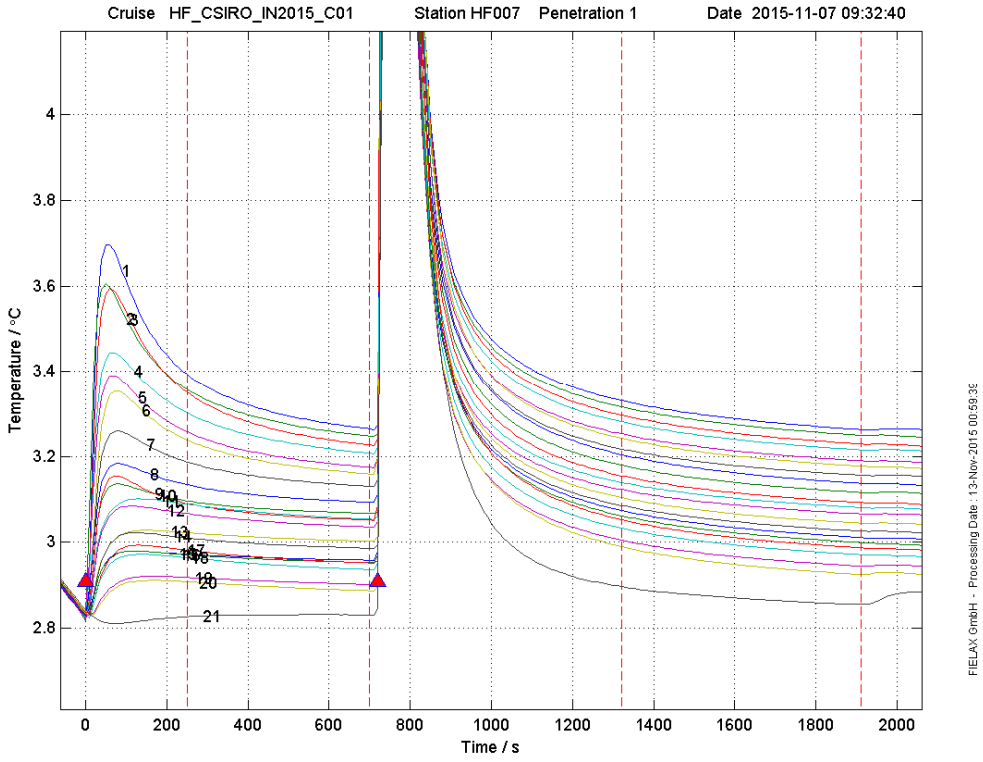

Sediment temperatures

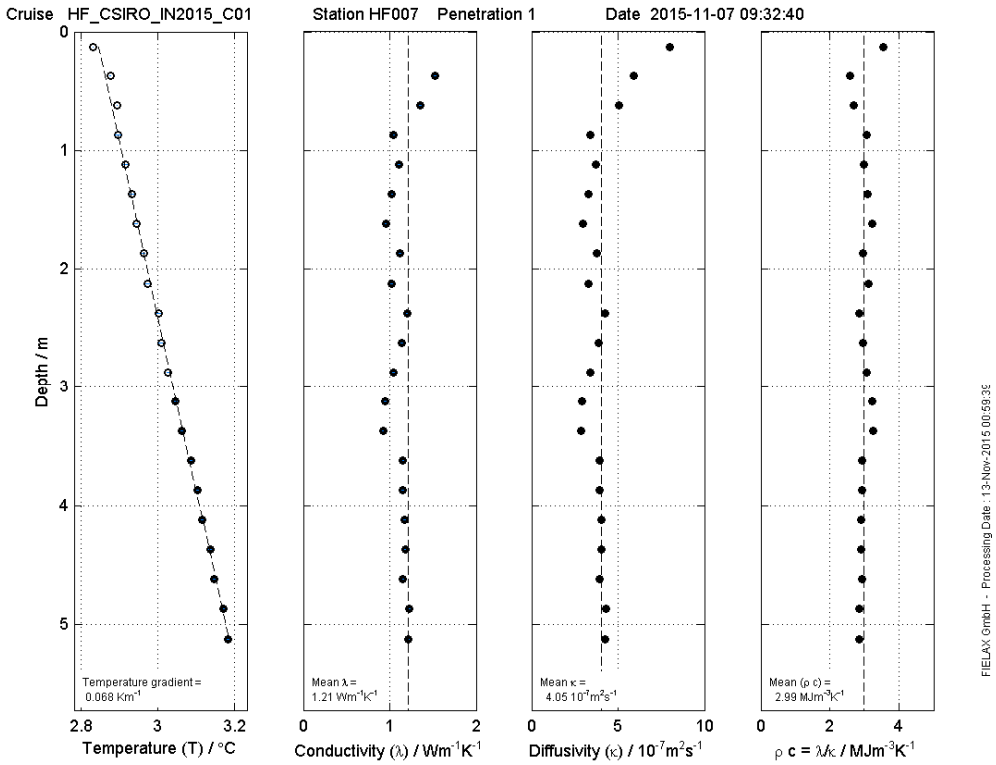

Sediment thermal properties

IN2015_C01 Station HF07 (TPRBE_046) Pen 1

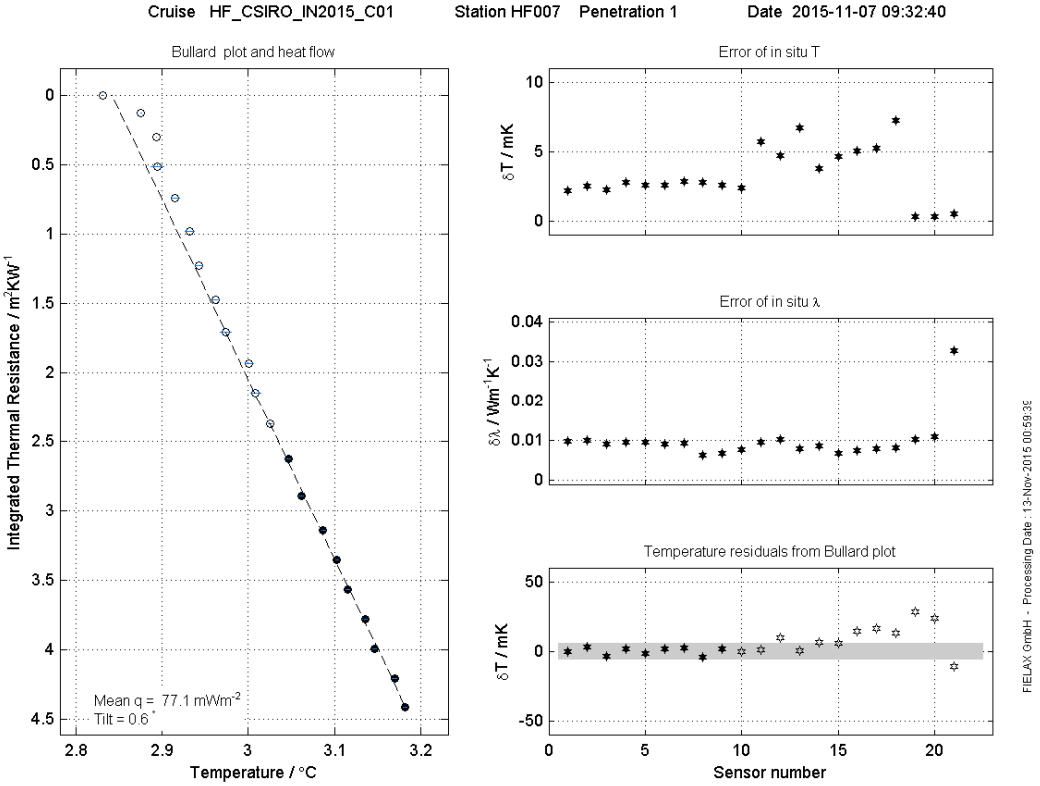

Bullard plot and error estimates

Cruise-Transect	HF_CSIRO_IN2015_C01
Station	HF07 (TPRBE_046)
Penetration No.	1
Date/Time of Penetration	2015-11-07 09:32:40
Latitude [°]	35.243246 S
Longitude [°]	132.494955 E
Depth [m]	1418.00
Device ID	CTM1000
String ID	T113SD
Heating wire length [m]	6.05
Pressure [dbar]	1409.8
Tilt [°]	0.6
Bottom water temperature [°C]	2.778
Heating power [J/m]	854.89
Mean thermal conductivity [W/(m K)]	1.214
Mean thermal resistivity [m K/W]	0.824
Mean thermal diffusivity [1e-07 m^2/s]	4.054
Mean volumetric capacity [MJ/m^3 K]	2.994
Temperature gradient dT/dz [K/m]	0.068
Heat flow Q [mW/m^2]	77.11

Sens_used #	Sens_depth m	Temp. °C	Bullard depth m^2 K/W	Th. conduct. W/(m K)	Th. res. m K/W	Th. diffus. 1e-07 m^2/s	Vol. capac. MJ/(m^3 K)
21	0.130	2.831	0.000	2.830	0.353	7.989	3.542
20	0.370	2.875	0.123	1.523	0.657	5.916	2.574
19	0.620	2.893	0.297	1.358	0.737	5.037	2.696
18	0.870	2.894	0.508	1.047	0.955	3.415	3.066
17	1.120	2.915	0.741	1.108	0.903	3.715	2.981
16	1.370	2.932	0.975	1.026	0.974	3.315	3.096
15	1.620	2.943	1.228	0.953	1.049	2.969	3.210
14	1.870	2.962	1.471	1.118	0.894	3.769	2.967
13	2.120	2.974	1.705	1.022	0.978	3.294	3.103
12	2.370	3.001	1.931	1.207	0.829	4.226	2.855
11	2.620	3.009	2.145	1.136	0.880	3.859	2.943
10	2.870	3.025	2.375	1.042	0.960	3.388	3.074
9	3.120	3.046	2.627	0.946	1.057	2.937	3.221
8	3.370	3.061	2.894	0.924	1.083	2.837	3.256
7	3.620	3.087	3.138	1.154	0.867	3.946	2.924
6	3.870	3.103	3.355	1.153	0.867	3.938	2.928
5	4.120	3.115	3.570	1.167	0.857	4.012	2.910
4	4.370	3.135	3.784	1.177	0.850	4.060	2.899
3	4.620	3.147	3.998	1.154	0.867	3.935	2.933
2	4.870	3.170	4.208	1.228	0.814	4.318	2.844
1	5.120	3.182	4.413	1.219	0.820	4.265	2.858

IN2015_C01 Station HF07 (TPRBE_046) Pen 2

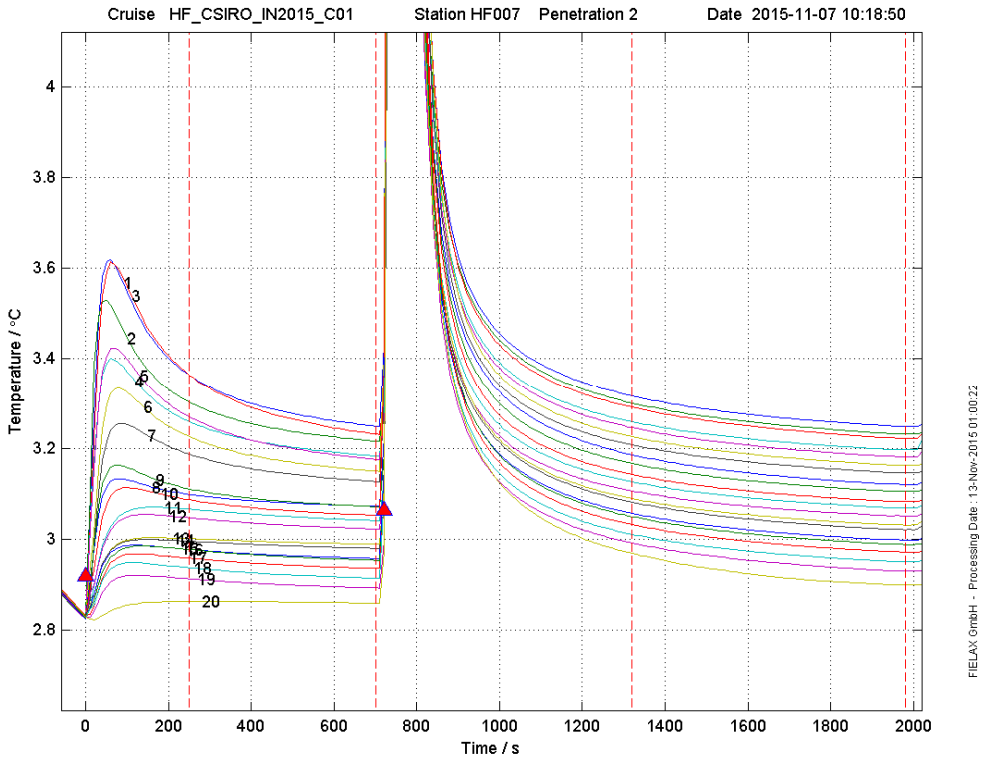

Sediment temperatures

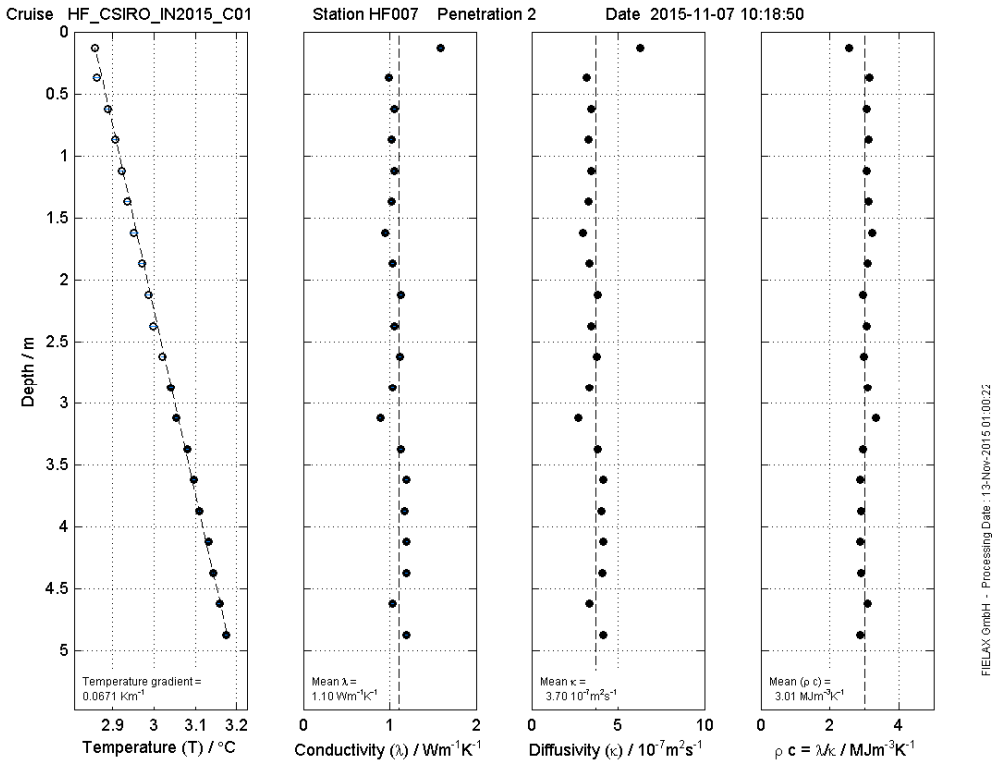

Sediment thermal properties

IN2015_C01 Station HF07 (TPRBE_046) Pen 2

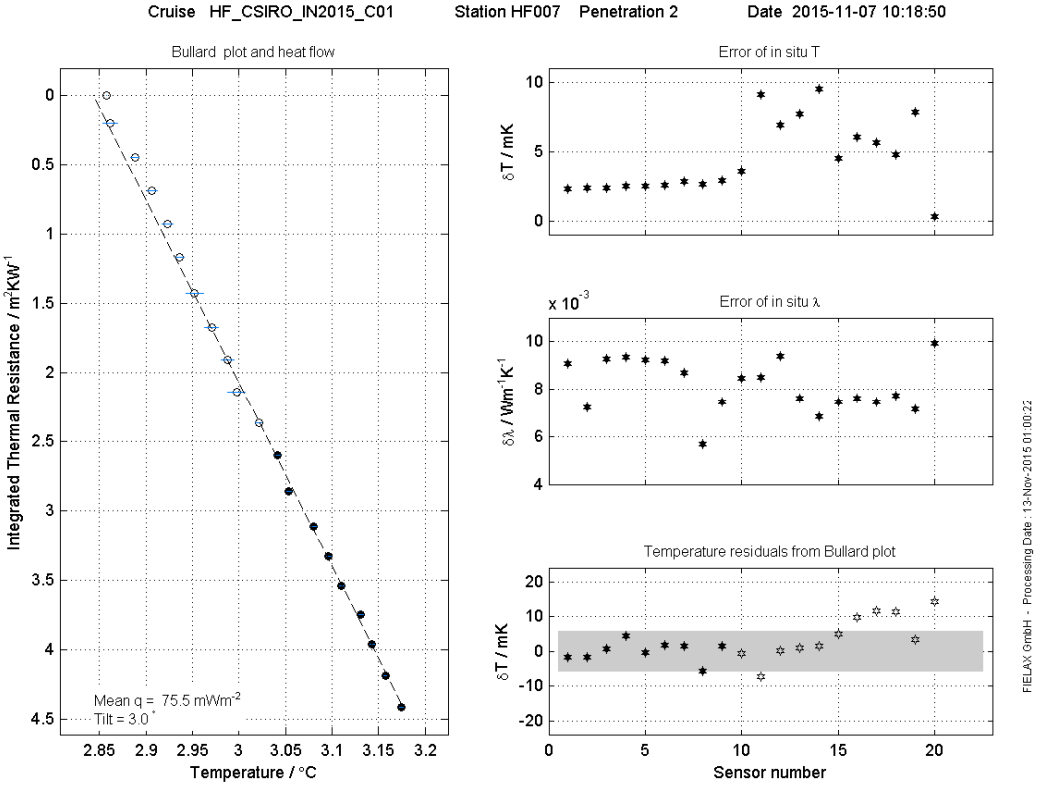

Bullard plot and error estimates

Cruise-Transect	HF_CSIRO_IN2015_C01
Station	HF07 (TPRBE_046)
Penetration No.	2
Date/Time of Penetration	2015-11-07 10:18:50
Latitude [°]	35.243246 S
Longitude [°]	132.494955 E
Depth [m]	1418.00
Device ID	CTM1000
String ID	T113SD
Heating wire length [m]	6.05
Pressure [dbar]	1409.5
Tilt [°]	3.0
Bottom water temperature [°C]	2.778
Heating power [J/m]	817.07
Mean thermal conductivity [W/(m K)]	1.102
Mean thermal resistivity [m K/W]	0.908
Mean thermal diffusivity [1e-07 m^2/s]	3.698
Mean volumetric capacity [MJ/m^3 K]	3.009
Temperature gradient dT/dz [K/m]	0.0671
Heat flow Q [mW/m^2]	75.49

Sens_used #	Sens_depth m	Temp. °C	Bullard depth m^2 K/W	Th. conduct. W/(m K)	Th. res. m K/W	Th. diffus. 1e-07 m^2/s	Vol. capac. MJ/(m^3 K)
20	0.130	2.858	0.000	1.592	0.628	6.260	2.542
19	0.370	2.862	0.198	0.993	1.007	3.156	3.147
18	0.620	2.888	0.443	1.052	0.950	3.441	3.058
17	0.870	2.907	0.684	1.018	0.983	3.273	3.109
16	1.120	2.923	0.926	1.050	0.952	3.430	3.061
15	1.370	2.936	1.168	1.019	0.982	3.279	3.107
14	1.620	2.952	1.422	0.952	1.051	2.963	3.212
13	1.870	2.971	1.674	1.032	0.969	3.344	3.087
12	2.120	2.988	1.906	1.126	0.888	3.810	2.955
11	2.370	2.997	2.136	1.051	0.951	3.437	3.059
10	2.620	3.021	2.367	1.117	0.895	3.761	2.969
9	2.870	3.041	2.600	1.033	0.968	3.345	3.087
8	3.120	3.054	2.862	0.888	1.126	2.678	3.316
7	3.370	3.080	3.113	1.131	0.884	3.829	2.953
6	3.620	3.096	3.328	1.194	0.837	4.150	2.877
5	3.870	3.110	3.540	1.172	0.853	4.033	2.906
4	4.120	3.131	3.751	1.197	0.835	4.164	2.874
3	4.370	3.143	3.960	1.190	0.840	4.115	2.892
2	4.620	3.158	4.187	1.031	0.970	3.334	3.092
1	4.870	3.175	4.413	1.196	0.836	4.148	2.882

8.4 Cruise IN2015_C01 Station HF04 (TPRBE_047)

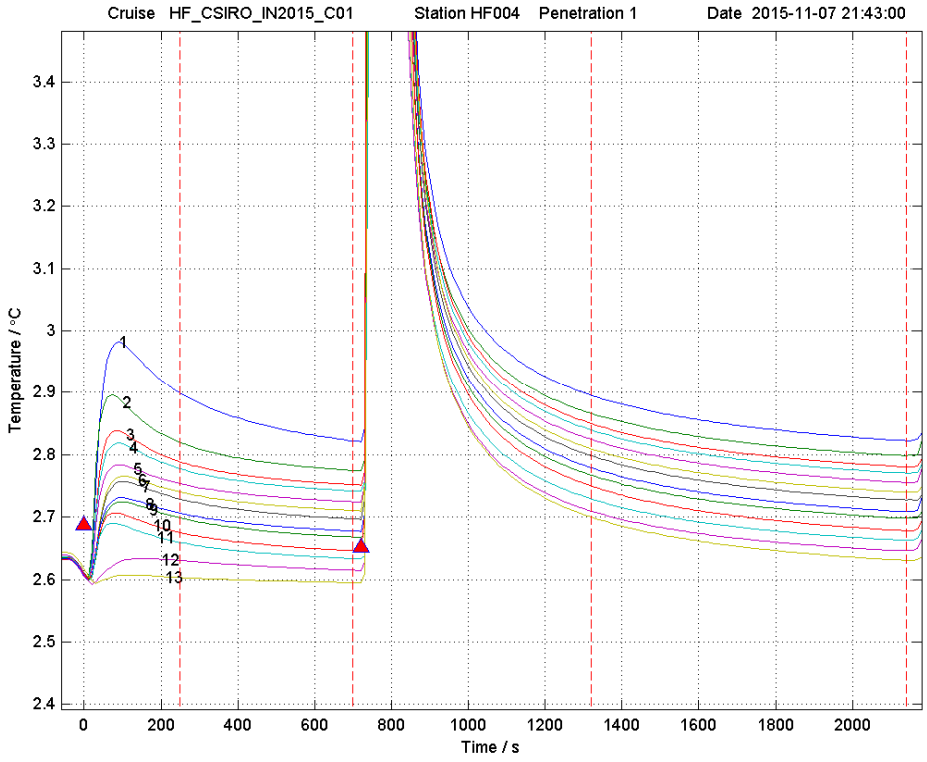

Sediment temperatures

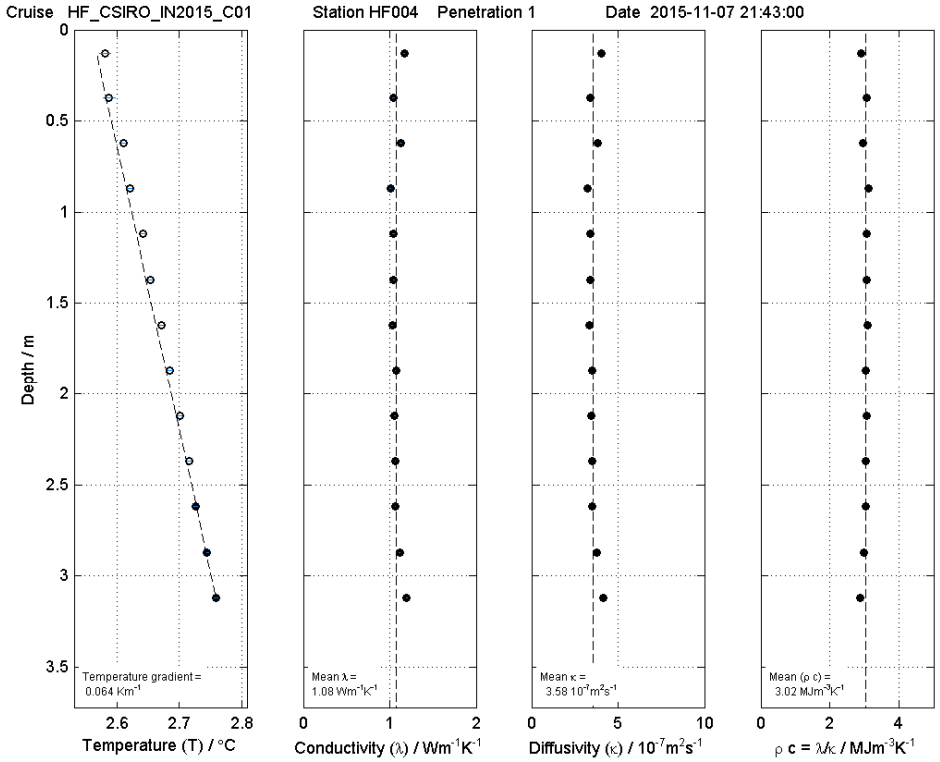

Sediment thermal properties

IN2015_C01 Station HF04 (TPRBE_047) Pen 1

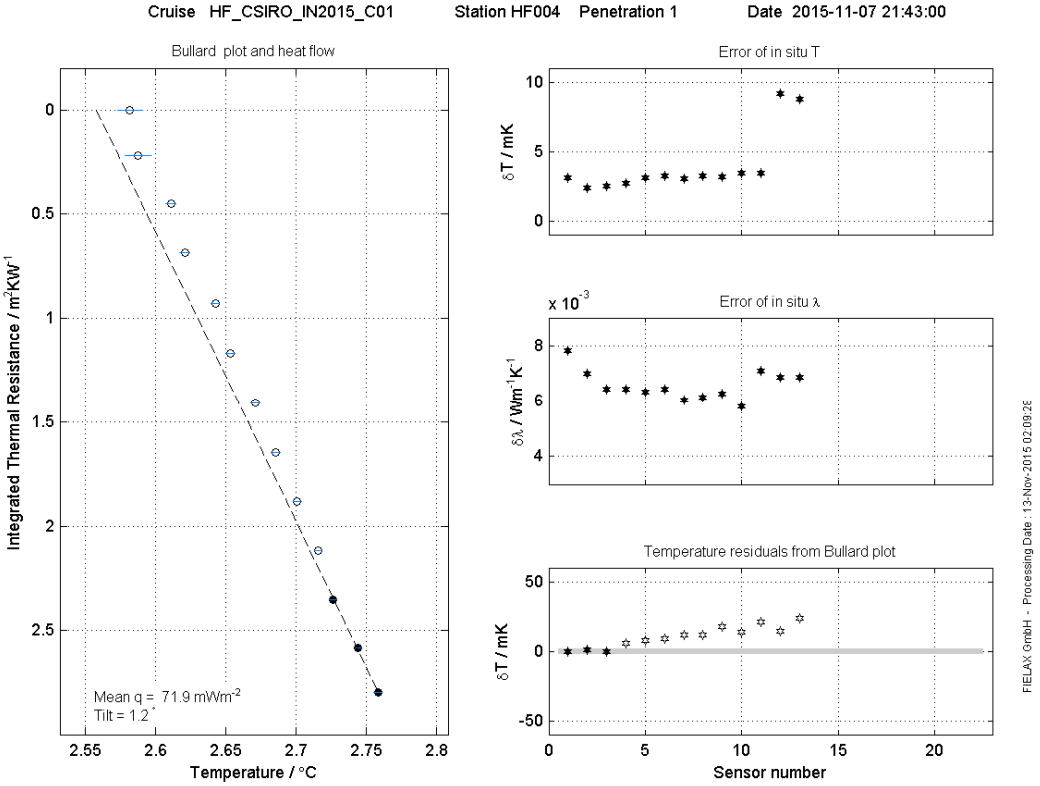

Bullard plot and error estimates

```
Cruise-Transect                          HF_CSIRO_IN2015_C01
Station                                  HF04 (TPRBE_047)
Penetration No.                          1

Date/Time of Penetration                 2015-11-07 21:43:00
Latitude [°]                             35.191869 S
Longitude [°]                            131.733369 E
Depth [m]                                1686.00

Device ID                                CTM1000
String ID                                T113SD
Heating wire length [m]                  6.05

Pressure [dbar]                          1689.9
Tilt [°]                                 1.2
Bottom water temperature [°C]            2.557
Heating power [J/m]                      826.71

Mean thermal conductivity [W/(m K)]      1.080
Mean thermal resistivity [m K/W]         0.926
Mean thermal diffusivity [1e-07 m^2/s]   3.578
Mean volumetric capacity [MJ/m^3 K]      3.022

Temperature gradient dT/dz [K/m]          0.064
Heat flow Q [mW/m^2]                     71.89
```

Sens_used #	Sens_depth m	Temp. °C	Bullard depth m^2 K/W	Th. conduct. W/(m K)	Th. res. m K/W	Th. diffus. 1e-07 m^2/s	Vol. capac. MJ/(m^3 K)
13	0.130	2.582	0.000	1.167	0.857	4.020	2.902
12	0.370	2.588	0.218	1.044	0.958	3.402	3.069
11	0.620	2.611	0.449	1.127	0.887	3.813	2.955
10	0.870	2.621	0.684	1.006	0.994	3.217	3.127
9	1.120	2.642	0.928	1.043	0.958	3.398	3.071
8	1.370	2.653	1.168	1.045	0.957	3.403	3.070
7	1.620	2.671	1.409	1.029	0.972	3.329	3.092
6	1.870	2.685	1.647	1.070	0.935	3.526	3.033
5	2.120	2.701	1.882	1.056	0.947	3.459	3.053
4	2.370	2.716	2.118	1.068	0.937	3.516	3.037
3	2.620	2.726	2.352	1.069	0.936	3.521	3.035
2	2.870	2.744	2.581	1.115	0.897	3.753	2.972
1	3.120	2.758	2.797	1.196	0.836	4.161	2.874

IN2015_C01 Station HF04 (TPRBE_047) Pen 2

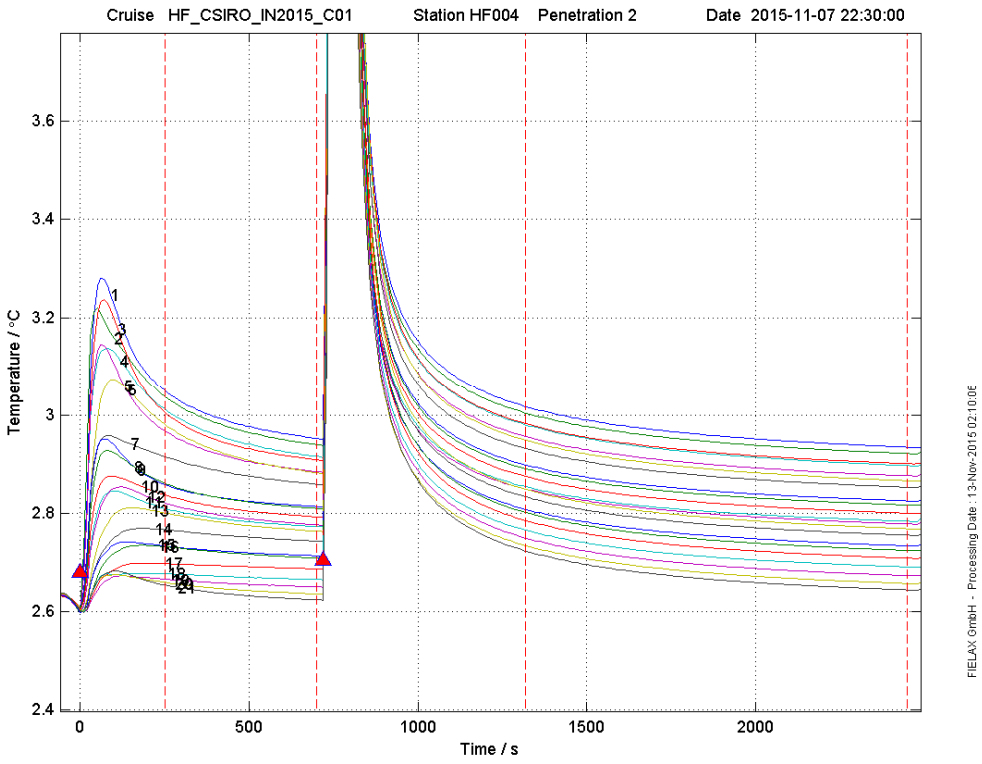

Sediment temperatures

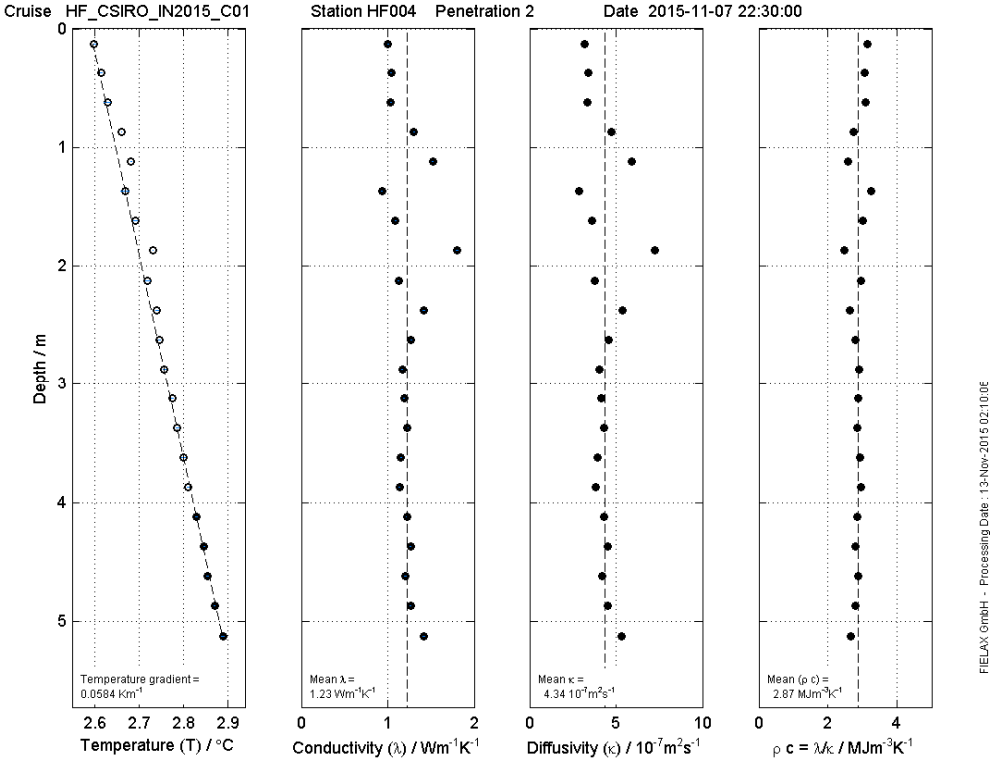

Sediment thermal properties

IN2015_C01 Station HF04 (TPRBE_047) Pen 2

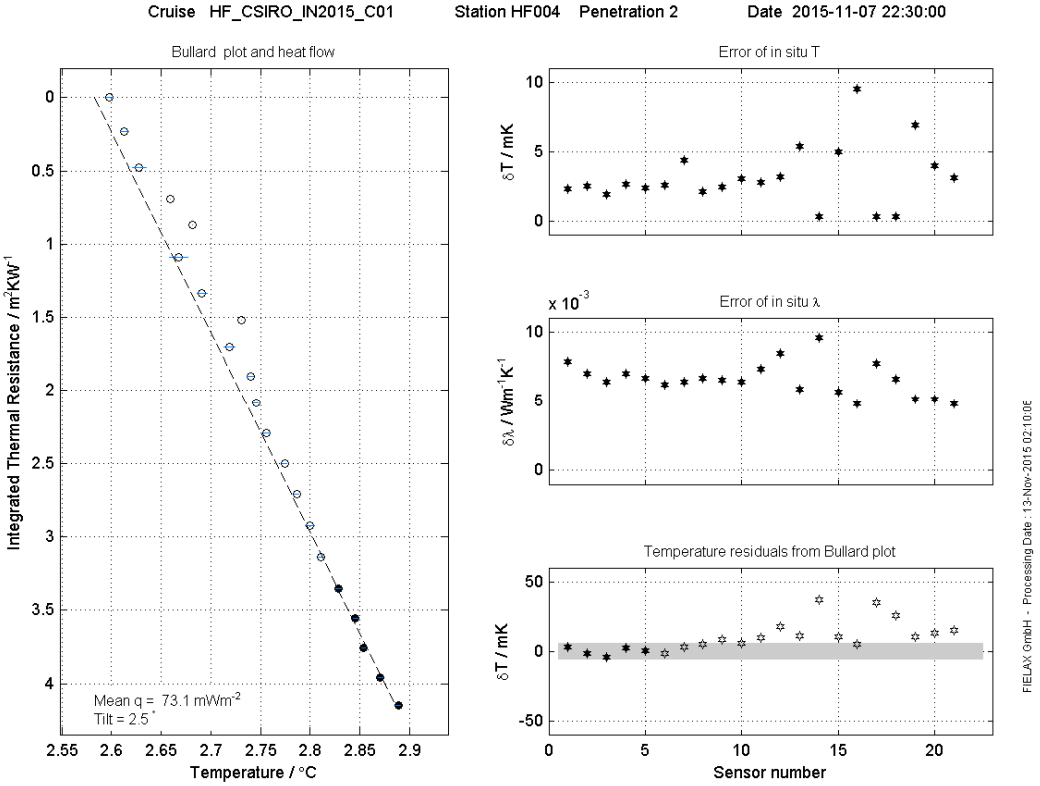

Bullard plot and error estimates

Cruise-Transect	HF_CSIRO_IN2015_C01
Station	HF04 (TPRBE_047)
Penetration No.	2
Date/Time of Penetration	2015-11-07 22:30:00
Latitude [°]	35.191869 S
Longitude [°]	131.733369 E
Depth [m]	1686.00
Device ID	CTM1000
String ID	T113SD
Heating wire length [m]	6.05
Pressure [dbar]	1693.5
Tilt [°]	2.5
Bottom water temperature [°C]	2.560
Heating power [J/m]	794.67
Mean thermal conductivity [W/(m K)]	1.228
Mean thermal resistivity [m K/W]	0.815
Mean thermal diffusivity [1e-07 m^2/s]	4.340
Mean volumetric capacity [MJ/m^3 K]	2.868
Temperature gradient dT/dz [K/m]	0.0584
Heat flow Q [mW/m^2]	73.09

Sens_used #	Sens_depth m	Temp. °C	Bullard depth m^2 K/W	Th. conduct. W/(m K)	Th. res. m K/W	Th. diffus. 1e-07 m^2/s	Vol. capac. MJ/(m^3 K)
21	0.130	2.598	0.000	1.002	0.998	3.200	3.132
20	0.370	2.613	0.235	1.042	0.960	3.390	3.073
19	0.620	2.628	0.476	1.034	0.968	3.350	3.085
18	0.870	2.659	0.692	1.303	0.767	4.751	2.743
17	1.120	2.682	0.871	1.521	0.658	5.916	2.571
16	1.370	2.668	1.087	0.932	1.073	2.869	3.247
15	1.620	2.691	1.336	1.088	0.919	3.621	3.006
14	1.870	2.731	1.520	1.801	0.555	7.248	2.484
13	2.120	2.719	1.701	1.123	0.890	3.795	2.959
12	2.370	2.740	1.900	1.419	0.704	5.363	2.647
11	2.620	2.745	2.087	1.271	0.787	4.566	2.784
10	2.870	2.756	2.292	1.167	0.857	4.020	2.904
9	3.120	2.774	2.504	1.191	0.839	4.140	2.877
8	3.370	2.786	2.711	1.226	0.816	4.323	2.836
7	3.620	2.800	2.922	1.151	0.869	3.937	2.924
6	3.870	2.811	3.140	1.135	0.881	3.843	2.954
5	4.120	2.829	3.353	1.221	0.819	4.287	2.849
4	4.370	2.845	3.554	1.264	0.791	4.508	2.804
3	4.620	2.853	3.757	1.204	0.831	4.189	2.874
2	4.870	2.871	3.959	1.263	0.792	4.498	2.807
1	5.120	2.889	4.147	1.418	0.705	5.324	2.664

8.5 Cruise IN2015_C01 Station HF03 (TPRBE_048)

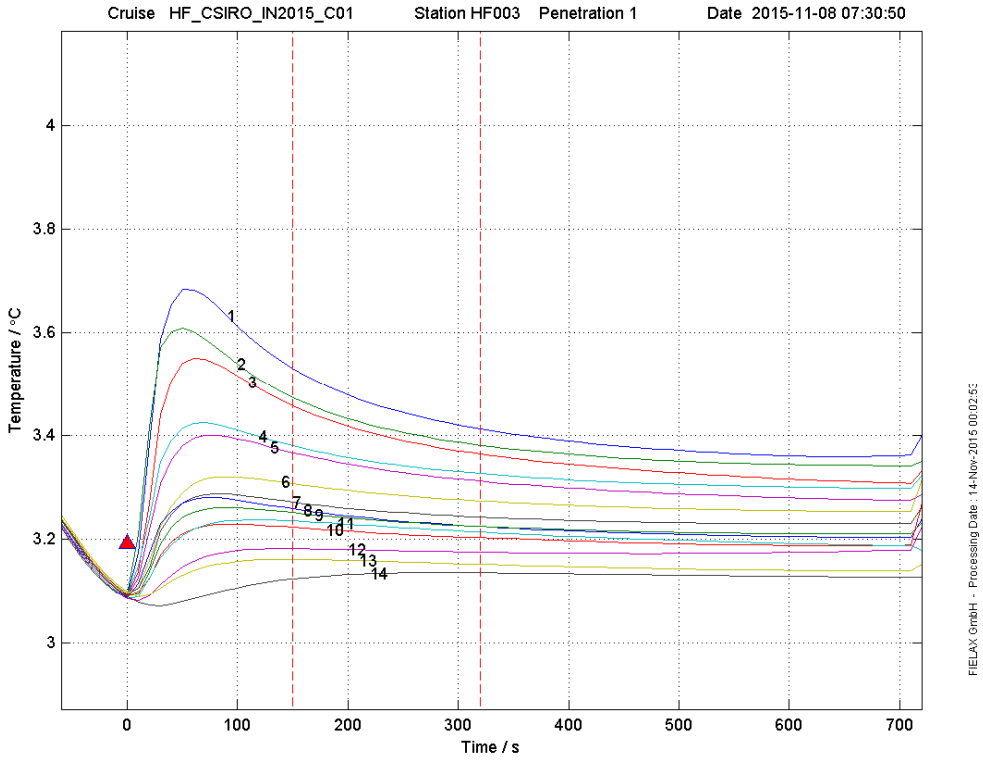

Sediment temperatures

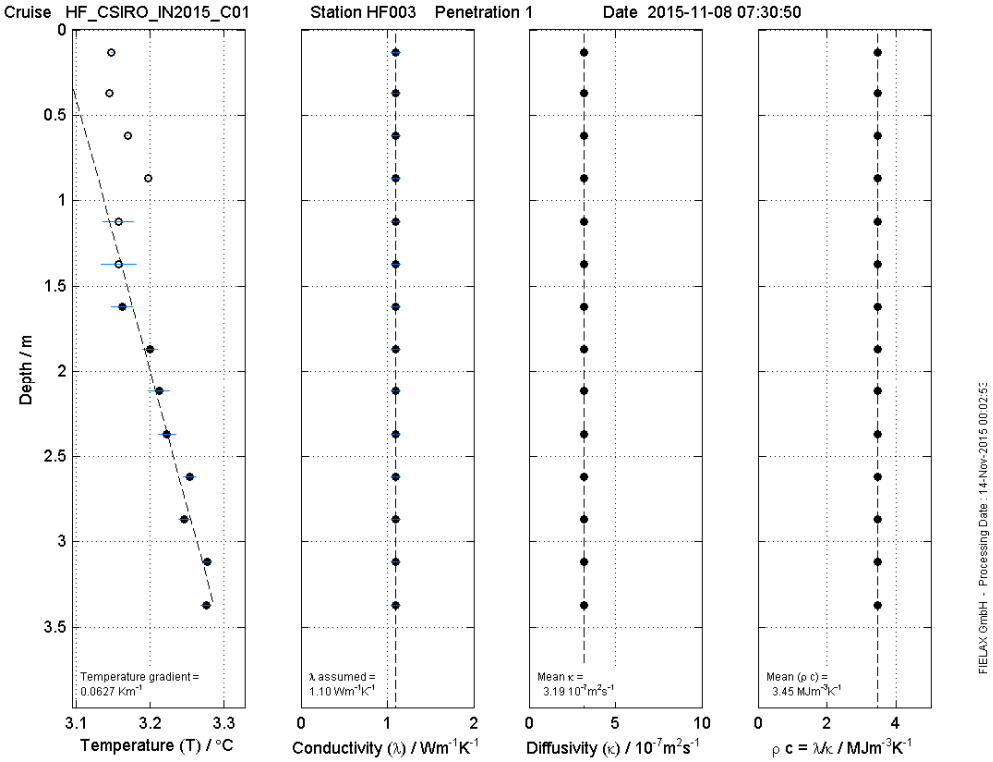

Sediment thermal properties

IN2015_C01 Station HF03 (TPRBE_048) Pen 1

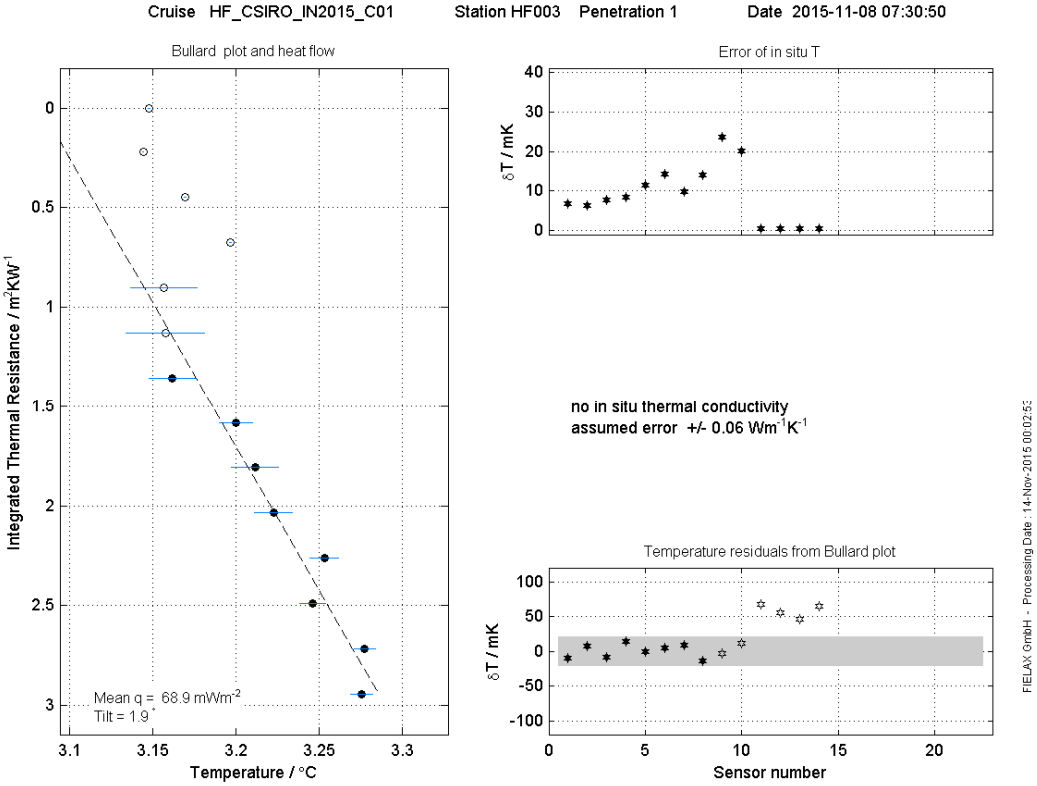

Bullard plot and error estimates

```
Cruise-Transect                          HF_CSIRO_IN2015_C01
Station                                  HF03 (TPRBE_048)
Penetration No.                          1

Date/Time of Penetration                 2015-11-08 07:30:50
Latitude [°]                             34.983634 S
Longitude [°]                            131.958528 E
Depth [m]                                1263.00

Device ID                                CTM1000
String ID                                T113SD
Heating wire length [m]                  6.05

Pressure [dbar]                          1270.0
Tilt [°]                                 1.9
Bottom water temperature [°C]            3.035
Heating power [J/m]                      0.00

Mean th. conductivity (assumed) [W/(m K)] 1.100
Temperature gradient dT/dz [K/m]         0.0627
Heat flow Q [mW/m^2]                     68.93
```

Sens_used #	Sens_depth [m]	T_insitu [K]	Bull_depth [m^2 K/W]	lambda_assumed [W/m K]
14	0.130	3.148	0.000	1.100
13	0.370	3.144	0.218	1.100
12	0.620	3.169	0.445	1.100
11	0.870	3.197	0.673	1.100
10	1.120	3.157	0.900	1.100
9	1.370	3.158	1.127	1.100
8	1.620	3.162	1.355	1.100
7	1.870	3.200	1.582	1.100
6	2.120	3.212	1.809	1.100
5	2.370	3.223	2.036	1.100
4	2.620	3.253	2.264	1.100
3	2.870	3.246	2.491	1.100
2	3.120	3.277	2.718	1.100
1	3.370	3.275	2.945	1.100

IN2015_C01 Station HF03 (TPRBE_048) Pen 2

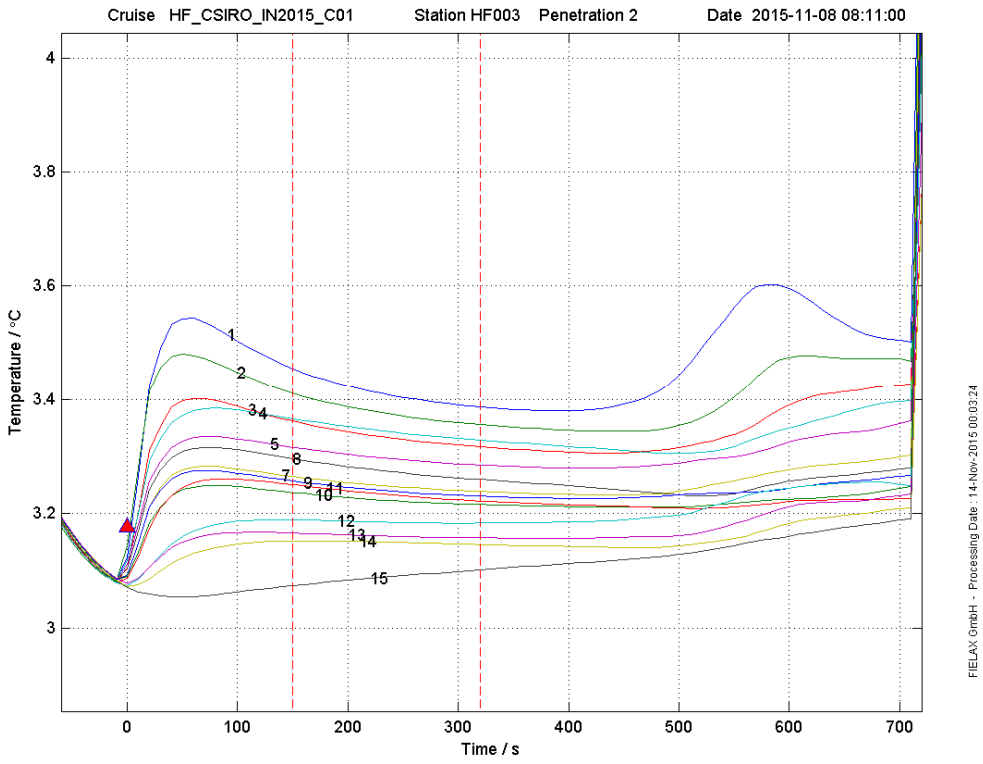

Sediment temperatures

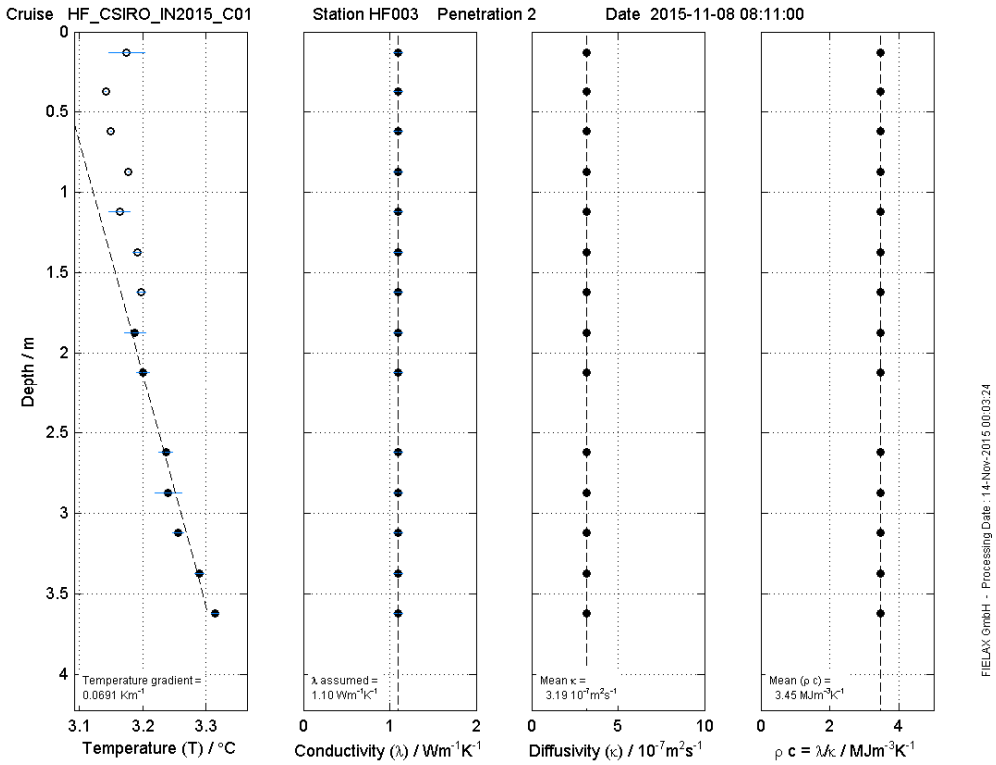

Sediment thermal properties

IN2015_C01 Station HF03 (TPRBE_048) Pen 2

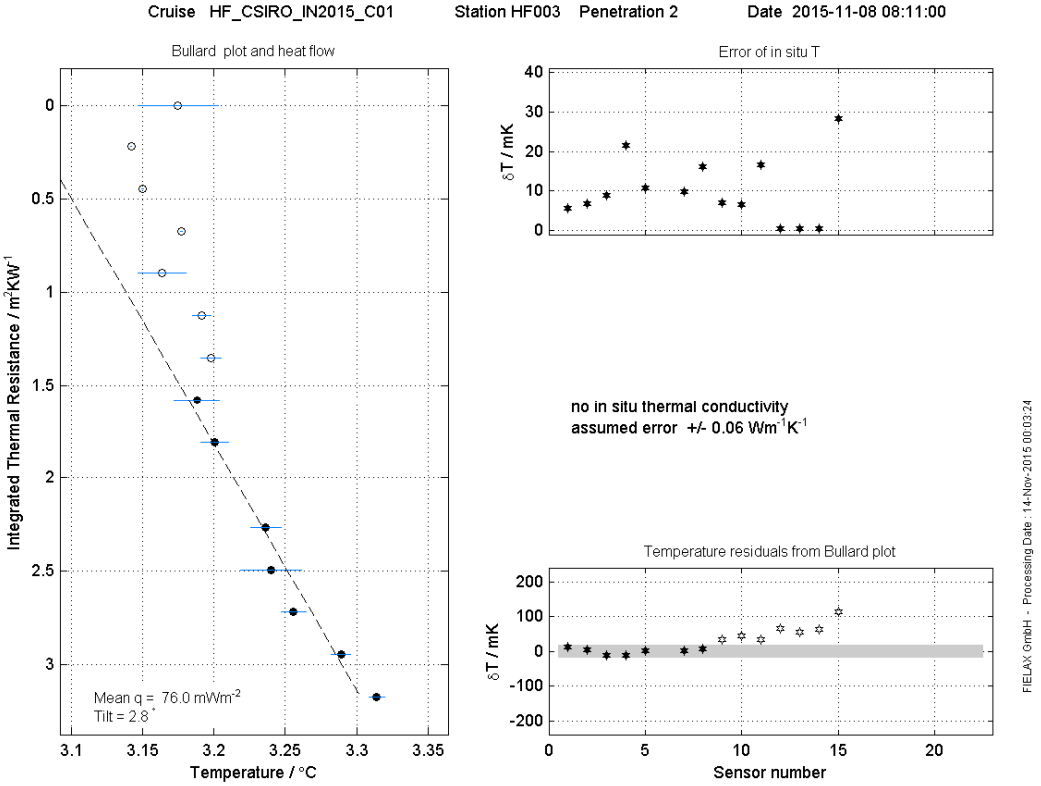

Bullard plot and error estimates

```
Cruise-Transect                          HF_CSIRO_IN2015_C01
Station                                  HF03 (TPRBE_048)
Penetration No.                          2

Date/Time of Penetration                 2015-11-08 08:11:00
Latitude [°]                             34.983634 S
Longitude [°]                            131.958528 E
Depth [m]                                1263.00

Device ID                                CTM1000
String ID                                T113SD
Heating wire length [m]                  6.05

Pressure [dbar]                          1271.0
Tilt [°]                                 2.8
Bottom water temperature [°C]            3.030
Heating power [J/m]                      0.00

Mean th. conductivity (assumed) [W/(m K)] 1.100
Temperature gradient dT/dz [K/m]         0.0691
Heat flow Q [mW/m^2]                     75.96
```

Sens_used #	Sens_depth [m]	T_insitu [K]	Bull_depth [m^2 K/W]	lambda_assumed [W/m K]
15	0.130	3.175	0.000	1.100
14	0.370	3.142	0.218	1.100
13	0.620	3.150	0.445	1.100
12	0.870	3.177	0.673	1.100
11	1.120	3.163	0.900	1.100
10	1.370	3.191	1.127	1.100
9	1.620	3.198	1.355	1.100
8	1.870	3.188	1.582	1.100
7	2.120	3.200	1.809	1.100
5	2.620	3.236	2.264	1.100
4	2.870	3.240	2.491	1.100
3	3.120	3.256	2.718	1.100
2	3.370	3.289	2.945	1.100
1	3.620	3.314	3.173	1.100

8.6 Cruise IN2015_C01 Station HF03 (TPRBE_049)

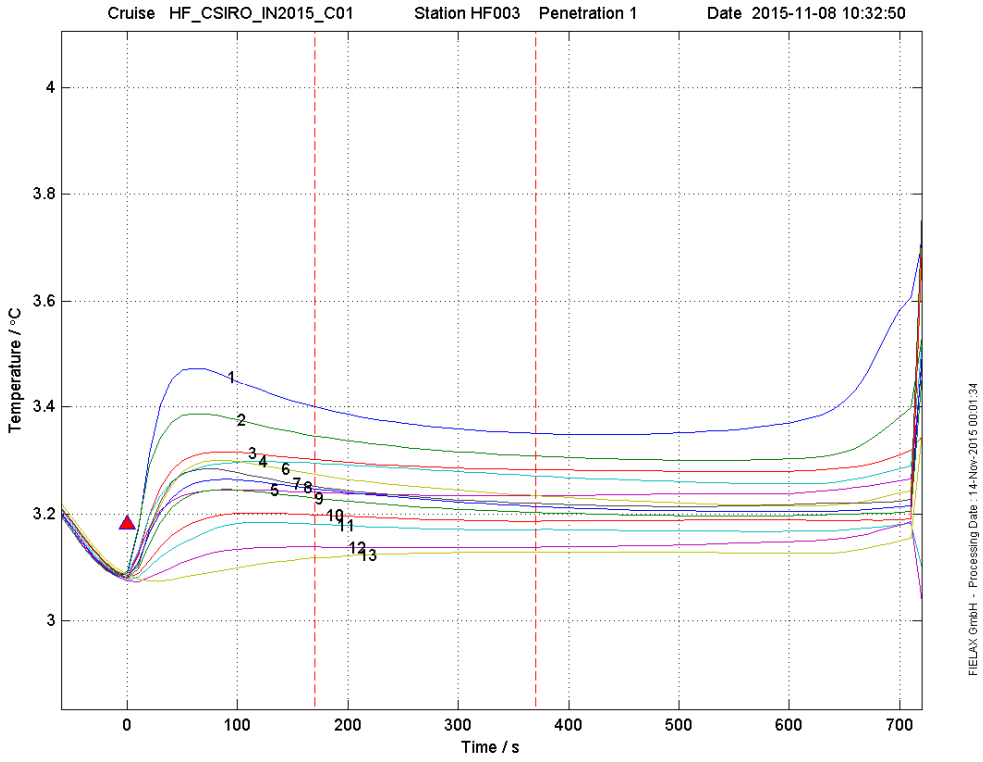

Sediment temperatures

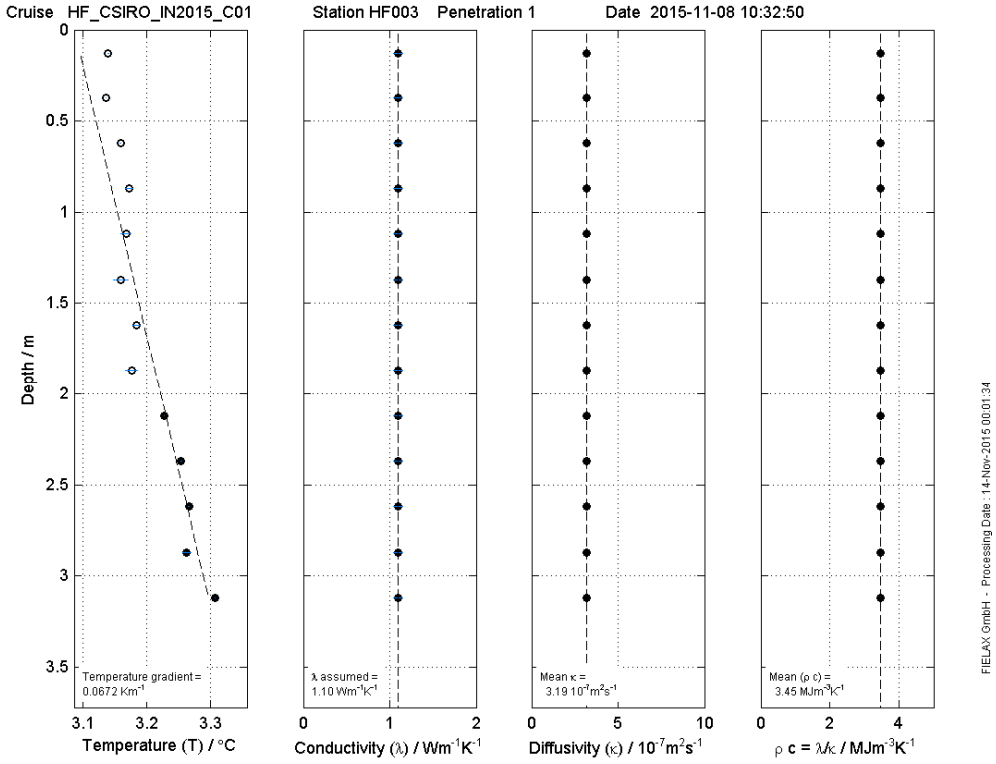

Sediment thermal properties

IN2015_C01 Station HF03 (TPRBE_049) Pen 1

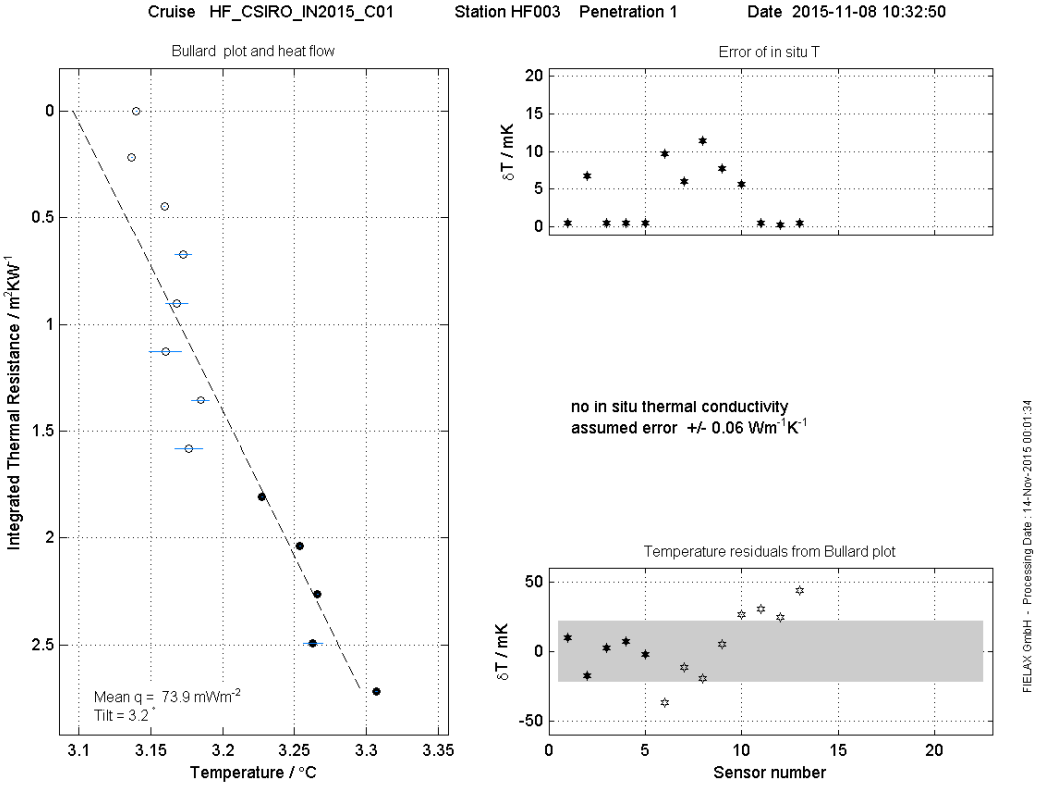

Bullard plot and error estimates

```
Cruise-Transect                          HF_CSIRO_IN2015_C01
Station                                  HF03 (TPRBE_049)
Penetration No.                          1

Date/Time of Penetration                 2015-11-08 10:32:50
Latitude [°]                             34.983729 S
Longitude [°]                            131.958444 E
Depth [m]                                1263.00

Device ID                                CTM1000
String ID                                T113SD
Heating wire length [m]                  6.05

Pressure [dbar]                          1270.5
Tilt [°]                                 3.2
Bottom water temperature [°C]            3.036
Heating power [J/m]                      0.00

Mean th. conductivity (assumed) [W/(m K)] 1.100
Temperature gradient dT/dz [K/m]         0.0672
Heat flow Q [mW/m^2]                     73.87
```

Sens_used #	Sens_depth [m]	T_insitu [K]	Bull_depth [m^2 K/W]	lambda_assumed [W/m K]
13	0.130	3.140	0.000	1.100
12	0.370	3.137	0.218	1.100
11	0.620	3.159	0.445	1.100
10	0.870	3.172	0.673	1.100
9	1.120	3.168	0.900	1.100
8	1.370	3.160	1.127	1.100
7	1.620	3.185	1.355	1.100
6	1.870	3.176	1.582	1.100
5	2.120	3.227	1.809	1.100
4	2.370	3.254	2.036	1.100
3	2.620	3.266	2.264	1.100
2	2.870	3.263	2.491	1.100
1	3.120	3.307	2.718	1.100

8.7 Cruise IN2015_C01 Station HF06 (TPRBE_056)

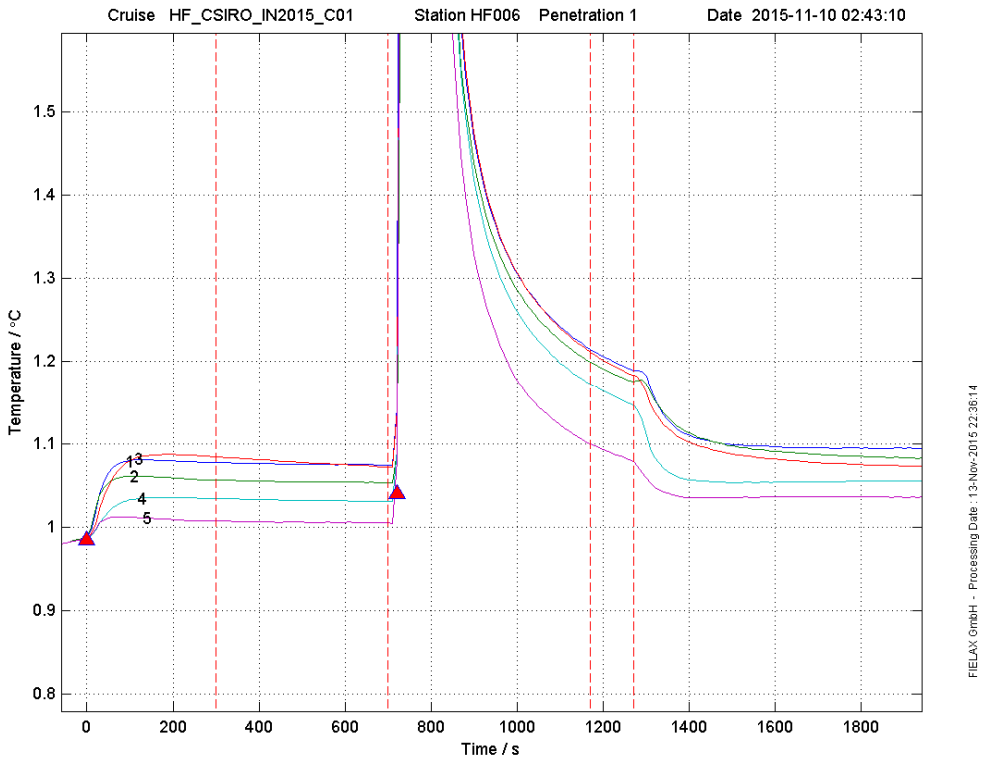

Sediment temperatures

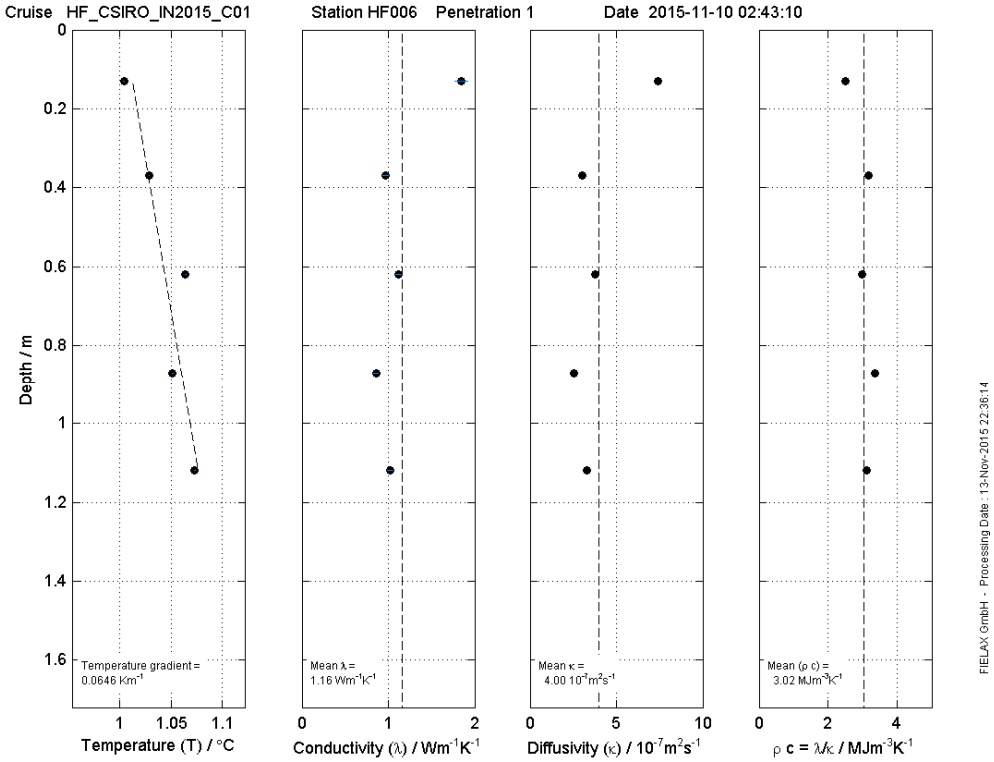

Sediment thermal properties

IN2015_C01 Station HF06 (TPRBE_056) Pen 1

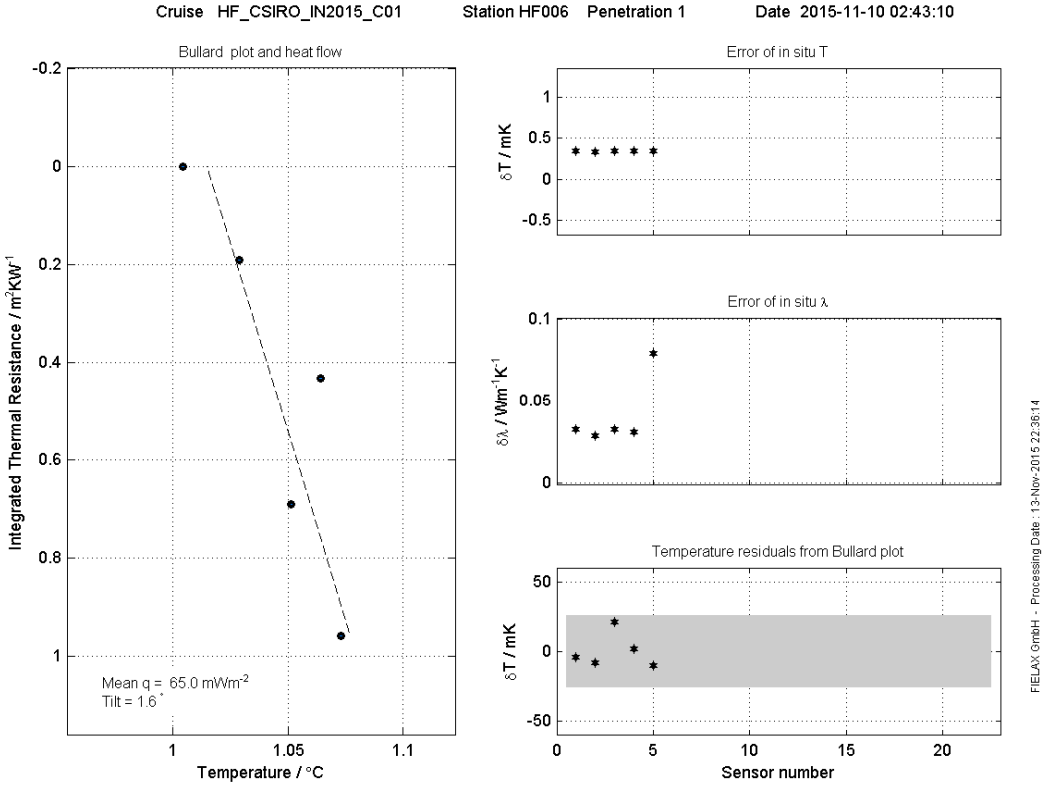

Bullard plot and error estimates

Cruise-Transect	HF_CSIRO_IN2015_C01
Station	HF06 (TPRBE_056)
Penetration No.	1
Date/Time of Penetration	2015-11-10 02:43:10
Latitude [°]	35.820164 S
Longitude [°]	130.563621 E
Depth [m]	5432.00
Device ID	CTM1000
String ID	T113SD
Heating wire length [m]	6.05
Pressure [dbar]	5533.7
Tilt [°]	1.6
Bottom water temperature [°C]	0.976
Heating power [J/m]	777.31
Mean thermal conductivity [W/(m K)]	1.162
Mean thermal resistivity [m K/W]	0.861
Mean thermal diffusivity [1e-07 m^2/s]	4.003
Mean volumetric capacity [MJ/m^3 K]	3.025
Temperature gradient dT/dz [K/m]	0.0646
Heat flow Q [mW/m^2]	65.03

Sens_used #	Sens_depth m	Temp. °C	Bullard depth m^2 K/W	Th. conduct. W/(m K)	Th. res. m K/W	Th. diffus. 1e-07 m^2/s	Vol. capac. MJ/(m^3 K)
5	0.130	1.004	0.000	1.846	0.542	7.380	2.501
4	0.370	1.029	0.191	0.969	1.032	3.046	3.181
3	0.620	1.064	0.432	1.117	0.895	3.752	2.978
2	0.870	1.051	0.690	0.857	1.167	2.553	3.357
1	1.120	1.073	0.958	1.020	0.980	3.283	3.107

8.8 Cruise IN2015_C01 Station HF05 (TPRBE_088)

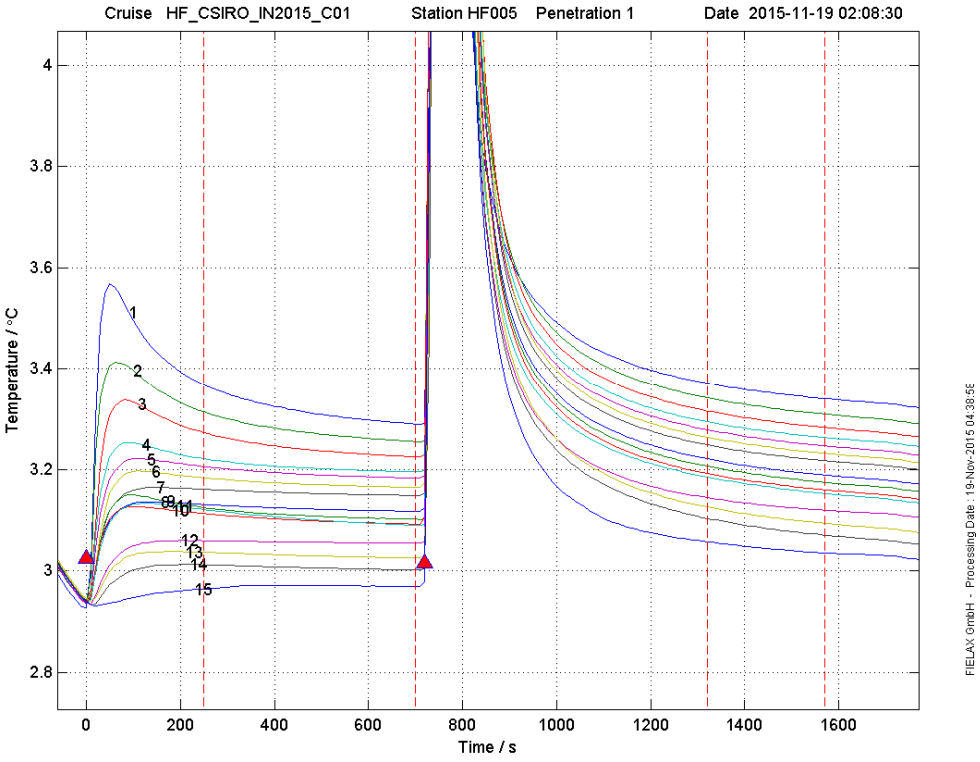

Sediment temperatures

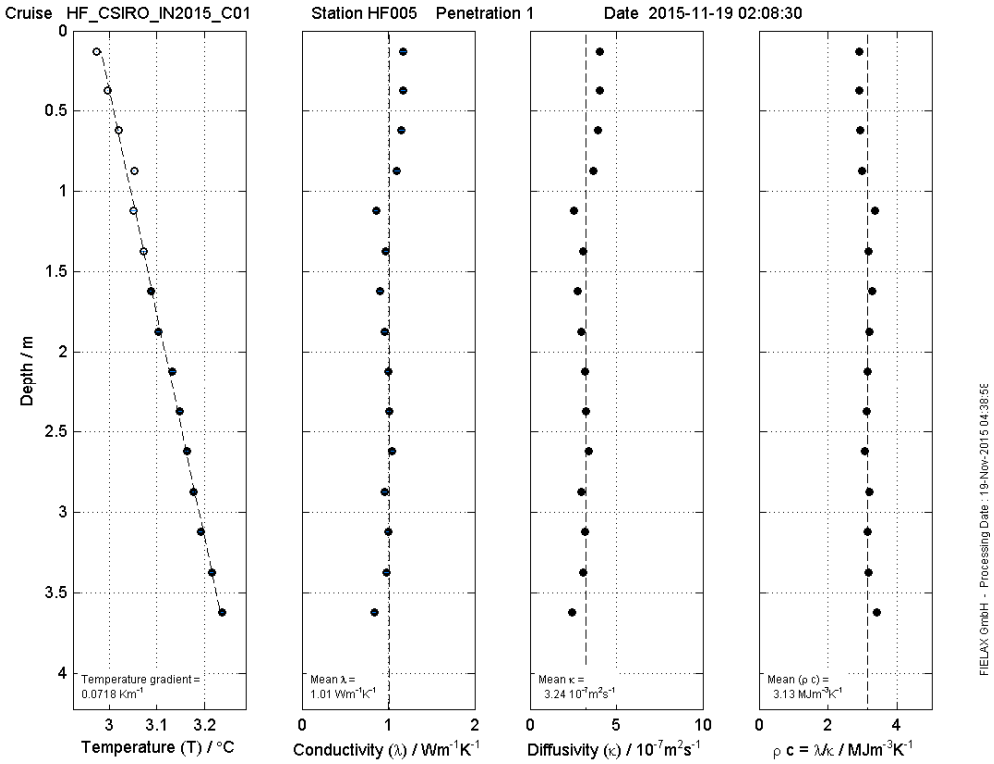

Sediment thermal properties

IN2015_C01 Station HF05 (TPRBE_088) Pen 1

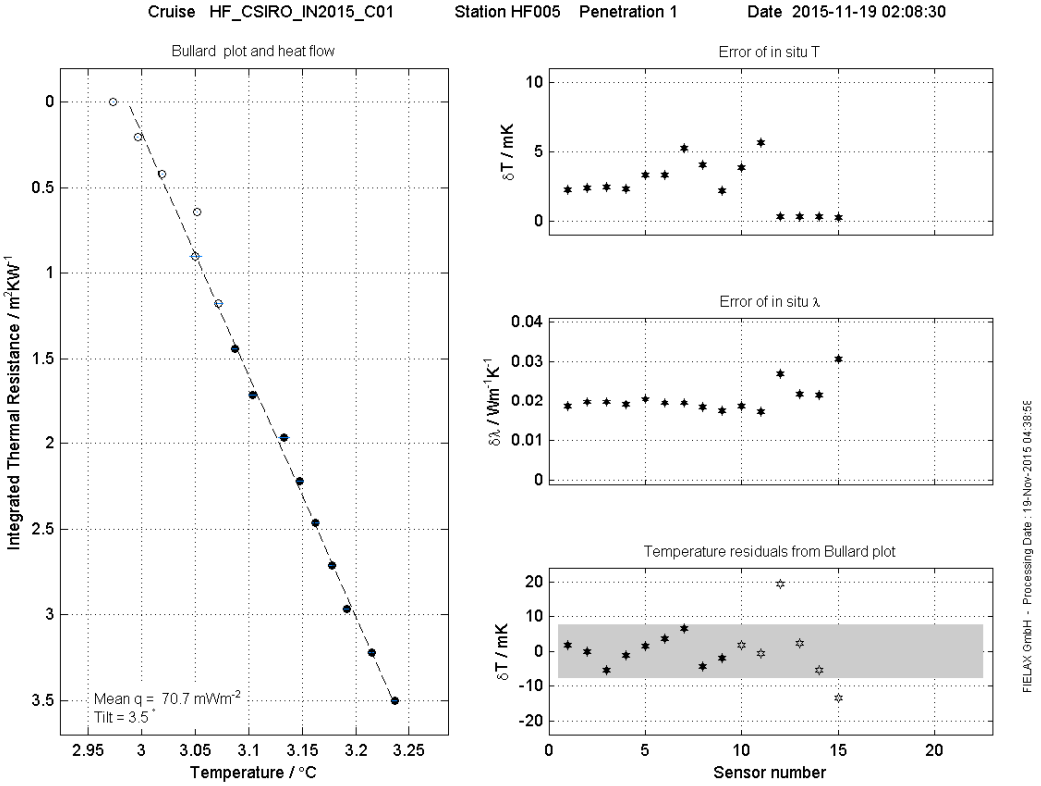

Bullard plot and error estimates

```
Cruise-Transect                          HF_CSIRO_IN2015_C01
Station                                  HF05 (TPRBE_088)
Penetration No.                          1

Date/Time of Penetration                 2015-11-19 02:08:30
Latitude [°]                             34.294436 S
Longitude [°]                            131.384343 E
Depth [m]                                1314

Device ID                                CTM1000
String ID                                T113SD
Heating wire length [m]                  6.05

Pressure [dbar]                          1317.3
Tilt [°]                                 3.5
Bottom water temperature [°C]            2.895
Heating power [J/m]                      812.34

Mean thermal conductivity [W/(m K)]      1.007
Mean thermal resistivity [m K/W]         0.993
Mean thermal diffusivity [1e-07 m^2/s]   3.236
Mean volumetric capacity [MJ/m^3 K]      3.133

Temperature gradient dT/dz [K/m]         0.0718
Heat flow Q [mW/m^2]                     70.73
```

Sens_used #	Sens_depth m	Temp. °C	Bullard depth m^2 K/W	Th. conduct. W/(m K)	Th. res. m K/W	Th. diffus. 1e-07 m^2/s	Vol. capac. MJ/(m^3 K)
15	0.130	2.974	0.000	1.170	0.855	4.037	2.898
14	0.370	2.996	0.205	1.173	0.853	4.048	2.897
13	0.620	3.019	0.420	1.155	0.866	3.957	2.918
12	0.870	3.052	0.642	1.097	0.912	3.665	2.993
11	1.120	3.050	0.902	0.858	1.166	2.546	3.369
10	1.370	3.072	1.176	0.971	1.030	3.053	3.181
9	1.620	3.087	1.443	0.904	1.106	2.748	3.289
8	1.870	3.104	1.712	0.957	1.045	2.989	3.203
7	2.120	3.133	1.968	0.995	1.005	3.166	3.144
6	2.370	3.148	2.218	1.006	0.994	3.217	3.127
5	2.620	3.163	2.462	1.047	0.955	3.415	3.067
4	2.870	3.178	2.712	0.957	1.045	2.986	3.204
3	3.120	3.191	2.968	0.996	1.004	3.169	3.143
2	3.370	3.215	3.221	0.979	1.022	3.088	3.169
1	3.620	3.236	3.498	0.836	1.196	2.459	3.400

8.9 Cruise IN2015_C01 Station HF02 (TPRBE_109)

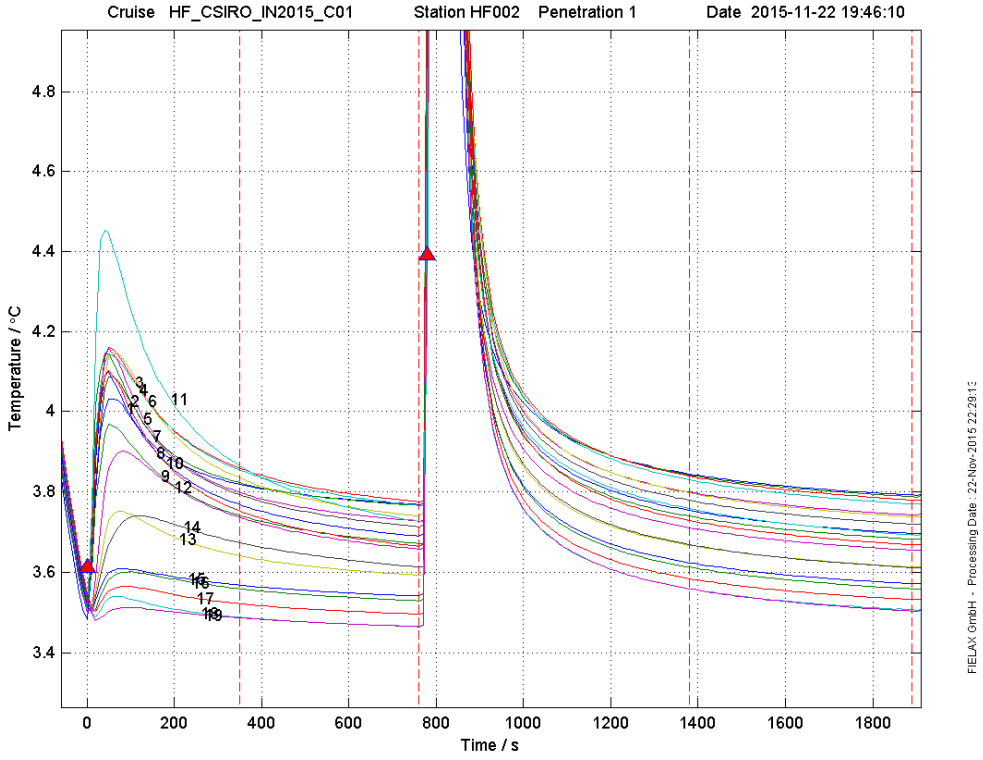

Sediment temperatures

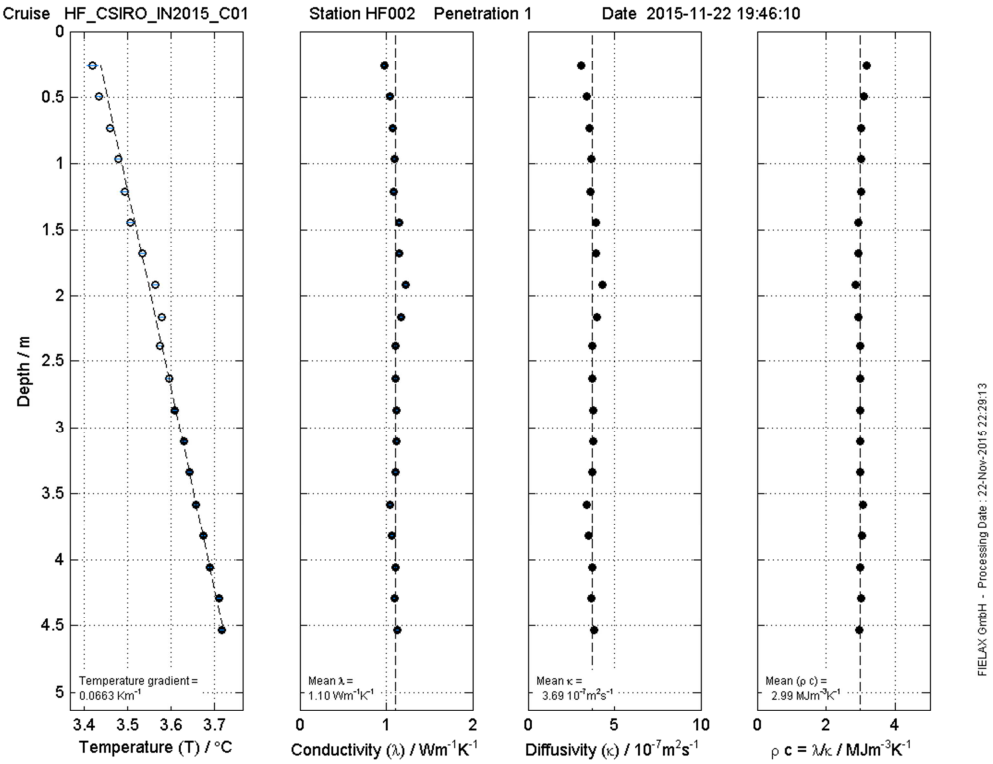

Sediment thermal properties

IN2015_C01 Station HF02 (TPRBE_109) Pen 1

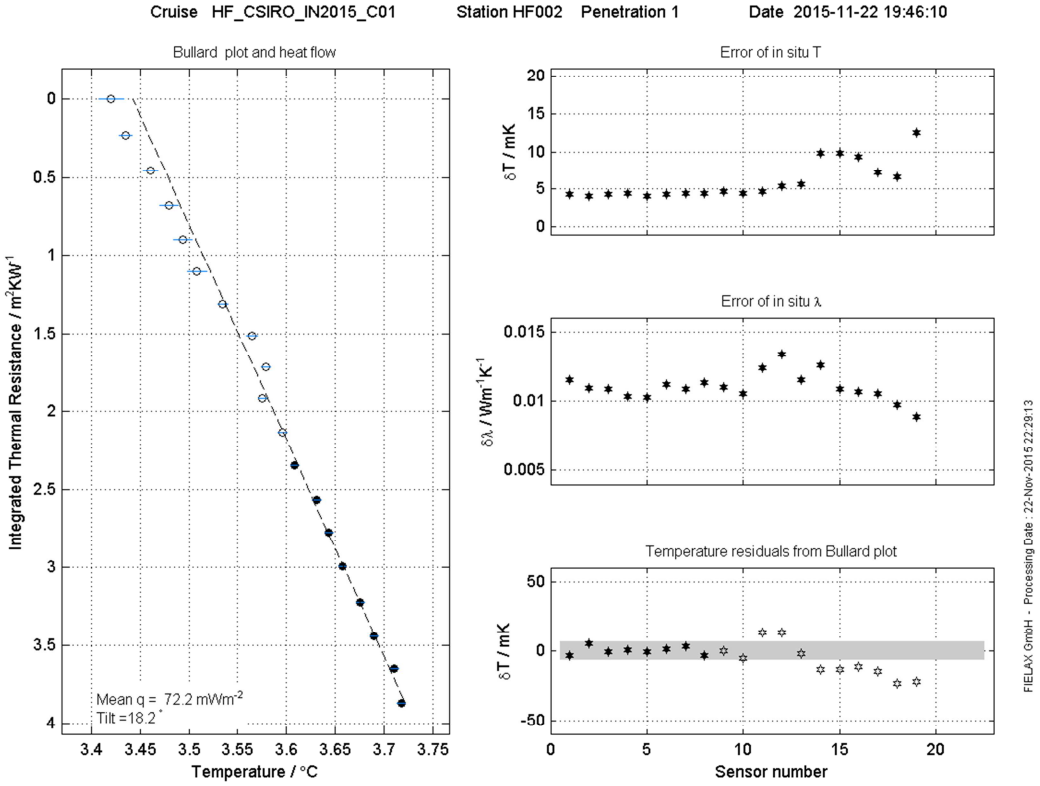

Bullard plot and error estimates

Cruise-Transect	HF_CSIRO_IN2015_C01
Station	HF002 (TPRBE_109)
Penetration No.	1
Date/Time of Penetration	2015-11-22 19:46:10
Latitude [°]	34.7571 S
Longitude [°]	132.1979 E
Depth [m]	1137.00
Device ID	CTM1000
String ID	T113SD
Heating wire length [m]	6.05
Pressure [dbar]	1136.4
Tilt [°]	18.2
Bottom water temperature [°C]	3.397
Heating power [J/m]	807.59
Mean thermal conductivity [W/(m K)]	1.104
Mean thermal resistivity [m K/W]	0.906
Mean thermal diffusivity [1e-07 m^2/s]	3.694
Mean volumetric capacity [MJ/m^3 K]	2.993
Temperature gradient dT/dz [K/m]	0.0663
Heat flow Q [mW/m^2]	72.25

Sens_used #	Sens_depth m	Temp. °C	Bullard depth m^2 K/W	Th. conduct. W/(m K)	Th. res. m K/W	Th. diffus. 1e-07 m^2/s	Vol. capac. MJ/(m^3 K)
19	0.260	3.420	0.000	0.974	1.027	3.066	3.177
18	0.490	3.435	0.229	1.039	0.963	3.373	3.079
17	0.730	3.460	0.455	1.079	0.927	3.573	3.020
16	0.970	3.480	0.676	1.092	0.916	3.637	3.003
15	1.210	3.494	0.897	1.086	0.921	3.606	3.011
14	1.440	3.508	1.103	1.151	0.869	3.934	2.926
13	1.680	3.535	1.311	1.150	0.870	3.927	2.928
12	1.920	3.565	1.513	1.225	0.816	4.310	2.842
11	2.160	3.579	1.714	1.168	0.856	4.001	2.919
10	2.390	3.575	1.917	1.105	0.905	3.693	2.992
9	2.630	3.596	2.134	1.105	0.905	3.699	2.989
8	2.870	3.609	2.349	1.120	0.893	3.772	2.970
7	3.110	3.631	2.564	1.117	0.895	3.756	2.975
6	3.340	3.644	2.770	1.112	0.900	3.725	2.984
5	3.580	3.658	2.993	1.047	0.956	3.408	3.071
4	3.820	3.676	3.221	1.065	0.939	3.495	3.046
3	4.060	3.690	3.442	1.107	0.904	3.702	2.989
2	4.290	3.711	3.650	1.099	0.910	3.666	2.997
1	4.530	3.718	3.865	1.133	0.883	3.837	2.951

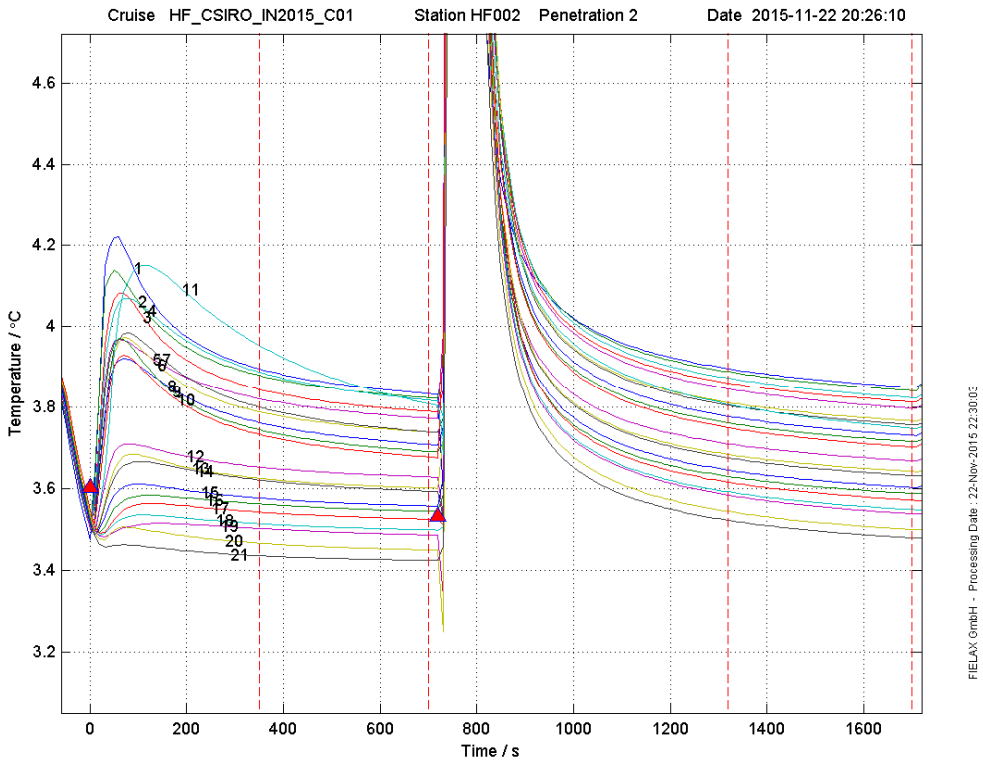

Sediment temperatures

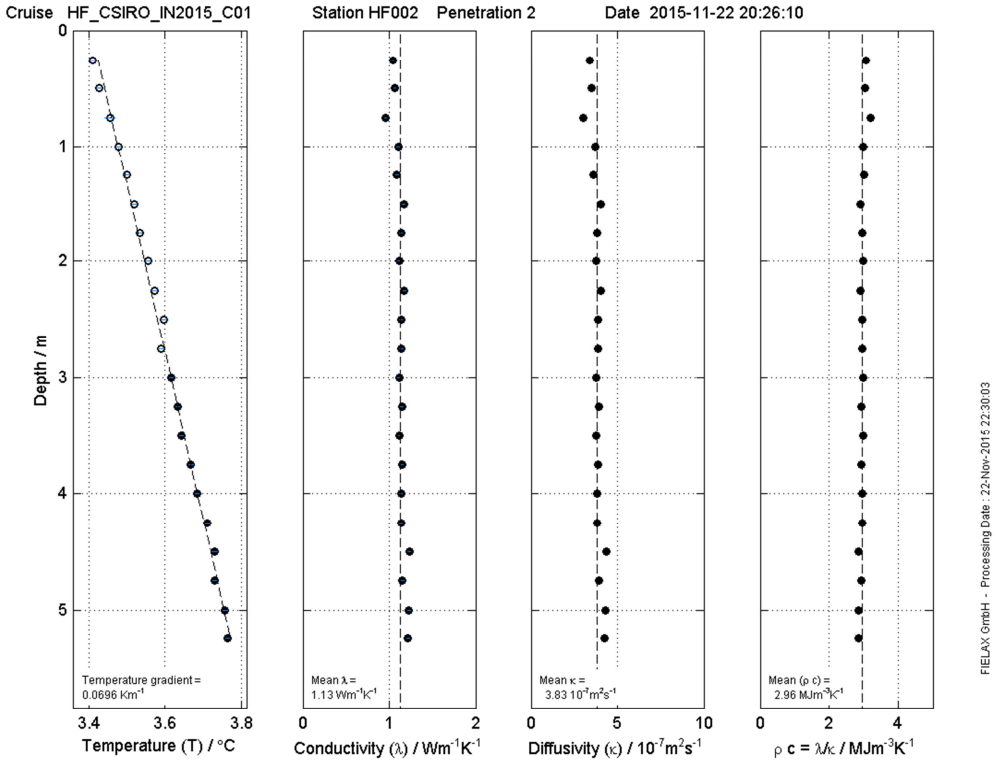

Sediment temperatures

IN2015_C01 Station HF02 (TPRBE_109) Pen 2

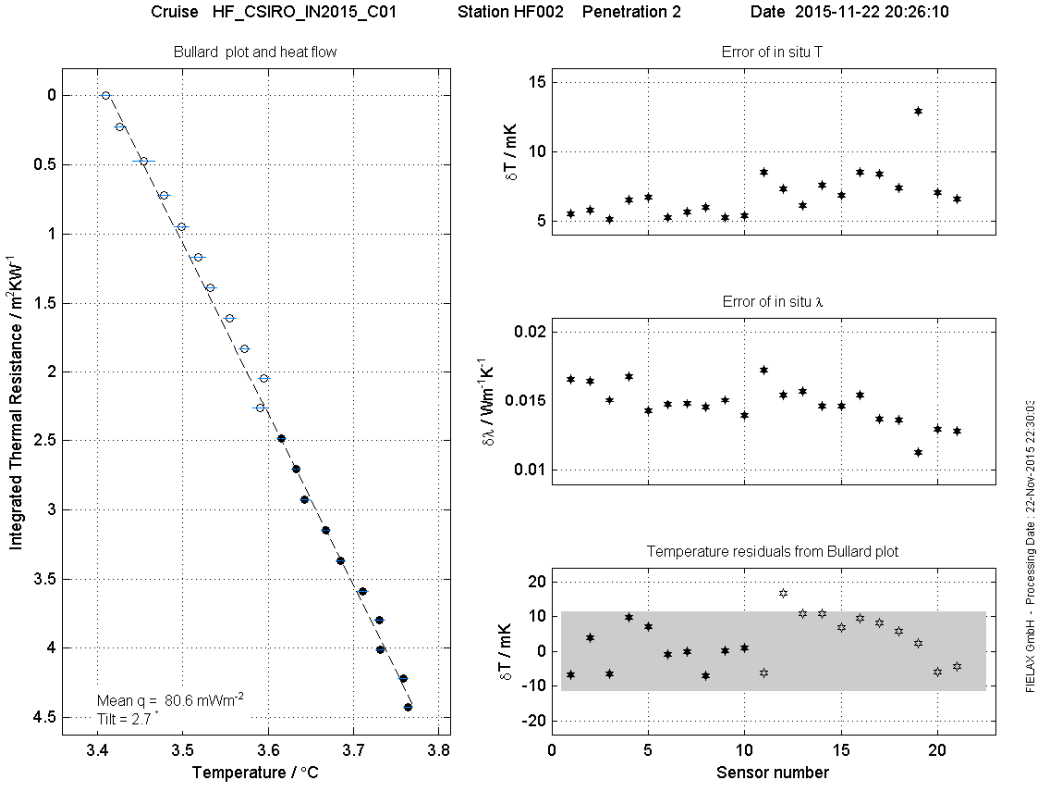

Bullard plot and error estimates

Cruise-Transect	HF_CSIRO_IN2015_C01
Station	HF002
Penetration No.	2
Date/Time of Penetration	2015-11-22 20:26:10
Latitude [°]	34.7571 S
Longitude [°]	132.1979 E
Depth [m]	1137.00
Device ID	CTM1000
String ID	T113SD
Heating wire length [m]	6.05
Pressure [dbar]	1136.5
Tilt [°]	2.7
Bottom water temperature [°C]	3.386
Heating power [J/m]	779.72
Mean thermal conductivity [W/(m K)]	1.131
Mean thermal resistivity [m K/W]	0.884
Mean thermal diffusivity [1e-07 m^2/s]	3.833
Mean volumetric capacity [MJ/m^3 K]	2.958
Temperature gradient dT/dz [K/m]	0.0696
Heat flow Q [mW/m^2]	80.64

Sens_used #	Sens_depth m	Temp. °C	Bullard depth m^2 K/W	Th. conduct. W/(m K)	Th. res. m K/W	Th. diffus. 1e-07 m^2/s	Vol. capac. MJ/(m^3 K)
21	0.260	3.410	0.000	1.043	0.959	3.393	3.073
20	0.500	3.427	0.228	1.065	0.939	3.504	3.041
19	0.750	3.455	0.475	0.959	1.043	2.997	3.200
18	1.000	3.478	0.719	1.104	0.906	3.693	2.988
17	1.250	3.499	0.947	1.089	0.918	3.622	3.007
16	1.500	3.518	1.169	1.166	0.857	4.014	2.906
15	1.750	3.533	1.386	1.134	0.881	3.849	2.947
14	2.000	3.555	1.608	1.115	0.897	3.749	2.974
13	2.250	3.572	1.827	1.173	0.852	4.048	2.899
12	2.500	3.596	2.043	1.138	0.879	3.867	2.943
11	2.750	3.591	2.263	1.140	0.877	3.859	2.954
10	3.000	3.616	2.485	1.115	0.897	3.747	2.977
9	3.250	3.633	2.706	1.148	0.871	3.911	2.935
8	3.500	3.643	2.926	1.119	0.894	3.764	2.972
7	3.750	3.668	3.147	1.145	0.874	3.894	2.940
6	4.000	3.685	3.367	1.135	0.881	3.847	2.951
5	4.250	3.710	3.587	1.135	0.881	3.848	2.950
4	4.500	3.730	3.798	1.232	0.812	4.344	2.836
3	4.750	3.731	4.008	1.153	0.867	3.935	2.929
2	5.000	3.758	4.219	1.228	0.814	4.324	2.840
1	5.250	3.764	4.423	1.219	0.820	4.276	2.851

8.10 Cruise IN2015_C01 Station HF01 (TPRBE_125)

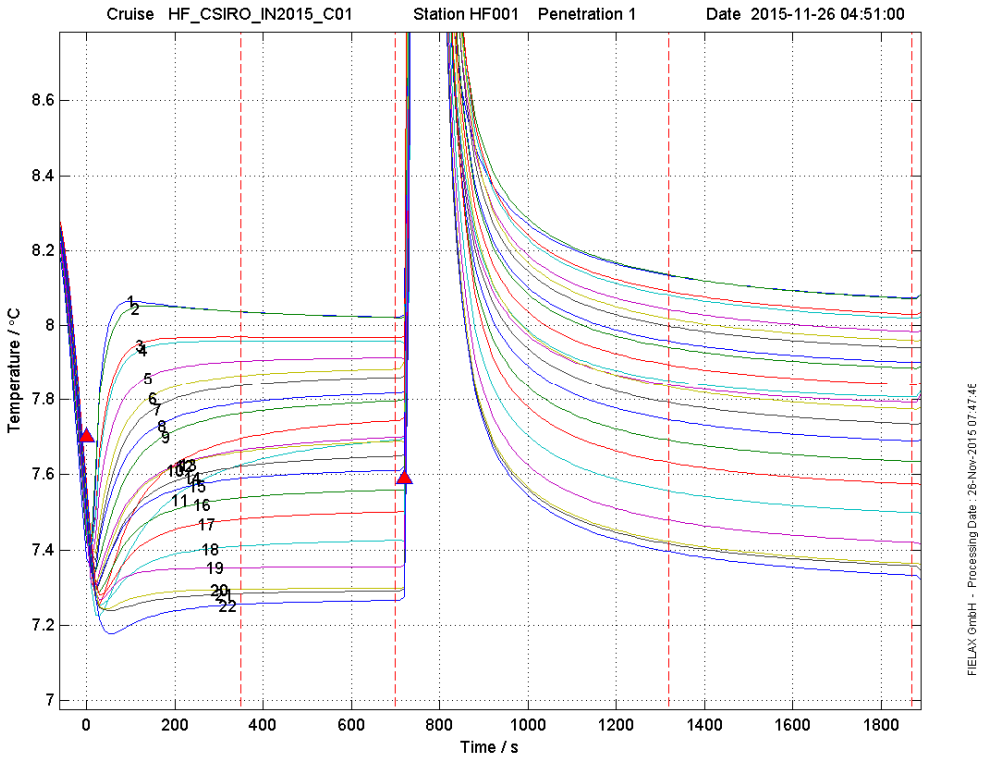

Sediment temperatures

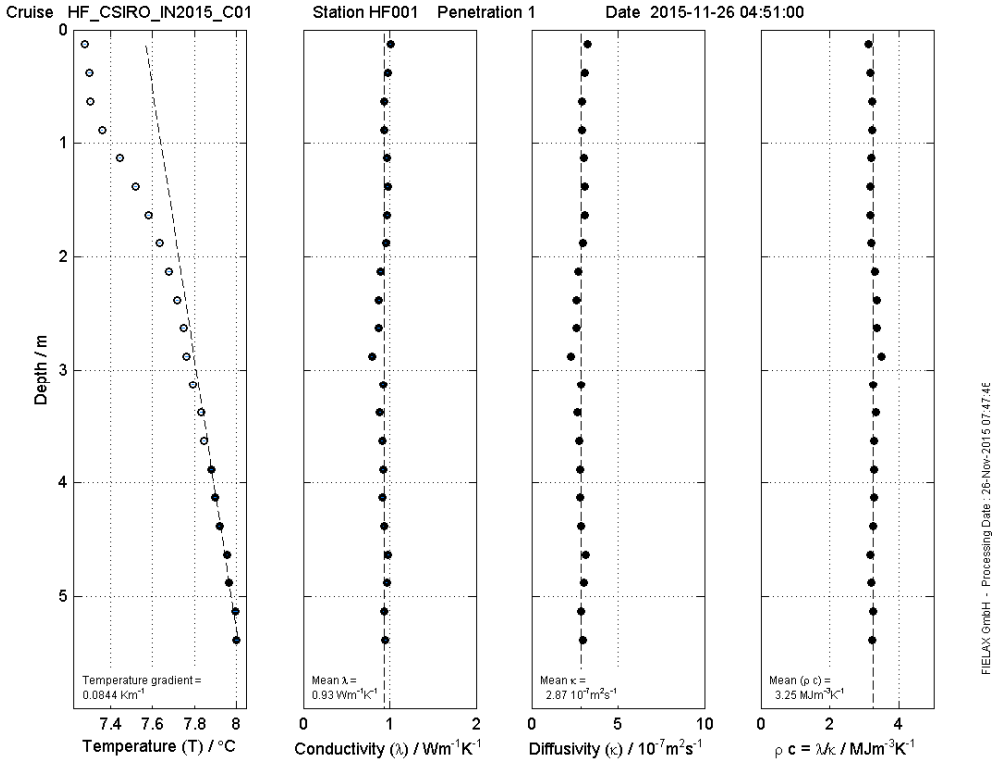

Sediment thermal properties

IN2015_C01 Station HF01 (TPRBE_125) Pen 1

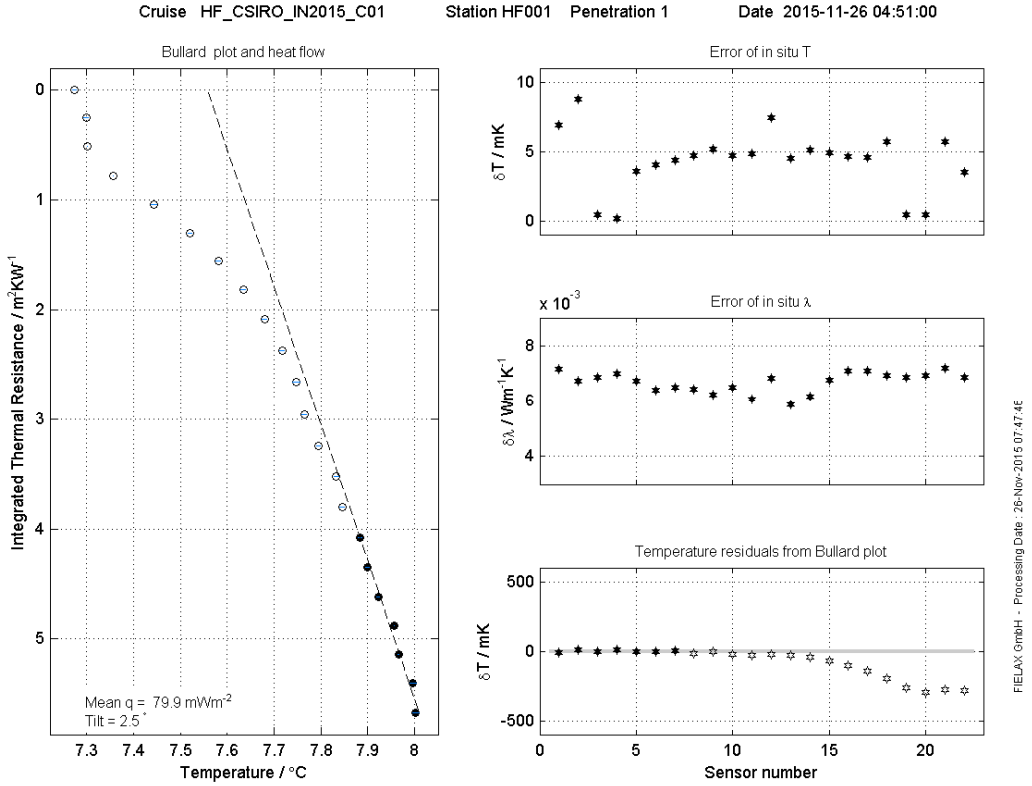

Bullard plot and error estimates

Cruise-Transect	HF_CSIRO_IN2015_C01
Station	HF01 (TPRBE_125
Penetration No.	1
Date/Time of Penetration	2015-11-26 04:51:00
Latitude [°]	34.359189 S
Longitude [°]	132.615812 E
Depth [m]	701.00
Device ID	CTM1000
String ID	T113SD
Heating wire length [m]	6.05
Pressure [dbar]	693.9
Tilt [°]	2.5
Bottom water temperature [°C]	6.825
Heating power [J/m]	841.29
Mean thermal conductivity [W/(m K)]	0.931
Mean thermal resistivity [m K/W]	1.074
Mean thermal diffusivity [1e-07 m^2/s]	2.871
Mean volumetric capacity [MJ/m^3 K]	3.249
Temperature gradient dT/dz [K/m]	0.0844
Heat flow Q [mW/m^2]	79.87

Sens_used #	Sens_depth m	Temp. °C	Bullard depth m^2 K/W	Th. conduct. W/(m K)	Th. res. m K/W	Th. diffus. 1e-07 m^2/s	Vol. capac. MJ/(m^3 K)
22	0.130	7.273	0.000	1.006	0.994	3.219	3.126
21	0.380	7.299	0.253	0.974	1.026	3.068	3.176
20	0.630	7.301	0.514	0.941	1.063	2.914	3.230
19	0.880	7.356	0.779	0.941	1.063	2.914	3.229
18	1.130	7.443	1.042	0.965	1.037	3.022	3.191
17	1.380	7.520	1.299	0.977	1.024	3.079	3.172
16	1.630	7.581	1.556	0.972	1.028	3.059	3.179
15	1.880	7.634	1.815	0.954	1.048	2.975	3.208
14	2.130	7.680	2.086	0.894	1.119	2.700	3.310
13	2.380	7.717	2.369	0.874	1.144	2.613	3.344
12	2.630	7.747	2.655	0.872	1.146	2.605	3.349
11	2.880	7.764	2.956	0.794	1.260	2.266	3.502
10	3.130	7.795	3.249	0.924	1.082	2.837	3.258
9	3.380	7.833	3.525	0.887	1.127	2.671	3.321
8	3.630	7.845	3.803	0.911	1.097	2.779	3.280
7	3.880	7.883	4.076	0.921	1.086	2.821	3.264
6	4.130	7.900	4.348	0.914	1.094	2.792	3.274
5	4.380	7.922	4.619	0.934	1.070	2.883	3.241
4	4.630	7.956	4.880	0.982	1.018	3.104	3.163
3	4.880	7.965	5.137	0.965	1.036	3.024	3.191
2	5.130	7.996	5.401	0.932	1.073	2.871	3.245
1	5.380	8.002	5.667	0.948	1.054	2.948	3.217

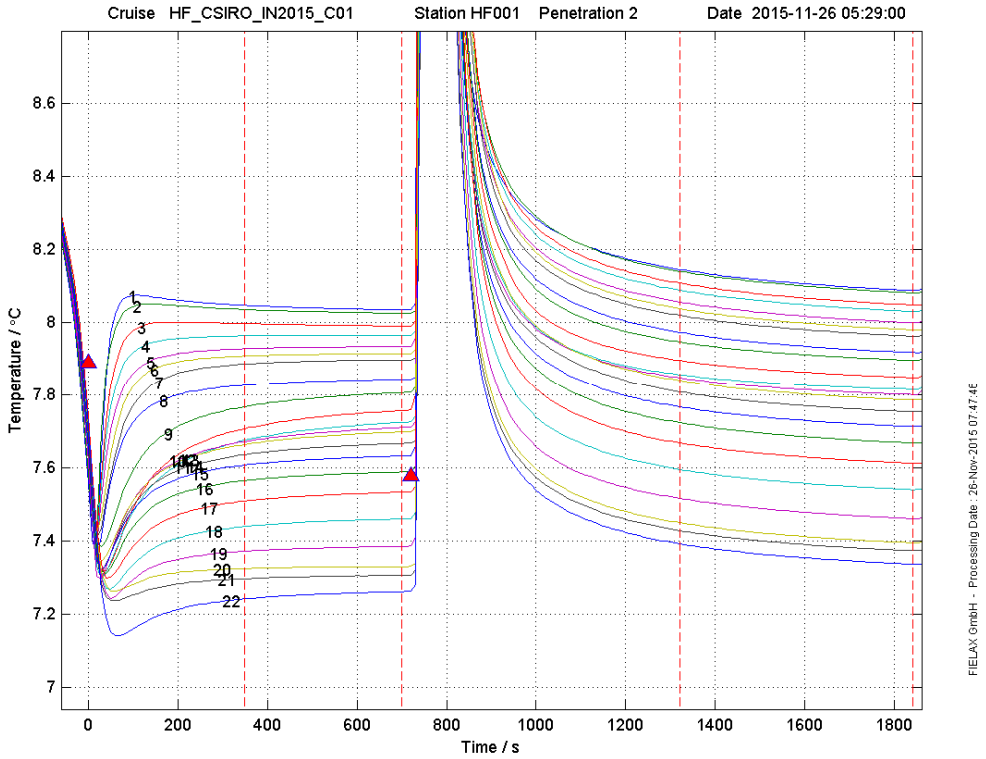

Sediment temperatures

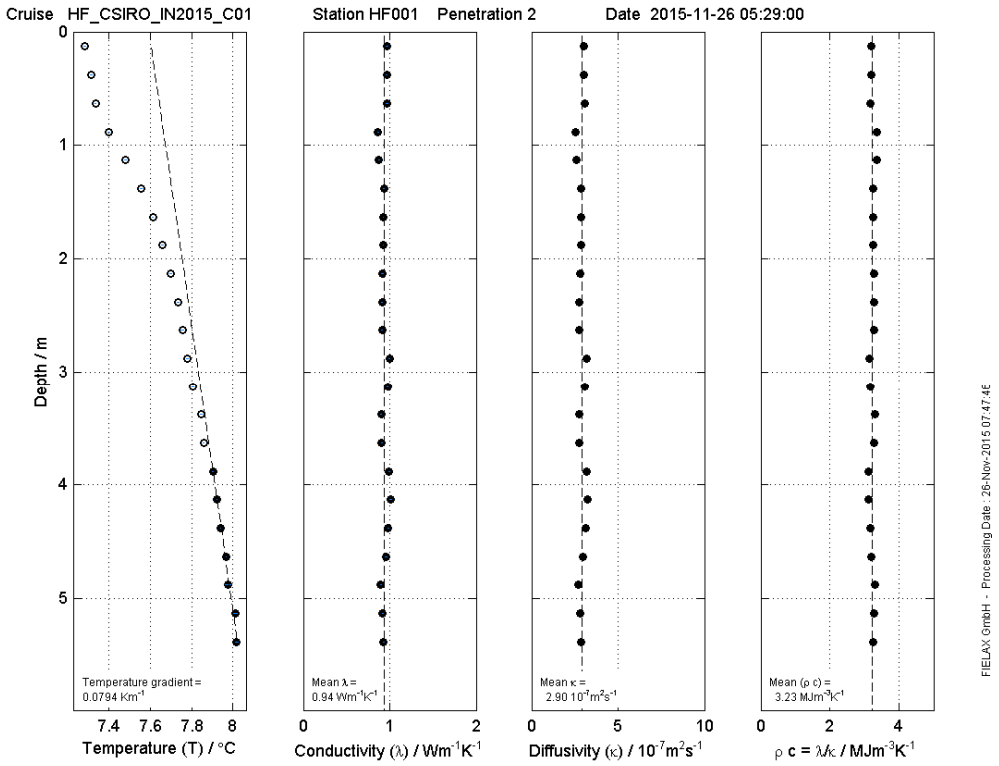

Sediment temperatures

IN2015_C01 Station HF01 (TPRBE_125) Pen 2

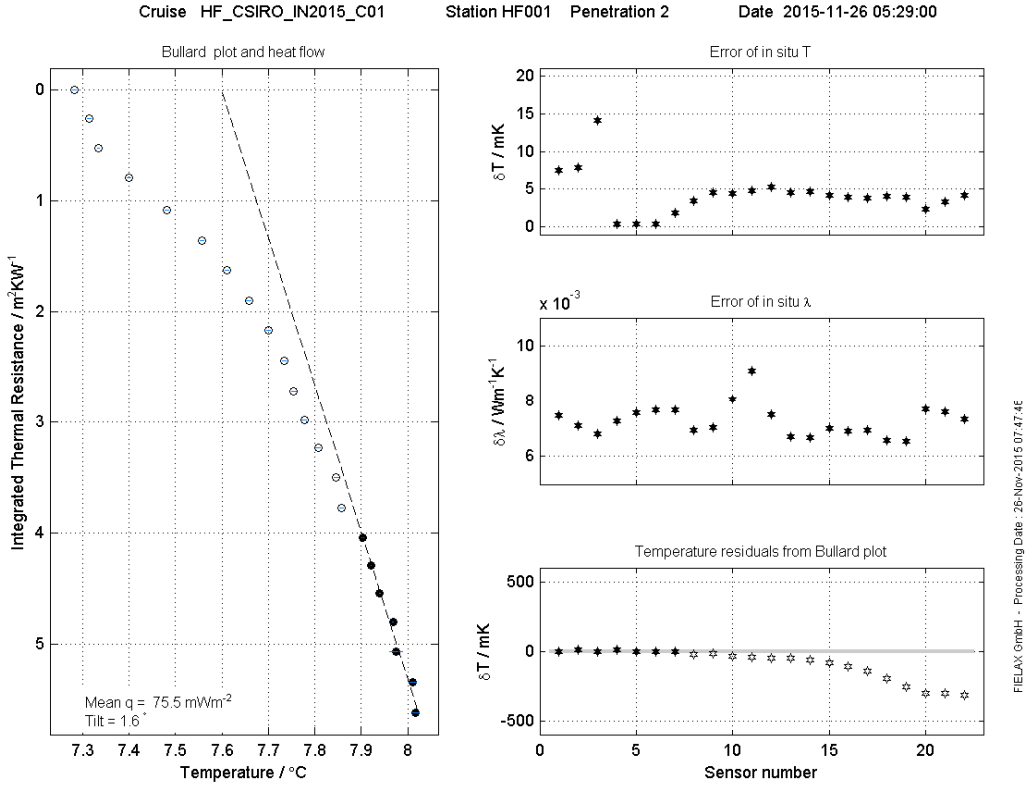

Bullard plot and error estimates

Cruise-Transect	HF_CSIRO_IN2015_C01
Station	HF01 (TPRBE_125
Penetration No.	2
Date/Time of Penetration	2015-11-26 05:29:00
Latitude [°]	34.359189 S
Longitude [°]	132.615812 E
Depth [m]	701.00
Device ID	CTM1000
String ID	T113SD
Heating wire length [m]	6.05
Pressure [dbar]	694.4
Tilt [°]	1.6
Bottom water temperature [°C]	6.830
Heating power [J/m]	809.00
Mean thermal conductivity [W/(m K)]	0.938
Mean thermal resistivity [m K/W]	1.066
Mean thermal diffusivity [1e-07 m^2/s]	2.905
Mean volumetric capacity [MJ/m^3 K]	3.233
Temperature gradient dT/dz [K/m]	0.0794
Heat flow Q [mW/m^2]	75.54

Sens_used #	Sens_depth m	Temp. °C	Bullard depth m^2 K/W	Th. conduct. W/(m K)	Th. res. m K/W	Th. diffus. 1e-07 m^2/s	Vol. capac. MJ/(m^3 K)
22	0.130	7.282	0.000	0.970	1.031	3.046	3.183
21	0.380	7.314	0.258	0.966	1.036	3.027	3.190
20	0.630	7.335	0.517	0.967	1.034	3.049	3.172
19	0.880	7.399	0.791	0.863	1.159	2.565	3.363
18	1.130	7.481	1.079	0.874	1.144	2.615	3.343
17	1.380	7.557	1.356	0.932	1.073	2.874	3.244
16	1.630	7.612	1.625	0.927	1.079	2.850	3.253
15	1.880	7.658	1.894	0.930	1.075	2.865	3.247
14	2.130	7.701	2.166	0.914	1.094	2.790	3.275
13	2.380	7.734	2.439	0.912	1.097	2.781	3.279
12	2.630	7.755	2.714	0.912	1.097	2.779	3.280
11	2.880	7.778	2.976	0.996	1.004	3.169	3.142
10	3.130	7.807	3.230	0.976	1.025	3.074	3.174
9	3.380	7.846	3.497	0.901	1.110	2.731	3.298
8	3.630	7.858	3.773	0.907	1.102	2.761	3.286
7	3.880	7.903	4.037	0.995	1.005	3.205	3.103
6	4.130	7.922	4.286	1.012	0.988	3.247	3.118
5	4.380	7.940	4.537	0.983	1.017	3.107	3.163
4	4.630	7.968	4.794	0.956	1.046	2.985	3.204
3	4.880	7.975	5.064	0.898	1.114	2.720	3.301
2	5.130	8.011	5.340	0.918	1.089	2.812	3.266
1	5.380	8.018	5.611	0.928	1.078	2.854	3.251

8.11 Cruise IN2015_C01 Station VSM03 (TPRBE_126)

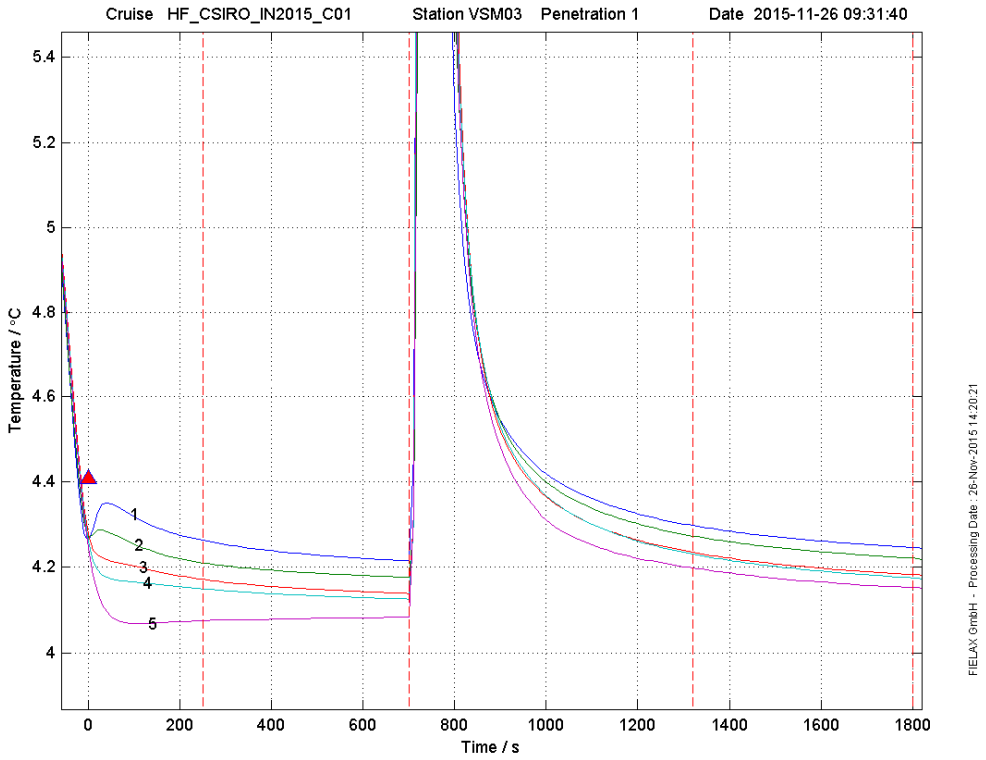

Sediment temperatures

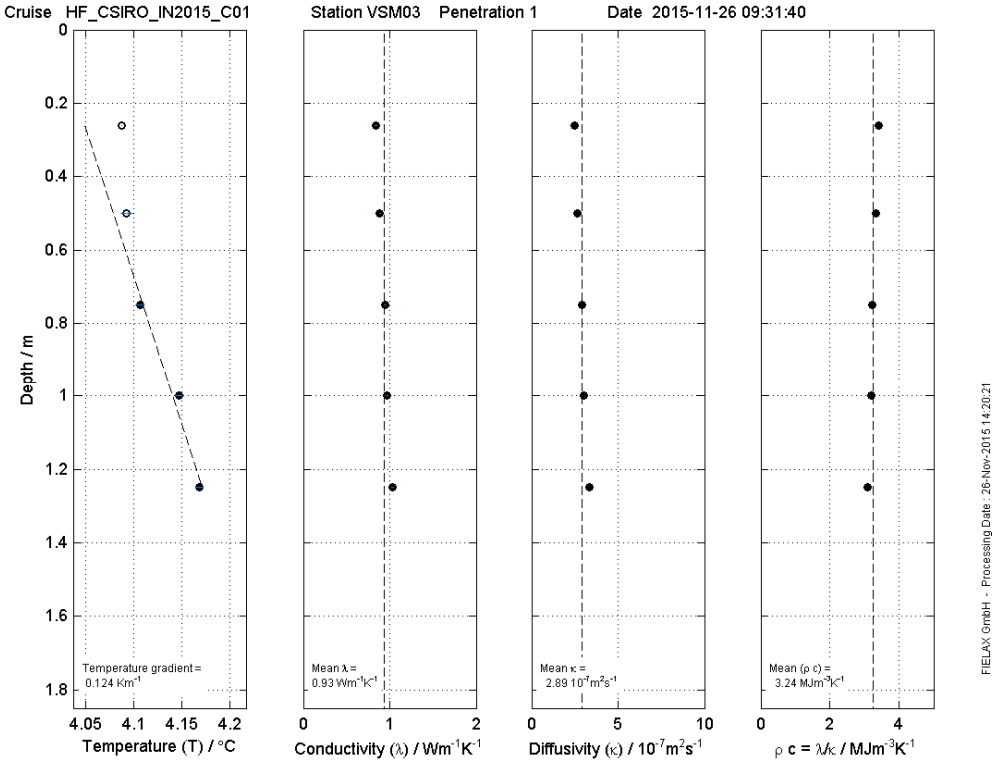

Sediment thermal properties

IN2015_C01 Station VSM03 (TPRBE_126) Pen 1

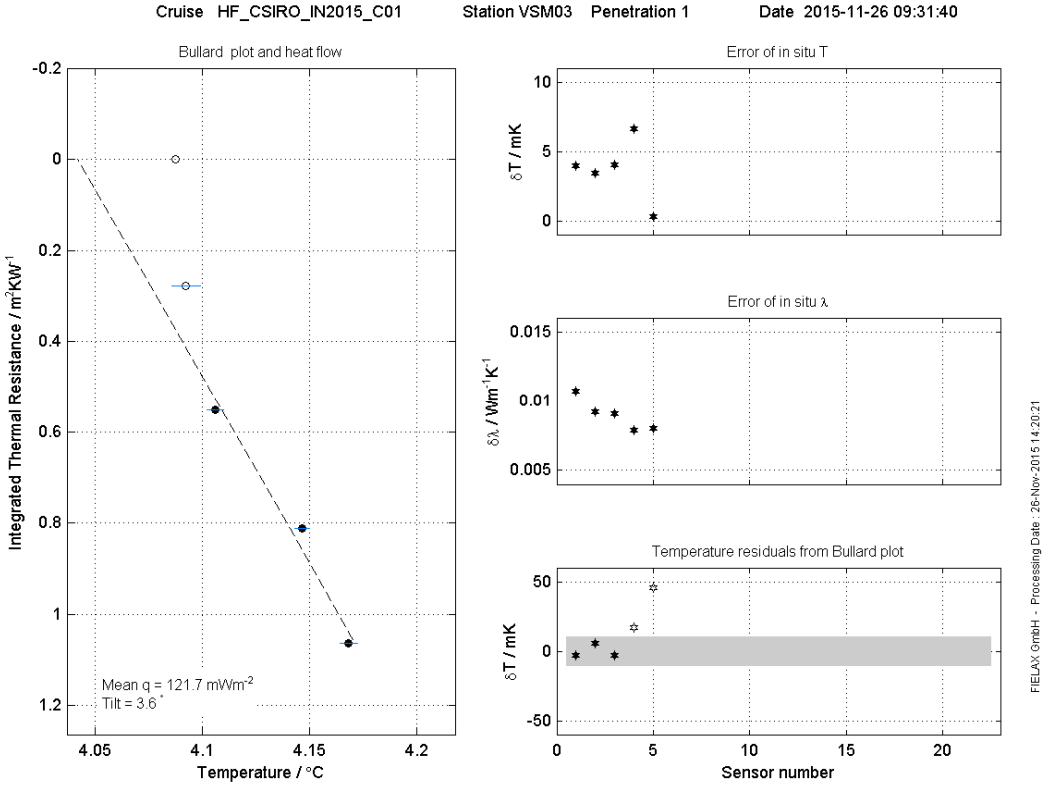

Bullard plot and error estimates

```
Cruise-Transect                          HF_CSIRO_IN2015_C01
Station                                  VSM03
Penetration No.                          1

Date/Time of Penetration                 2015-11-26 09:31:40
Latitude [°]                             34.704162 S
Longitude [°]                            132.524754 E
Depth [m]                                996.00

Device ID                                CTM1000
String ID                                T113SD
Heating wire length [m]                  6.05

Pressure [dbar]                          989.6
Tilt [°]                                 3.6
Bottom water temperature [°C]            4.120
Heating power [J/m]                      799.37

Mean thermal conductivity [W/(m K)]      0.934
Mean thermal resistivity [m K/W]         1.071
Mean thermal diffusivity [1e-07 m^2/s]   2.888
Mean volumetric capacity [MJ/m^3 K]      3.245

Temperature gradient dT/dz [K/m]          0.124
Heat flow Q [mW/m^2]                     121.71
```

Sens_used #	Sens_depth m	Temp. °C	Bullard depth m^2 K/W	Th. conduct. W/(m K)	Th. res. m K/W	Th. diffus. 1e-07 m^2/s	Vol. capac. MJ/(m^3 K)
5	0.260	4.087	0.000	0.838	1.193	2.461	3.405
4	0.500	4.092	0.278	0.887	1.127	2.673	3.319
3	0.750	4.106	0.551	0.947	1.056	2.939	3.220
2	1.000	4.147	0.813	0.966	1.035	3.029	3.189
1	1.250	4.168	1.063	1.032	0.969	3.339	3.090

8.12 Cruise IN2015_C01 Station VSM03 (TPRBE_127)

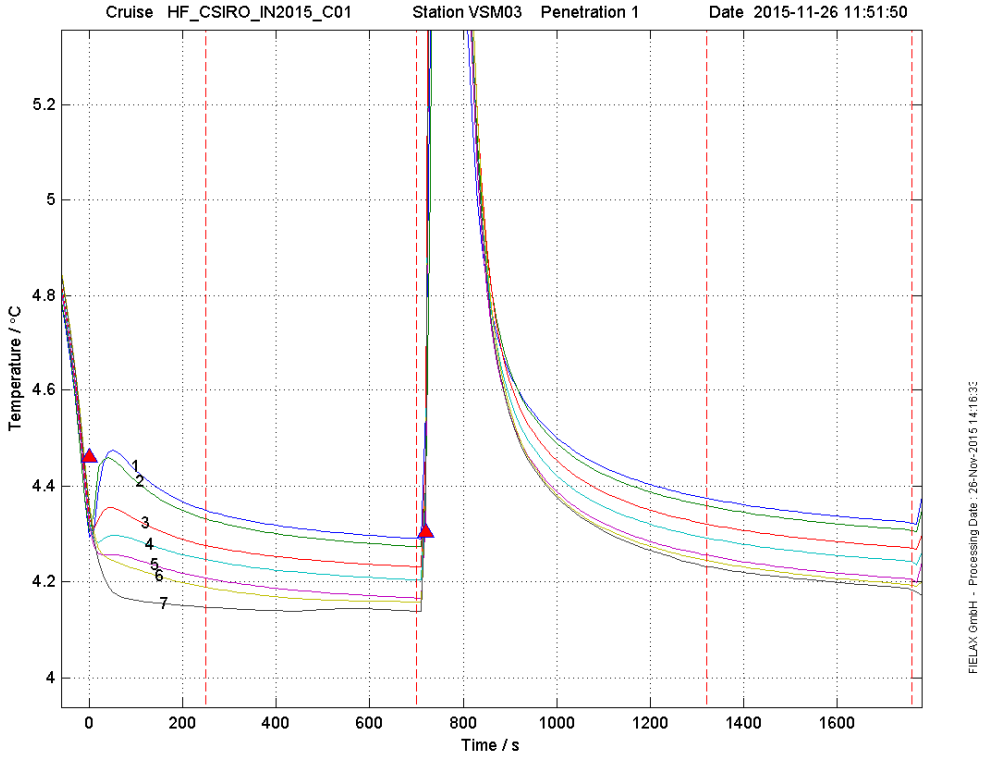

Sediment temperatures

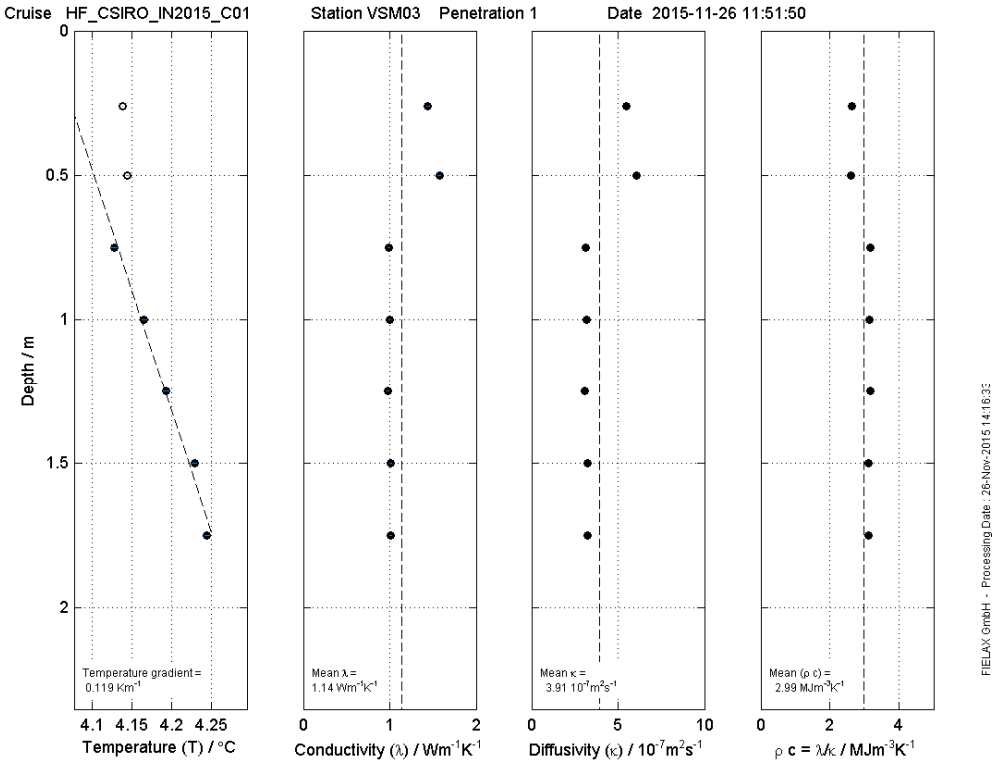

Sediment thermal properties

IN2015_C01 Station VSM03 (TPRBE_127) Pen 1

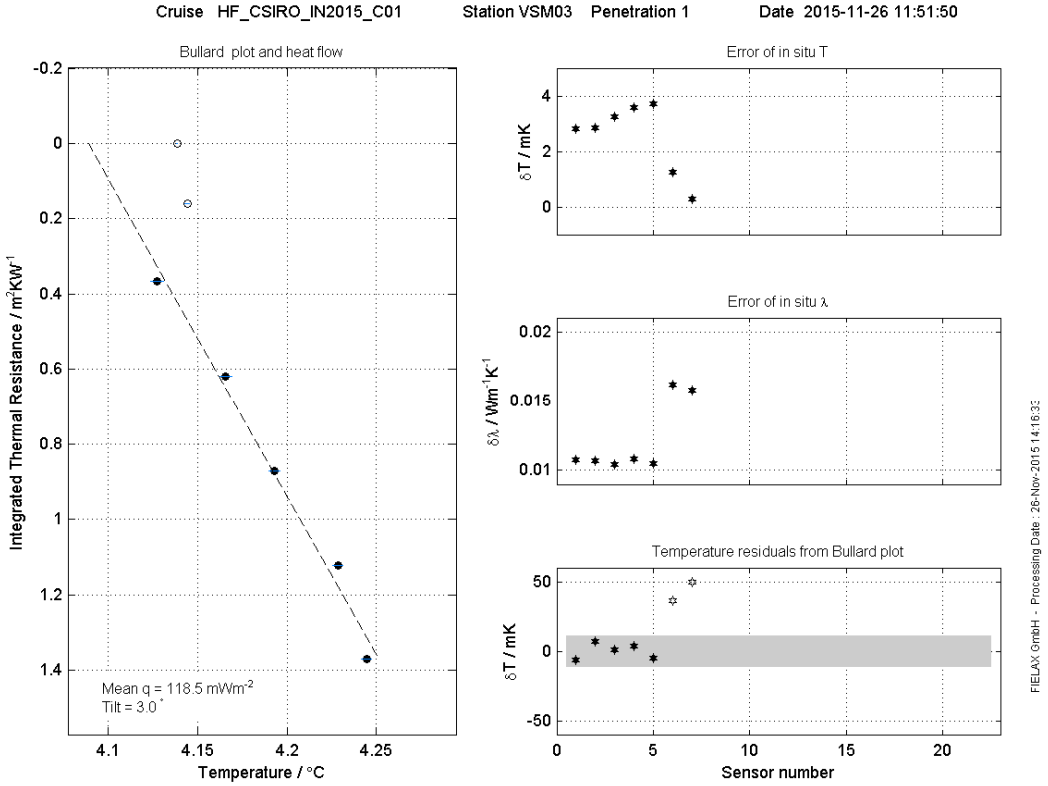

Bullard plot and error estimates

Cruise-Transect	HF_CSIRO_IN2015_C01
Station	VSM03
Penetration No.	1
Date/Time of Penetration	2015-11-26 11:51:50
Latitude [°]	34.704162 S
Longitude [°]	132.524754 E
Depth [m]	996.00
Device ID	CTM1000
String ID	T113SD
Heating wire length [m]	6.05
Pressure [dbar]	991.1
Tilt [°]	3.0
Bottom water temperature [°C]	4.086
Heating power [J/m]	767.79
Mean thermal conductivity [W/(m K)]	1.142
Mean thermal resistivity [m K/W]	0.876
Mean thermal diffusivity [1e-07 m^2/s]	3.909
Mean volumetric capacity [MJ/m^3 K]	2.993
Temperature gradient dT/dz [K/m]	0.119
Heat flow Q [mW/m^2]	118.51

Sens_used #	Sens_depth m	Temp. °C	Bullard depth m^2 K/W	Th. conduct. W/(m K)	Th. res. m K/W	Th. diffus. 1e-07 m^2/s	Vol. capac. MJ/(m^3 K)
7	0.260	4.138	0.000	1.439	0.695	5.463	2.634
6	0.500	4.144	0.159	1.572	0.636	6.051	2.598
5	0.750	4.127	0.366	0.984	1.016	3.114	3.161
4	1.000	4.165	0.618	0.998	1.002	3.178	3.140
3	1.250	4.193	0.871	0.981	1.019	3.100	3.165
2	1.500	4.229	1.122	1.007	0.993	3.222	3.126
1	1.750	4.245	1.370	1.009	0.991	3.230	3.124

9 Appendix 3: Water temperatures

All penetration sites are presented in appending figures and data:

9.1 Cruise IN2015_C01 Station HFTest (TPRBE_006)

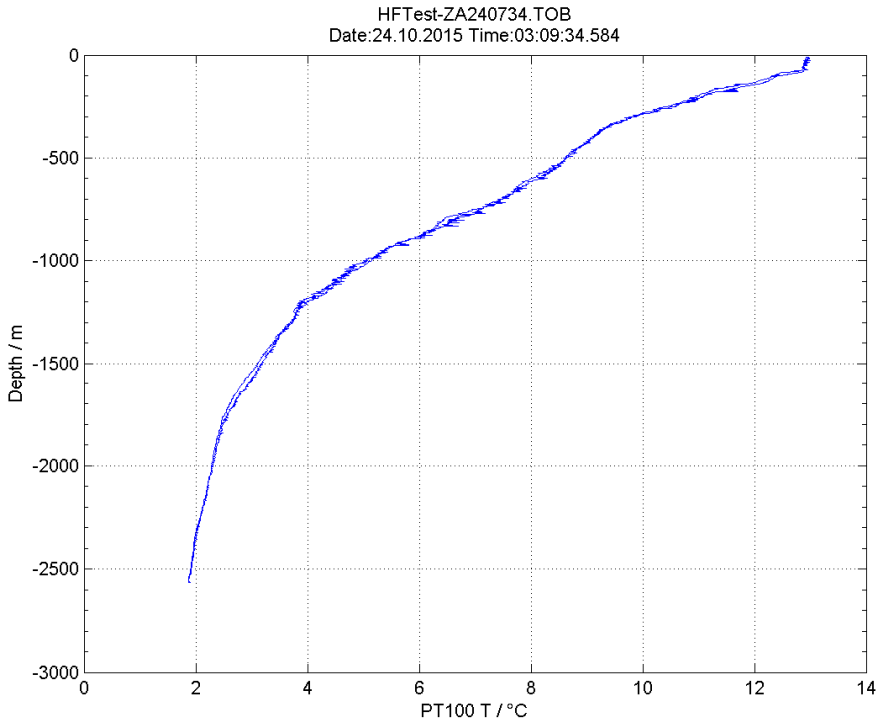

9.2 Cruise IN2015_C01 Station HF08 (TPRBE_030)

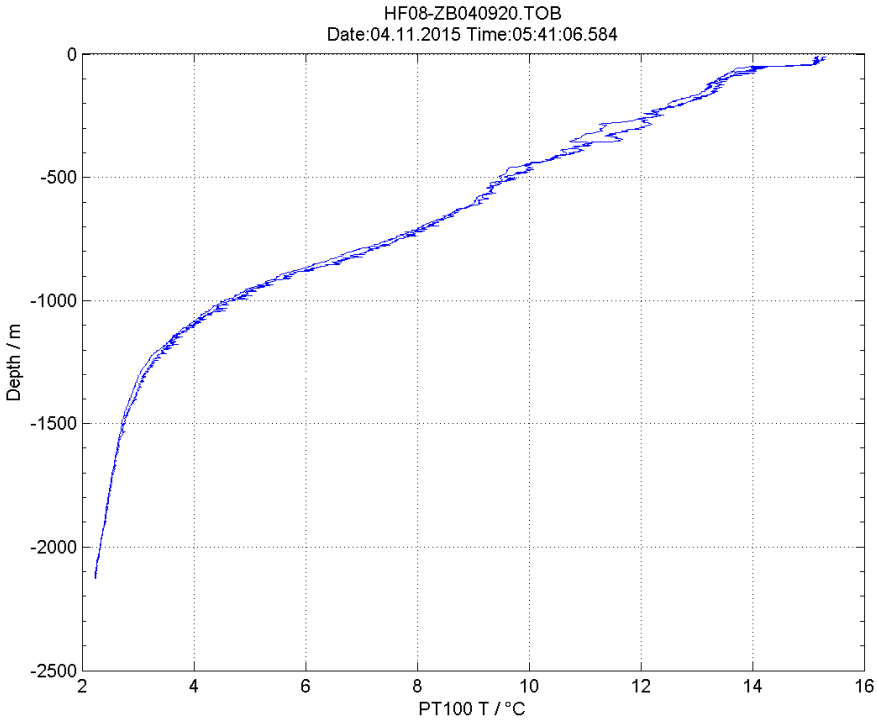

9.3 Cruise IN2015_C01 Station HF07 (TPRBE_046)

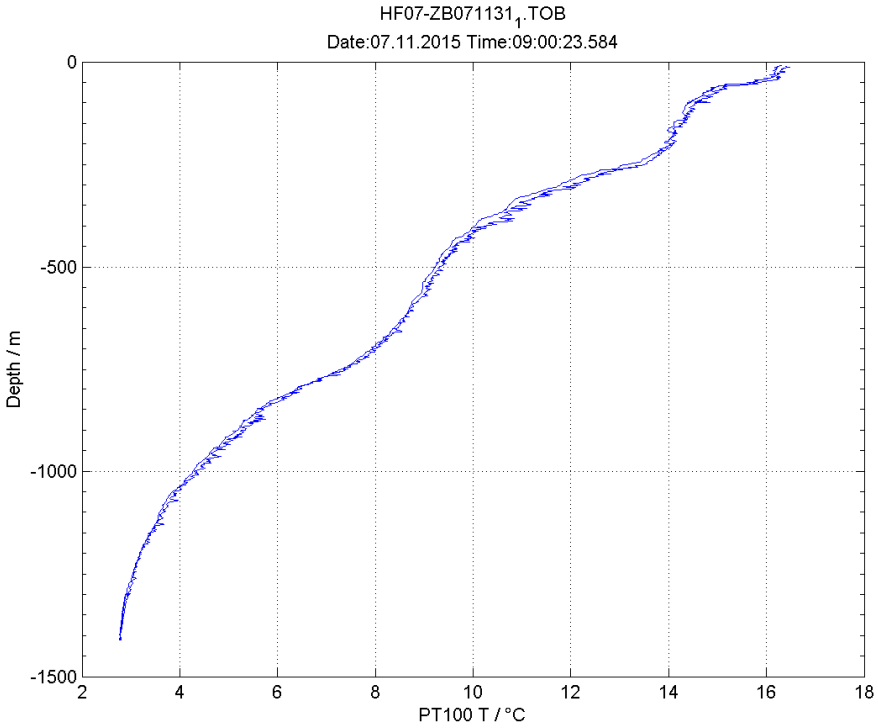

9.4 Cruise IN2015_C01 Station HF04 (TPRBE_047)

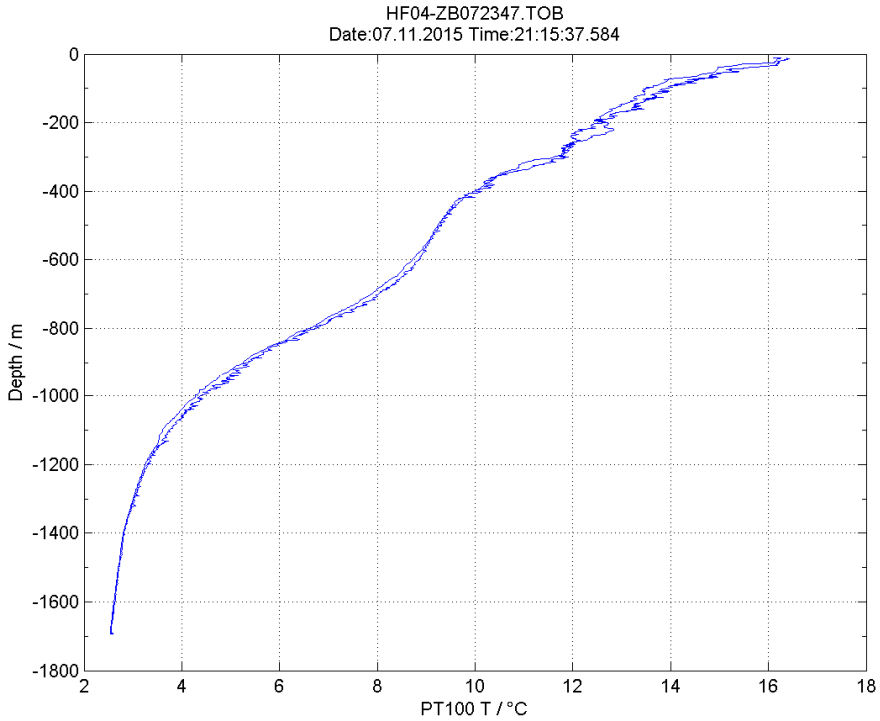

9.5 Cruise IN2015_C01 Station HF03 (TPRBE_048)

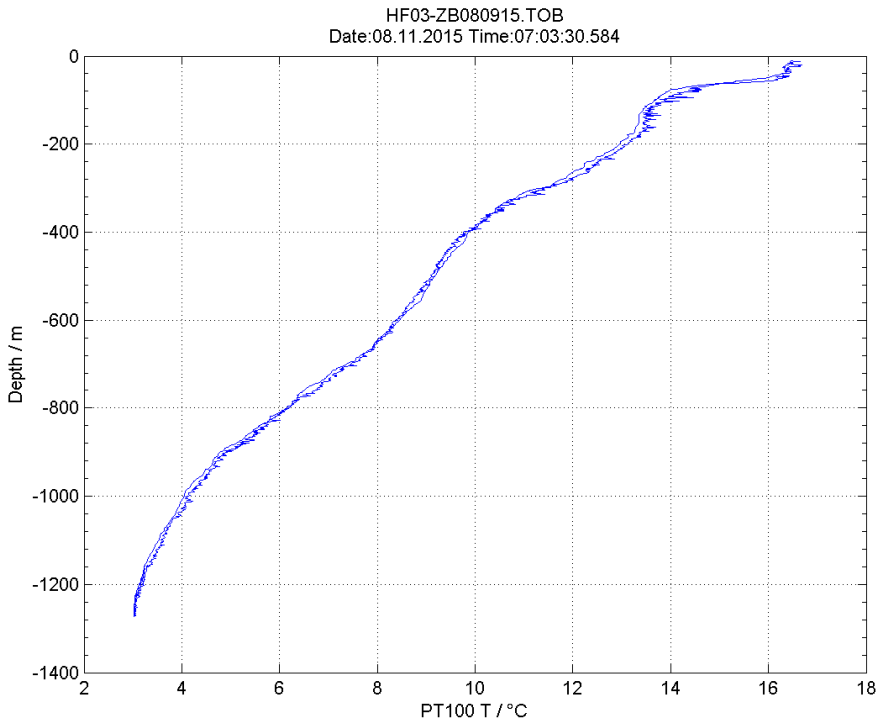

9.6 Cruise IN2015_C01 Station HF03 (TPRBE_049)

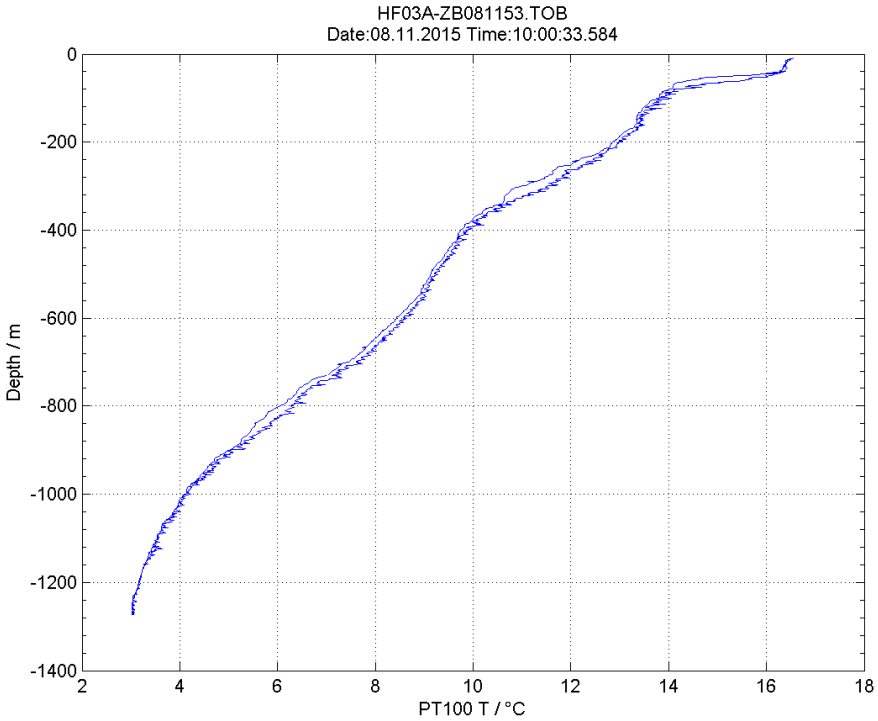

9.7 Cruise IN2015_C01 Station HF06 (TPRBE_056)

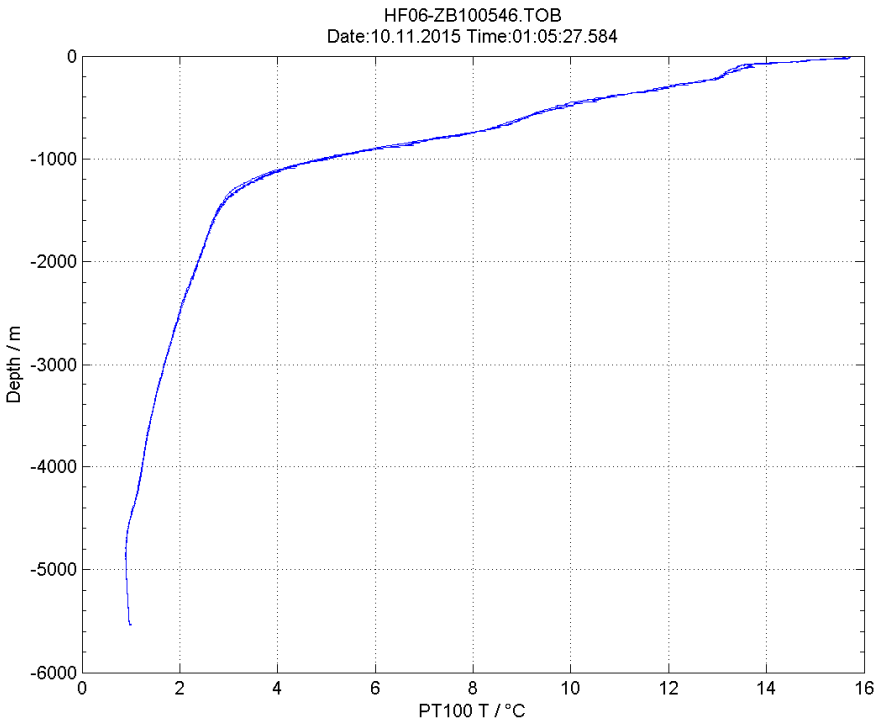

9.8 Cruise IN2015_C01 Station HF05 (TPRBE_088)

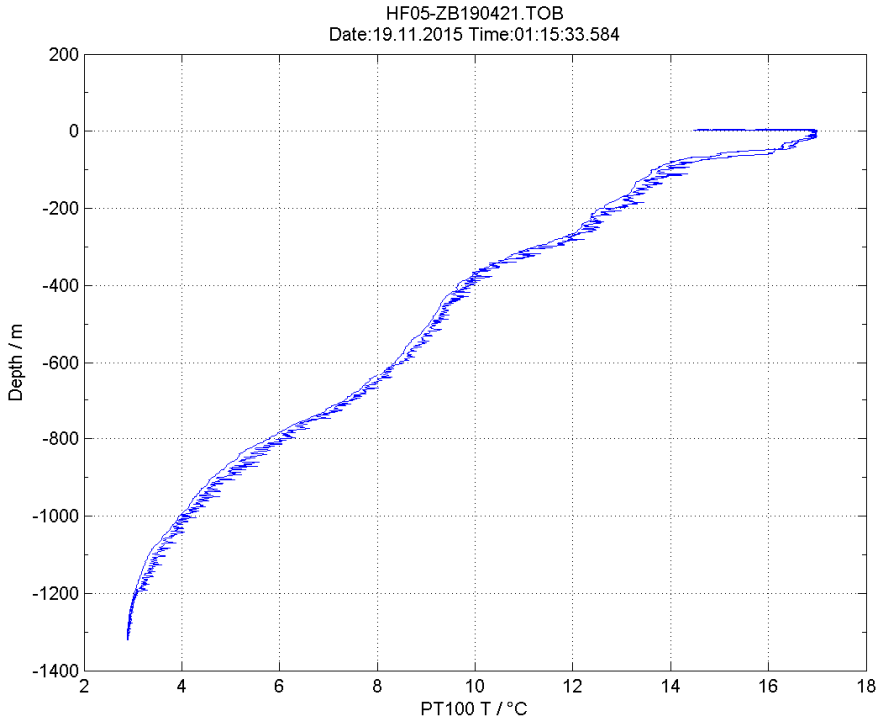

9.9 Cruise IN2015_C01 Station HF02 (TPRBE_109)

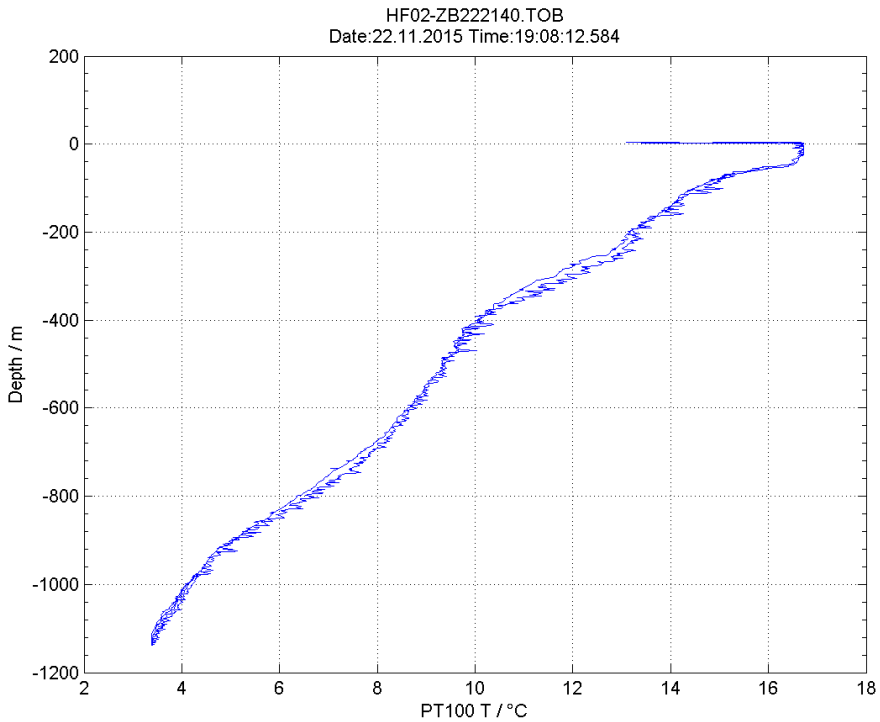

9.10 Cruise IN2015_C01 Station HF01 (TPRBE_125)

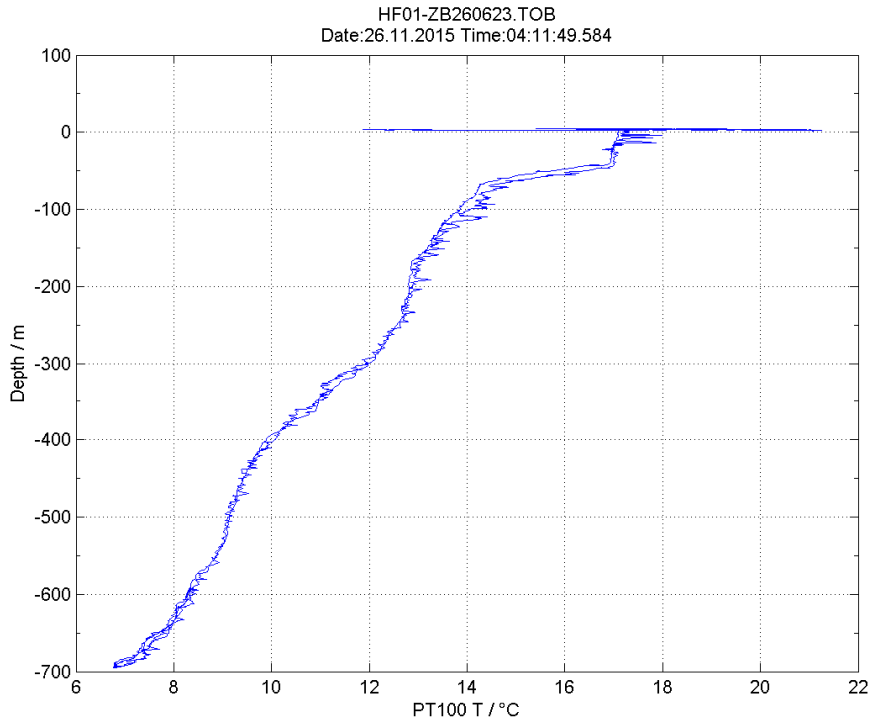

9.11 Cruise IN2015_C01 Station VSM03 (TPRBE_126)

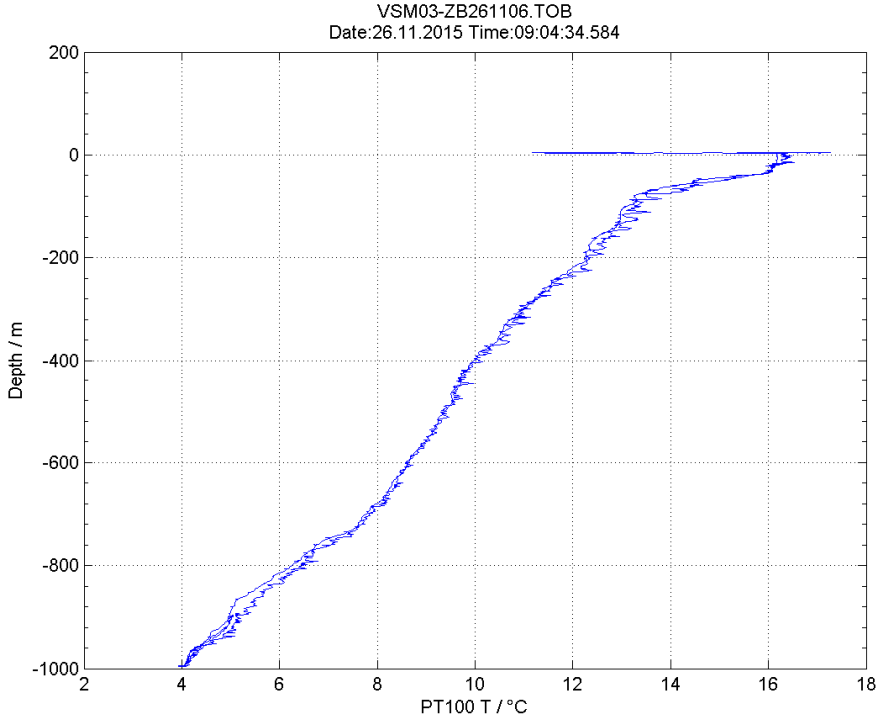

9.12 Cruise IN2015_C01 Station VSM03 (TPRBE_127)

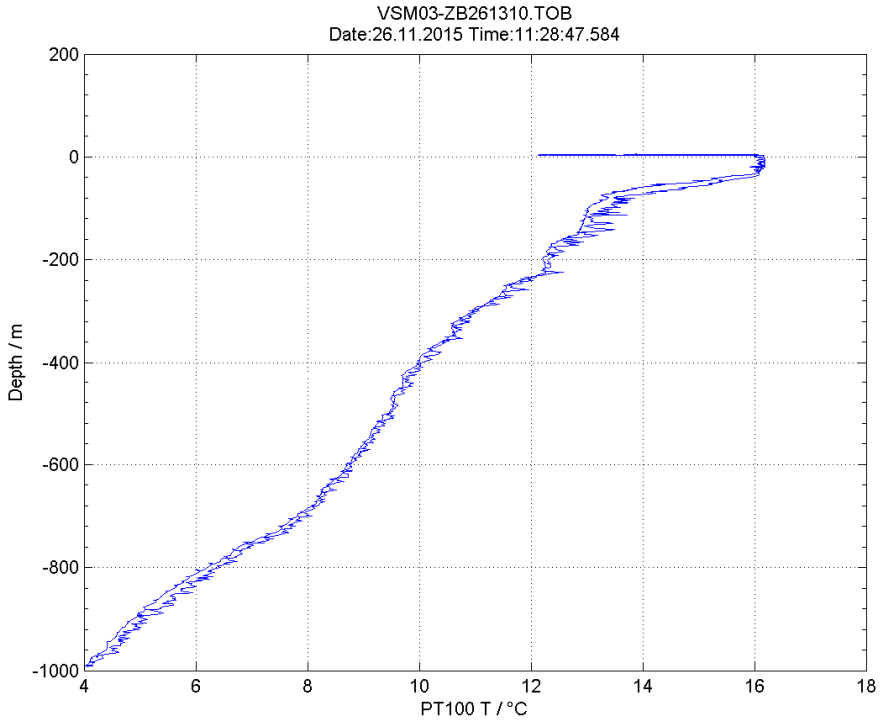

10 Appendix 4: Heat flow data description

10.1 Directory structure of heat flow data and processing results

Data, inversion parameters used and results are organized in each of the following station directory

```
data/TPRBE_006        + Station HF-Test     (TPRBE_048, Pen 1, Pen 2)
data/TPRBE_030        + Station HF08        (TPRBE_030, Pen 1, Pen 2)
data/TPRBE_046        + Station HF07        (TPRBE_046, Pen 1, Pen 2)
data/TPRBE_047        + Station HF04        (TPRBE_047, Pen 1, Pen 2)
data/TPRBE_048        + Station HF03        (TPRBE_048, Pen 1, Pen 2)
data/TPRBE_049        + Station HF03        (TPRBE_049, Pen 1)
data/TPRBE_047        + Station HF04        (TPRBE_047, Pen 1, Pen 2)
data/TPRBE_088        + Station HF05        (TPRBE_088, Pen 1, Pen 2)
data/TPRBE_109        + Station HF02        (TPRBE_109, Pen 1, Pen 2)
data/TPRBE_125        + Station HF01        (TPRBE_125, Pen 1, Pen 2)
data/TPRBE_126        + Station VSM03       (TPRBE_126, Pen 1, Pen 2)
data/TPRBE_127        + Station VSM03       (TPRBE_127, Pen 1)
```

according to the following scheme:

Parameter files used for pre-processing and inversion:

```
parameter
  ghf_6m_CTM1000_T113SD.m     + MATLAB-m-file containing probe parameters
  HF???.m                     + MATLAB-m-file containing station parameters
  HF???.pick                  + Time of penetration, heat pulse and end of measurement
  HF???k_ass.dat              + List of sensors with assumed thermal conductivities
  HF???omit.dat               + List of sensors used for processing
  init_var_6mv8.m             + MATLAB-m-file containing inversion parameters
  TOffset_HF06-ZB100546.dat   + Calibration file
```

Data after pre-processing:

```
penfiles
  HF0??P0?.pen.dat            + Data after pre-processing in ASCII format
  HF0??P0?.pen.mat            + Data after pre-processing in MATLAB format
```

Raw data:

```
raw_data
  HF*.SRD                     + Raw data in binary format
  HF*.TOB                     + Raw data in ASCII format
raw_data/QC/QC?.png           + Quality Control plots
```

Processing results:

```
results
  HF0??P0?.pen_t2c.mat                              + Data and results in MATLAB format
  HF_CSIRO_IN2015_C01_HF???P0?_HF???P0?.dat         + Results in ASCII-format
```

Plots of results in png graphic format:

```
results/png
  HF_CSIRO_IN2015_C01_HF???P0?_q.png                + Bullard-plot and error estimation
  HF_CSIRO_IN2015_C01_HF???P0?_raw.png              + Plot of temperatures
  HF_CSIRO_IN2015_C01_HF???P0?_scatf.png            + Scatter plot for frictional decay
  HF_CSIRO_IN2015_C01_HF???P0?_scatp.png            + Scatter plot for heat pulse decay
  HF_CSIRO_IN2015_C01_HF???P0?_temp.png             + Plot of temperature evolution
  HF_CSIRO_IN2015_C01_HF???P0?_Tk.png               + Plot of thermal properties
```

Plots of results in MATLAB fig format:

```
results/fig
  HF_CSIRO_IN2015_C01_HF???P0?_q.fig                + Bullard-plot and error estimation
  HF_CSIRO_IN2015_C01_HF???P0?_raw.fig              + Plot of temperature evolution
  HF_CSIRO_IN2015_C01_HF???P0?_scatf.fig            + Scatter plot for frictional decay
  HF_CSIRO_IN2015_C01_HF???P0?_scatp.fig            + Scatter plot for heat pulse decay
  HF_CSIRO_IN2015_C01_HF???P0?_temp.fig             + Plot of temperatures
  HF_CSIRO_IN2015_C01_HF???P0?_Tk.fig               + Plot of thermal properties
```

10.2 Raw data (*.TOB) format

```
Lines 1-17            Header information
Lines 18-50           Calibration Coefficients
Line 51               blank
Line 52               Path to data (not mandatory)
Line 53               Number of lines
Line 54               “;”
Line 55               “; Datasets Vbatt  Press  Temp Vheat  Iheat TiltX TiltY ACCz
      NTC01 NTC02 NTC03 NTC04 NTC05 NTC06 NTC07 NTC08 NTC09 NTC10 NTC11 NTC12 NTC13 NTC14
      NTC15 NTC16 NTC17 NTC18 NTC19 NTC20 NTC21 NTC22 Vaccu  Stat    IntT   IntT”
Line 55               “;       [Volt]  [dbar] [°C] [Volt] [A]   [°]  [°]    [g]
      [°C]  [°C]  [°C]  [°C]  [°C]  [°C]  [°C]  [°C]  [°C]  [°C]  [°C]  [°C]  [°C]  [°C]
      [°C]  [°C]  [°C]  [°C]  [°C]  [°C]  [°C]  [°C]  [Volt] [Bits]  [Time] [Time]”
Line 57               blank
Line 58               Data
 .                    .
.                     .
.                     .
.                     .
```

Datasets	- Running number / s since start / Sample rate: 1 sample/s
Vbatt	- voltage of internal battery / V
Press	- press / dbar
Temp	- PT100 water temperature / °C
Vheat	- voltage of heat pulse / V
Iheat	- current during heat pulse / A
TilX	- horizontal component of tilt / °
TiltY	- horizontal component of tilt / °
ACCz	- acceleration in fraction of g (earth acceleration)
NTC01-NTC22	- temperatures of NTCs / °C
Vaccu	- voltage of heat pulse battery / V
Stat	- heat probe status information
IntT	- time stamp [hh:mm:ss]
IntT	- time stamp [dd:mm:yyy]

Example of data row:

```
Datasets Vbatt  Press  Temp   Vheat  Iheat TiltX  TiltY ACCz   NTC01  … NTC22  Vaccu
       Stat    IntT          IntT
        [Volt] [dbar]  [°C]   [Volt] [A]   [°]    [°]   [g]    [°C]   … [°C]   [Volt]
       [Bits]  [Time]        [Time]
1       1.531   10.549 15.317 0.00   0.00  0.158  0.200 -0.986 15.085 … 15.078 24.818
       0x0000EB 05:41:06.584 04.11.2015
```